

NUMERICAL MODELING OF
BALÇOVA GEOTHERMAL FIELD

A THESIS SUBMITTED TO
THE GRADUATE SCHOOL OF NATURAL AND APPLIED SCIENCES
OF
MIDDLE EAST TECHNICAL UNIVERSITY

BY

CAN POLAT

IN PARTIAL FULFILLMENT OF THE REQUIREMENTS
FOR
THE DEGREE OF MASTER OF SCIENCE
IN
PETROLEUM AND NATURAL GAS ENGINEERING

FEBRUARY 2010

Approval of the thesis:

NUMERICAL MODELING OF BALÇOVA GEOTHERMAL FIELD

submitted by **CAN POLAT** in partial fulfillment of the requirements for the degree of **Master of Science in Petroleum and Natural Gas Engineering, Middle East Technical University** by,

Prof. Dr. Canan Özgen
Dean, Graduate School of **Natural and Applied Sciences** _____

Prof. Dr. Mahmut Parlaktuna
Head of Department, **Petroleum and Natural Gas Engineering** _____

Prof. Dr. Mahmut Parlaktuna
Supervisor, **Petroleum and Natural Gas Engineering Dept., METU** _____

Prof. Dr. Serhat Akin
Co-Supervisor, **Petroleum and Natural Gas Engineering Dept., METU** _____

Examining Committee Members:

Prof. Dr. Ender Okandan
Petroleum and Natural Gas Engineering Dept., METU _____

Prof. Dr. Mahmut Parlaktuna
Petroleum and Natural Gas Engineering Dept., METU _____

Prof. Dr. Serhat Akin
Petroleum and Natural Gas Engineering Dept., METU _____

Prof. Dr. Nurkan Karahanoğlu
Geological Engineering Dept., METU _____

Prof. Dr. Nilgün Güleç
Geological Engineering Dept., METU _____

Date: 29.01.2010

I hereby declare that all information in this document has been obtained and presented in accordance with academic rules and ethical conduct. I also declare that, as required by these rules and conduct, I have fully cited and referenced all material and results that are not original to this work.

Name, Last name : Can POLAT

Signature :

ABSTRACT

NUMERICAL MODELING OF BALÇOVA GEOTHERMAL FIELD

Polat, Can

M.Sc., Department of Petroleum and Natural Gas Engineering

Supervisor : Prof. Dr. Mahmut Parlaktuna

Co-Supervisor : Prof. Dr. Serhat Akın

February 2010, 153 pages

The aim of this study is to construct a numerical reservoir model for Balçova geothermal field, which is located in the İzmir bay area of the Aegean coast. A commercial numerical simulation program, TOUGH2 was utilized with a graphical interface, PETRASIM to model the Balçova geothermal field.

Natural state modeling of the field was carried out based on the conceptual model of the field, then history matching of production – injection practices of the field was established for the period of 1996 – 2008. The final stage of modeling was the future performance prediction of the field by using three different Scenarios. In Scenario-1, production and injection rates in year 2008 were repeated for 20 years. In Scenario-2, production and injection rates in year 2008 were repeated for the first 3 years, then they were increased at every 3 years. In Scenario-3, a new well (BT-1) that is assumed to be drilled to 1000 m depth is added for injecting some portion of water that was injected through BD-8 well. In that scenario, similar to Scenario-2, production and injection rates in year 2008 were repeated during the first 3 years, and then the rates of these wells (except the new well) were increased every three years.

Analysis of the results indicated that in Scenario-2, compared to Scenario-1, both the temperatures of deep wells located at the eastern portion of the field (BD-6, BD-2, BD-14, BD-9, BD-11, BD-12) and the temperatures of deep wells located at the western portion (BD-4, BD-15, BD-7, BD-5) decreased more. In Scenario-3, compared to Scenario-1, the deep wells located at the eastern side experienced less temperature drops while the deep wells located at the western side experienced higher temperature drops. Such temperature differences were not encountered in shallow wells. No significant changes in bottom hole pressures of deep wells occurred in all three scenarios. On the other hand, shallow wells, especially B-10 and B-5, responded to Scenario-2 and Scenario-3 as decrease in bottom hole pressures.

Keywords: Balçova Geothermal Field, TOUGH2, Petrasim, Numerical Modeling.

ÖZ

BALÇOVA JEOTERMAL SAHASININ SAYISAL MODELLENMESİ

Polat, Can

Yüksek Lisans, Petrol ve Doğal Gaz Mühendisliği Bölümü

Tez Yöneticisi : Prof. Dr. Mahmut Parlaktuna

Ortak Tez Yöneticisi : Prof. Dr. Serhat Akın

Şubat 2010, 153 sayfa

Bu çalışmanın amacı Ege kıyısının İzmir körfezinde yer alan Balçova jeotermal sahası için sayısal bir model oluşturmaktır. Çalışmada sayısal modelleme için simülasyon programı olan TOUGH2 ve bu programın grafiksel arayüzü olan Petrasim kullanılmıştır.

Sahanın doğal durum modellemesi sahanın kavramsal modeli temel alınarak yapılmıştır. Daha sonra, üretim ve enjeksiyon faaliyetlerini içeren 1996 – 2008 dönemi için tarihsel çakışma yapılmıştır. Modelleme çalışmasının son aşaması sahanın gelecekteki performansını üç farklı senaryo ile belirlemek olmuştur. Birinci senaryoda, 2008 yılındaki üretim ve enjeksiyon debileri 20 yıl boyunca tekrarlanmıştır. İkinci senaryoda, 2008 yılındaki üretim ve enjeksiyon debileri ilk üç yıl boyunca tekrarlanmış, daha sonra her üç yılda bir bu debiler artırılmıştır. Üçüncü senaryoda, 1000 m derinliğe kadar delindiği var sayılan BT-1 kuyusu daha önceden BD-8 kuyusuna basılan suyun bir kısmını bu kuyuya basmak için eklenmiştir. Bu senaryoda, ikinci senaryoya benzer olarak 2008 yılındaki üretim ve enjeksiyon debileri ilk üç yıl boyunca tekrarlanmış daha sonra yeni kuyu dışındaki kuyuların debileri her üç yılda bir artırılmıştır.

Senaryolardan elde edilen sonuçların analizi ikinci senaryoda sahanın dođu kısmında yer alan derin kuyuların (BD-6, BD-2, BD-14, BD-9, BD-11, BD-12) ve sahanın batı kısmında yer alan derin kuyuların (BD-4, BD-15, BD-7, BD-5) sıcaklıklarının birinci senaryoya kıyasla daha fazla düřtüđünü göstermiştir. Üçüncü senaryoda, sahanın dođu kısmında yer alan kuyuların sıcaklıkları birinci senaryoya kıyasla daha az, sahanın batı kısmında yer alan kuyuların sıcaklıkları ise yine aynı senaryoya kıyasla daha fazla düřmüřtür. Derin kuyularda görölen sıcaklık farklılıkları sıđ kuyularda gözlenmemiřtir. Her üç senaryoda da, derin kuyularının kuyu dibi basıçlarında önemli deđiřiklikler gözlenmemiřtir. Fakat, ikinci ve üçüncü senaryoda sıđ kuyularının özellikle B-5 ve B-10 kuyularının kuyu dibi basıçlarında düřmeler olmuřtur.

Anahtar kelimeler: Balçova jeotermal sahası, TOUGH2, Petrasim, Sayısal Modelleme

ACKNOWLEDGEMENTS

I would like to thank to Prof. Dr. Mahmut Parlaktuna for his support throughout the study and for his guidance, advice and assistance during writing the thesis.

I would also like to thank to the company, İzmir Geothermal A.Ş, for providing me well data necessary to prepare this thesis.

TABLE OF CONTENTS

ABSTRACT.....	iv
ÖZ.....	vi
ACKNOWLEDGEMENTS.....	viii
TABLE OF CONTENTS.....	ix
LIST OF TABLES.....	xi
LIST OF FIGURES.....	xii
CHAPTERS.....	1
1. INTRODUCTION.....	1
2. HYDROGEOLOGICAL INVESTIGATIONS ON BALÇOVA GEOTHERMAL SYSTEM.....	4
2.1. Stratigraphic Units.....	4
2.2. Tectonics.....	7
2.3. Temperature Structure.....	10
2.4. Hydrologic Balance.....	18
2.5. Chemical and Isotopic Characteristics of Balçova Waters.....	20
2.6. Conceptual Model.....	25
3. RESERVOIR SIMULATION AND FLOW IN FRACTURED MEDIA.....	28
3.1. Reservoir Simulation.....	28
3.1.1. The Need for Reservoir Simulation.....	28
3.1.2. The Modeling Approach.....	29
3.1.3. Numerical Models.....	29
3.1.4. Reservoir Simulation Application.....	30
3.1.5. Benefits of Simulation.....	32
3.2. Flow in Fractured Media.....	32
4. TOUGH2.....	34
4.1. General Concepts in TOUGH2.....	34
4.2. Equation of State Modules.....	35
4.3. Petrasim.....	37
5. STATEMENT OF THE PROBLEM.....	39
6. RESULTS AND DISCUSSION.....	40
6.1. Methodology.....	40
6.2. Model Creation.....	41
6.3. Natural State Modeling.....	47

6.4. History Matching.....	58
6.5. Future Forecasting.....	73
7. CONCLUSIONS AND RECOMMENDATION.....	119
REFERENCES.....	122
APPENDICES	
A. PERMEABILITY STRUCTURE.....	125
B. POROSITY DISTRIBUTION.....	128
C. GENERAL EQUATIONS AND CALCULATION PROCEDURE IN TOUGH2.....	132
C.1. General Equations.....	132
C.2. Space and Time Discretization.....	135
C.3. Calculation Procedure.....	137
C.4. Relative Permeability Functions.....	140
C.5. Capillary Pressure Functions.....	142
C.6. Deliverability Model.....	143
C.7. Heat Exchange with Confining Beds.....	145
C.8. Coupled Wellbore Flow.....	145
D. Petrasim.....	147

LIST OF TABLES

TABLES

Table 2.1- Properties of the wells in Balçova geothermal field (Çetiner, 1999, Çetiner, 2004, Yilmazer et al., 1998, Yilmazer et al., 1999, Aksoy, 2001).....	11
Table 2.2- Results of analysis of waters in Balçova region (Aksoy, 2001).....	21
Table 2.3- Isotopic composition of balçova area waters (Aksoy, 2001).....	24
Table 6.1- Properties of the materials used in the program.	43
Table 6.2- Coloring of materials used in grid model.....	43
Table 6.3- RMSD values of temperatures for different wells at initial condition.....	55
Table 6.4- Total production and injection (m ³) of the wells and their share (%) between 2004 and 2008.	60
Table 6.5- RMSD values of temperatures for different wells for the injection and production period.	72
Table 7.1- Explanation of Scenarios used in the future forecasting study.....	120
Table A.1-Transmissivity values of İzmir flysh (Onur et al., 2002).....	126

LIST OF FIGURES

FIGURES

Figure 1.1- Location map of Balçova Geothermal field (Aksoy and Filiz, 2001).....	1
Figure 1.2- Balçova geothermal field geological map (Yilmazer, 1989).	2
Figure 2.1- Location of Balçova field and regional geological map (after Öngür, 1972; Genç et.al., 2001).	5
Figure 2.2- Stratigraphic sequence of the area around Balçova geothermal field (Serpen, 2003).	6
Figure 2.3- Fault systems and well locations of Balçova geothermal field.....	7
Figure 2.4- Fault systems and well location of Balçova geothermal field (Satman et al., 2001).	9
Figure 2.5- Temperature profiles of deep wells (Satman et al., 2001).	12
Figure 2.6- Temperature profiles of shallow wells (Satman et al., 2001).....	13
Figure 2.7- Temperature of deep wells (BD-2, BD-4, BD-5, BD-6, BD-7, BD-8) with respect to time.	16
Figure 2.8- Temperature of deep wells (BD-3, BD-9, BD-10, BD-11, BD-12, BD-14, BD-15) with respect to time.	16
Figure 2.9- Temperature of shallow wells with respect to time.	17
Figure 2.10- Static water level of shallow wells with respect to time.....	17
Figure 2.11- Static water level of deep wells with respect to time.	18
Figure 2.12- Streams and fault zones of the area around Balçova field (Serpen and Kayan, 2001).	19
Figure 2.13- Chloride distribution (in mg/kg) in the Balçova geothermal field.....	22
Figure 2.14- Ternary diagram of Cl, SO ₄ and HCO ₃ (Serpen, 2003).....	22
Figure 2.15- Ternary diagram of Na, K, Mg (Aksoy et al., 2007).....	23
Figure 2.16- Conceptual model of the Balçova geothermal field (Aksoy et al., 2007).	26
Figure 6.1- Dimensions of grid model of Balçova geothermal field.....	44
Figure 6.2- Material distribution for the cross-section Z=-15.	44
Figure 6.3- Material distribution for the cross-section Z=-150.	45
Figure 6.4- Material distribution for the cross-section Z=-400.	45
Figure 6.5- Material distribution for the cross-section X=3075.	46
Figure 6.6- Material distribution for the cross-section X=3470.	46
Figure 6.7- Material distribution for the cross-section X=3920.	47
Figure 6.8- Temperature vs. depth profiles for the shallow well B-4.	49

Figure 6.9- Temperature vs. depth profiles for the shallow well B-7.	49
Figure 6.10- Temperature vs. depth profiles for the shallow well B-8.	50
Figure 6.11- Temperature vs. depth profiles for the shallow well B-10.	50
Figure 6.12- Temperature vs. depth profiles for the shallow well B-11.	51
Figure 6.13- Temperature vs. depth profiles for the deep well BD-1.	51
Figure 6.14- Temperature vs. depth profiles for the deep well BD-2.	52
Figure 6.15- Temperature vs. depth profiles for the deep well BD-3.	52
Figure 6.16- Temperature vs. depth profiles for the deep well BD-4.	53
Figure 6.17- Temperature vs. depth profiles for the deep well BD-5.	53
Figure 6.18- Temperature vs. depth profiles for the deep well ND-1.	54
Figure 6.19- A comprasion of the observed and calculated temperatures for initial condition.....	54
Figure 6.20- Initial temperature distributions for cross-sections x=2800 and x=3000.....	56
Figure 6.21- Initial temperature distribuitons for cross-sections X=3700 and X=4400.....	56
Figure 6.22- Initial temperature distributions for cross-sections Z=0 and Z=-15.....	57
Figure 6.23- Initial temperature distributions for cross-sections Z=-85 and Z=-350.....	57
Figure 6.24- Initial temperature distribution for cross-section Z=-550.....	57
Figure 6.25- Model pressure vs. depth profile for initial condition.....	58
Figure 6.26- A comprasion of the simulated and measured temperatures for well B-1.	61
Figure 6.27- A comprasion of the simulated and measured temperatures for well B-4.	62
Figure 6.28- A comparison of the simulated and measured temperatures for well B-5.	62
Figure 6.29- A comparison of the simulated and measured temperatures for well B-10.	63
Figure 6.30- A comprasion of the simulated and measured temperatures for well B-11.	63
Figure 6.31- A comprasion of the simulated and measured temperatures for well BD-1.....	64
Figure 6.32- A comprasion of the simulated and measured temperatures for well BD-2.....	64
Figure 6.33- A comprasion of the simulated and measured temperatures for well BD-3.....	65

Figure 6.34- A comparison of the simulated and measured temperatures for well BD-4.....	65
Figure 6.35- A comparison of the simulated and measured temperatures for well BD-6.....	66
Figure 6.36- A comparison of the simulated and measured temperatures for well BD-11.....	66
Figure 6.37- A comparison of the simulated and measured temperatures for well BD-12.....	67
Figure 6.38- A comparison of the simulated and measured temperatures for well BD-14.....	67
Figure 6.39- A comparison of the simulated and measured temperatures for well BD-15.....	68
Figure 6.40- A comparison of the model pressure and measured water level at well BD-1.....	68
Figure 6.41- A comparison of the model pressure and measured water level at well BD-5.....	69
Figure 6.42- A comparison of the model pressure and measured water level at well BD-9.....	69
Figure 6.43- A comparison of the model pressure and measured water level at well ND-1.....	70
Figure 6.44- A comparison of the model pressure and measured water level at well N-1.....	70
Figure 6.45- A comparison of the model pressure and measured water level at well B-2.....	71
Figure 6.46- A comparison of the model pressure and measured water level at well B-12.....	71
Figure 6.47- A comparison of the observed and calculated temperatures for the production and injection period.....	72
Figure 6.48- Production and injection wells used in Scenario-1.....	75
Figure 6.49- Production and injection wells used in Scenario-2.....	76
Figure 6.50- Production and injection wells used in Scenario-3.....	77
Figure 6.51- The areal temperature profile for cross-section Z=0 and year 2014 (Scenario 1, 2, 3).....	82
Figure 6.52- The areal temperature profile for cross-section Z=0 and year 2019 (Scenario 1, 2, 3).....	83
Figure 6.53- The areal temperature profile for cross-section Z=0 and year 2024 (Scenario 1, 2).....	84

Figure 6.54- The areal temperature profile for cross-section Z=-15 and year 2014 (Scenario 1, 2, 3).....	85
Figure 6.55- The areal temperature profile for cross-section Z=-15 and year 2019 (Scenario 1, 2, 3).....	86
Figure 6.56- The areal temperature profile for cross-section Z=-15 and year 2024 (Scenario 1, 2).....	87
Figure 6.57- The areal temperature profile for cross-section Z=-85 and year 2014 (Scenario 1, 2, 3).....	88
Figure 6.58- The areal temperature profile for cross-section Z=-85 and year 2019 (Scenario 1, 2, 3).....	89
Figure 6.59- The areal temperature profile for cross-section Z=-85 and year 2024 (Scenario 1, 2).....	90
Figure 6.60- The areal temperature profile for cross-section Z=-350 and year 2014 (Scenario 1, 2, 3).....	91
Figure 6.61- The areal temperature profile for cross-section Z=-350 and year 2019 (Scenario 1, 2, 3).....	92
Figure 6.62- The areal temperature profile for cross-section Z=-350 and year 2024 (Scenario 1, 2).....	93
Figure 6.63- The areal temperature profile for cross-section Z=-550 and year 2014 (Scenario 1, 2, 3).....	94
Figure 6.64- The areal temperature profile for cross-section Z=-550 and year 2019 (Scenario 1, 2, 3).....	95
Figure 6.65- The areal temperature profile for cross-section Z=-550 and year 2024 (Scenario 1, 2).....	96
Figure 6.66- The areal temperature profile for cross-section X=2500 and year 2014 (Scenario 1, 2, 3).....	97
Figure 6.67- The areal temperature profile for cross-section X=2500 and year 2019 (Scenario 1, 2, 3).....	98
Figure 6.68- The areal temperature profile for cross-section X=2500 and year 2024 (Scenario 1, 2).....	99
Figure 6.69- The areal temperature profile for cross-section X=2800 and year 2014 (Scenario 1, 2, 3).....	100
Figure 6.70- The areal temperature profile for cross-section X=2800 and year 2019 (Scenario 1, 2, 3).....	101
Figure 6.71- The areal temperature profile for cross-section X=2800 and year 2024 (Scenario 1, 2, 3).....	102
Figure 6.72- The areal temperature profile for cross-section X=3000 and year 2014 (Scenario 1, 2, 3).....	103

Figure 6.73- The areal temperature profile for cross-section X=3000 and year 2019 (Scenario 1, 2, 3).....	104
Figure 6.74- The areal temperature profile for cross-section X=3000 and year 2024 (Scenario 1, 2).....	105
Figure 6.75- The areal temperature profile for cross-section X=3700 and year 2014 (Scenario 1, 2, 3).....	106
Figure 6.76- The areal temperature profile for cross-section X=3700 and year 2019 (Scenario 1, 2, 3).....	107
Figure 6.77- The areal temperature profile for cross-section X=3700 and year 2024 (Scenario 1, 2).....	108
Figure 6.78- The areal temperature profile for cross-section X=4400 and year 2014 (Scenario 1, 2, 3).....	109
Figure 6.79- The areal temperature profile for cross-section X=4400 and year 2019 (Scenario 1, 2, 3).....	110
Figure 6.80- The areal temperature profile for cross-section X=4400 and year 2024 (Scenario 1, 2).....	111
Figure 6.81- Simulated bottomhole temperature of BD-1 and BD-2 (Scenario 1, 2, 3).....	113
Figure 6.82- Simulated botomhole temperature of BD-4 and BD-6 (Scenario 1, 2, 3).....	114
Figure 6.83- Simulated bottomhole temperature of BD-7 and BD-9 (Scenario 1, 2, 3).....	114
Figure 6.84- Simulated bottomhole temperature of BD-11 and BD-12 (Scenario 1, 2, 3).....	114
Figure 6.85- Simulated bottomhole temperature of BD-14 and BD-15 (Scenario 1, 2, 3).....	115
Figure 6.86- Simulated bottomhole temperature of B-1 and B-4 (Scenario 1, 2, 3).....	115
Figure 6.87- Simulated bottomhole temperature of B-5 and B-10 (Scenario 1, 2, 3).....	115
Figure 6.88- Simulated bottomhole pressure of ND-1 and N-1 (Scenario 1, 2, 3).....	116
Figure 6.89- Simulated bottomhole pressure of B-12 and BD-1 (Scenario 1, 2, 3).....	116
Figure 6.90- Simulated bottomhole pressure of BD-2 and BD-4 (Scenario 1, 2, 3).....	116
Figure 6.91- Simulated bottomhole pressure of BD-6 and BD-7 (Scenario 1, 2, 3).....	117

Figure 6.92- Simulated bottomhole pressure of BD-11 and BD-12 (Scenario 1, 2, 3).....	117
Figure 6.93- Simulated bottomhole pressure of BD-14 and BD-15 (Scenario 1, 2, 3).....	117
Figure 6.94- Simulated bottomhole pressure of B-5 and B-10 (Scenario 1, 2, 3).....	118
Figure A.1- Reservoir pressures of Balçova field with respect to depth (Serpen, 2003).	125
Figure B.1- Balçova BG-1 well gamma ray and neutron porosity logs (Tuncay, 1989).....	129
Figure B.2- Balçova BG-2 well gamma ray and neutron porosity logs (Tuncay, 1989).....	130
Figure B.3- Balçova BG-3 well gamma ray and neutron porosity logs (Tuncay, 1989).....	130
Figure B.4-Balçova BG-4 well gamma ray, neutron porosity logs and density logs (Tuncay, 1989).....	131
Figure B.5- Balçova B-3 well gamma ray and neutron porosity logs (Tuncay, 1989).....	131
Figure D.1- Defining the boundary of the model.....	147
Figure D.2- Defining an internal boundary.....	148
Figure D.3- Creating grid data.....	149
Figure D.4- Material Properties.....	149
Figure D.5- Editting Cell Data	150
Figure D.6- Running TOUGH2.....	151
Figure D.7- The 3D results window	151
Figure D.8- 3D view of a model with top surface defined	152
Figure D.9- Editing well data	152
Figure D.10- Subgridding in the method of MINC.....	153

CHAPTER 1

INTRODUCTION

Balçova geothermal field, the first field utilized in Turkey for direct heat application, is located in the İzmir bay area of the Aegean coast and is situated 11 km southwest of İzmir city (38.2 latitude, 27.0 longitudes) (Figure 1.1).

The temperature of the produced waters have changed between 80 and 140 °C. They have low dissolved solids and very low non condensable gas content.



Figure 1.1- Location map of Balçova Geothermal field (Aksoy and Filiz, 2001).

The first known study on Agamemnon thermal spring was made in 1961. Resistivity and SP studies were conducted in year 1962. In year 1963, three shallow wells were drilled in the field. S1 well produced 124 °C water with 27 L/s rate from the depth 39 m. S2 well produced 102 °C water with 11 L/s from the depth 69 m and S3 well produced 101 °C water with rate 1.25 L/s from the depth 140 m. Due to scaling problems these wells were clogged. Today the location of these wells is not known as they have disappeared with time. The Balçova field was first exploited in the early 1980s. In year 1983, 9 shallow wells represented with letter B were drilled to heat Balçova Thermal facilities and Dokuz Eylül University. To overcome scaling problems downhole heat exchangers were used in those wells. In year 1989, ten gradient wells were drilled to determine hot zones and temperature distribution of the field. Temperature and well logs were taken from those wells and temperature gradients were evaluated. In year 1989 and 1990, 4 wells named as BTF were drilled to heat Dokuz Eylül University and at the same years B-10 and B-11 wells were drilled. Deep wells were started to be drilled in year 1994 with the well BD-1 (Figure 1.2). Balçova district heating system started in 1996 and Narlıdere district heating system started in 1998 (Satman et al., 2001).

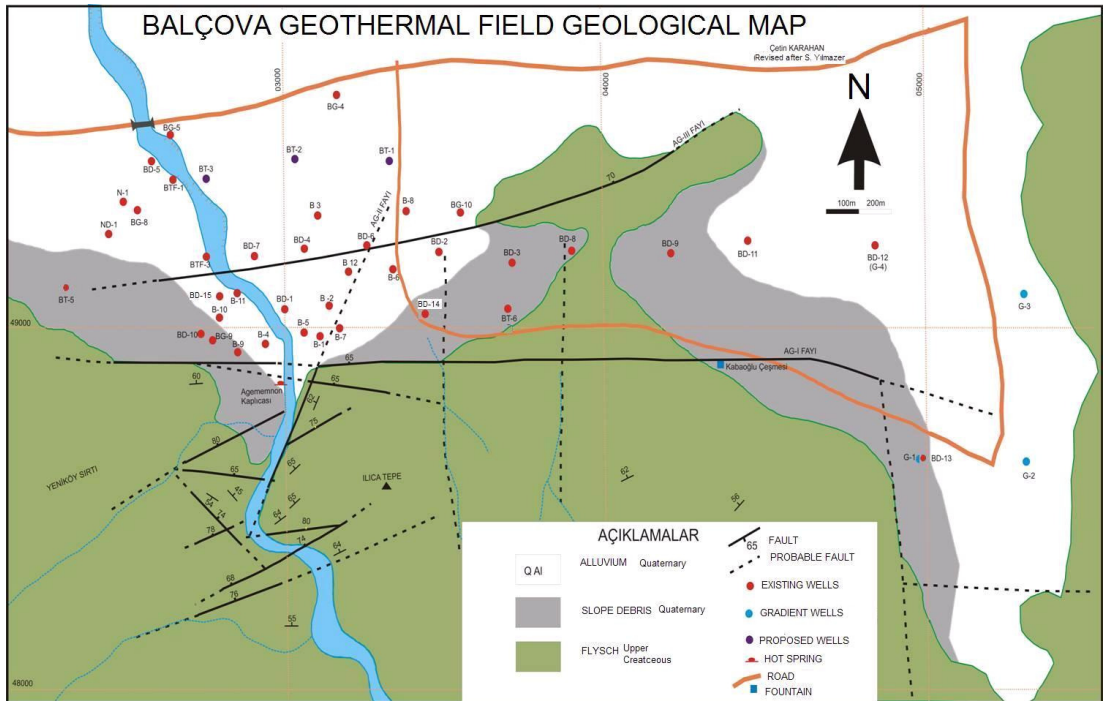


Figure 1.2- Balçova geothermal field geological map (Yilmazer, 1989).

In 2000, 0.64 million m² of indoor space corresponding to 5489 houses, hotels, schools and a university hospital and campus were being heated. In year 2003 hot water that had the capacity to heat 15000 house (72 MWt) (Toksoy, 2003) were produced (Aksoy and Serpen, 2005). By the end of 2005, the heated area had increased to 1.6 million m², and the project supplied heat to 10 ha of greenhouses. In November 2007 the heated area increased to 1.9 million m² (Aksoy et al., 2007).

There is a continuous increase in production and injection amount from 2000 to 2009. In year 2000, 2.13E6 m³ water was produced from the field and 1.29E6 m³ (%60 of production) water was injected. In year 2005, water production and injection were realized as 4.20E6 m³ and 1.87E6 m³ (%45 of production), respectively. Water production and injection in year 2008 were as 4.86E6 m³ and 3.79E6 m³ (% 80 of production), respectively.

In brief, it is seen that there has been increase in heat energy demand obtained from the field. This brings the need of producing more and as a result water injection will have to be increased, which may cause the production zones cool more. As increasing the production and so the injection, new production and injection scenarios should be conducted and new wells should be drilled for both injection and production purposes to minimize the cooling in production zone. Modeling studies are one of the tools utilized to study the effect of different scenarios before the development plans are realized.

The aim of this study is to construct a numerical model in a computer environment for Balçova geothermal field thus future performance predictions can be made to give directions for the possible operations in the field.

CHAPTER 2

HYDROGEOLOGICAL INVESTIGATIONS ON BALÇOVA GEOTHERMAL SYSTEM

2.1. Stratigraphic Units

The area around the Balçova geothermal field consists of Alluvium, talus, Cumovası volcanites, Yeniköy formation and İzmir flysch and Menderes metamorphics (Figure 2.1). Although alluvium has some permeability, most parts of talus, Cumovası volcanites, Yeniköy formation and İzmir flysch are impermeable. Permeability in these zones is created by faults and fractures.

Alluvium, talus and flysch constitute the lithology of the Balçova geothermal field (Figure 2.2). Flysch formation exceeding 2000 m depth, occupies the most of the volume of the field. Above the flysch formation alluvium and talus thickness of which change between 0 and 200 m take place. While talus exists in small amounts in southern part of the field, alluvium covers the rest of the field above the flysch formation. Balçova area wells intersect mainly lightly metamorphosed sandstones, clays and siltstones of the İzmir Flysch sequence.

Upper Cretaceous İzmir flysch, comprising most of the region, consists of metasandstones, limestone, granodiorites, serpentinite-diabase, rhyolites and phyllites. The thickness of the İzmir flysch exceeds 2000 m in some regions. Fractured metasandstones and fault zones existing in limestone and granodiorites are permeable. Other zones existing in the İzmir flysch formation can be thought as impermeable.

Metasandstones exist in the sequence of lightly metamorphosed sandstone, clay and siltstone. Metasandstones in the İzmir flysch formation has nil porosity. They have some fissures and they have some permeability created by fractures and faults.

Limestone and granodiorites have fractures and faults that create secondary permeability and so easily transmit water.

Serpentinite and rhyolites are thought as impermeable zones.

Phyllites have nil porosity and permeability so do not contain any ground water.

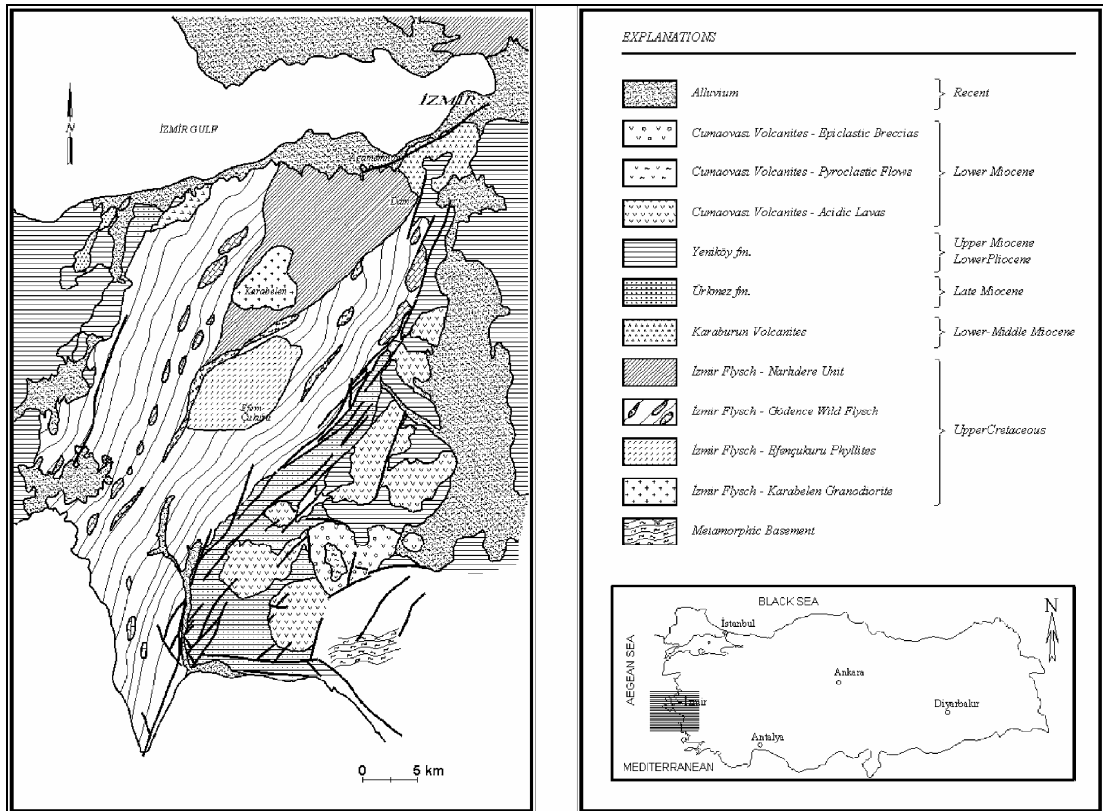


Figure 2.1- Location of Balçova field and regional geological map (after Öngür, 1972; Genç et.al., 2001).

The Miocene Yeniköy formation, existing in the southern east and southern west of the area, includes sandstones, limestones, claystones and conglomerates. The thickness of it varies between 800 and 1000 m. It has nil primary permeability. Fractures and faults are the reason of secondary permeability existing in the formation.

The Pliocene Cumaovası volcanites, existing in the east and southern east of the area, includes rhyolite, latite-andesite, volcanic Breccia-Tuffs. The thickness of it varies between 300 and 500 m. Fractured zones are permeable (Satman et al., 2001).

Alluvium existing over the field has good porosity and some permeability. Some shallow wells produce water mainly from this zone. The thickness of it varies between 0 and 200 m.

Talus exists in southern part of the field in small amounts compared to area covered by alluvium. Talus serves as cap rock and so is impermeable as indicated by temperature distribution of the wells in the field. The thickness of it varies between 0 and 200.

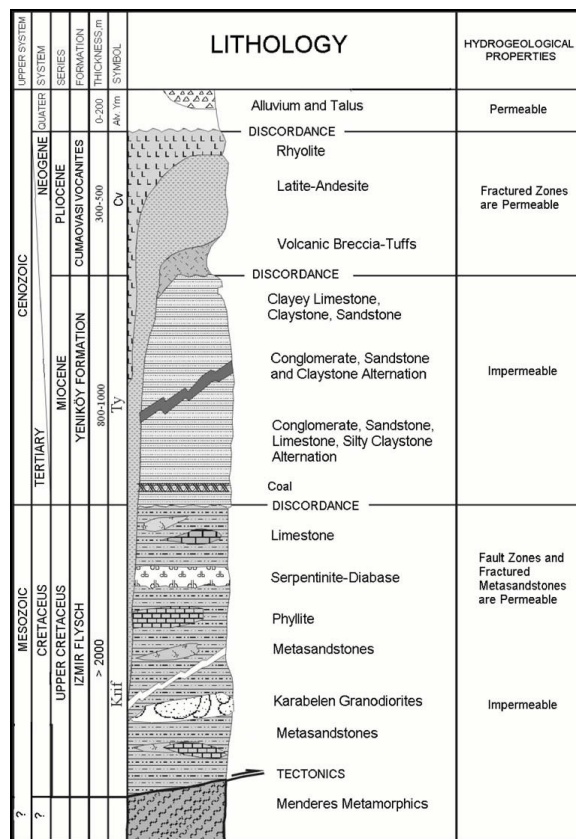


Figure 2.2- Stratigraphic sequence of the area around Balçova geothermal field (Serpel, 2003).

Satman et al., (2001) presented the second structural map of the field in their study (Figure 2.4). In that map, faults that are confirmed with observations from the surface are represented by bold continuous lines. The first group consisting of four faults is represented by the letter A. These faults are nearly vertical and the rock north of these faults moved downward with respect to the rock south of the fault. The second group of faults that are in the same category are represented by the letter B (BI-BIII). They locate at the south of the field and they are N-S trending faults.

Faults that are confirmed with the help of underground geology are represented by bold dashed lines. Some of them are E-W trending faults (CI-CII). The south of CI fault moved 10-30 m downward relative to the north. The CII fault locates close to BD-7, BD-4 and BD-6 wells. The magnitude of the throw is around 65 m. The rock north of the CII fault moved downward relative to the rock on the other side. It is thought that CI and CII faults have dips around 70°.

The other groups of faults shown by bold dashed lines are represented by the letter D (DI-DIV). They are N-S trending faults. DI fault which locates between BTF-4 and BD-7 well is nearly vertical. The magnitude of the throw is around 70 m. The rock east of the DI fault moved downward relative to the rock on the other side. East of this fault, DII fault whose throw has the magnitude of 30 m and DIII fault whose throw has the magnitude of 10 m locate. DIV fault locating close to BD-5 well has the throw of magnitude 40 m. The rock west of the DIV fault moved downward relative to the rock on the other side.

Other faults that were proposed in the previous studies are represented by thin dashed lines. It was mentioned that the fault named as Agamemnon II was not compatible with geological data, the suggested fault locating close to CI fault had a different throw direction compared to CI fault and the suggested fault locating close to CII fault should locate at the place where CII fault is shown (Satman et al., 2001).

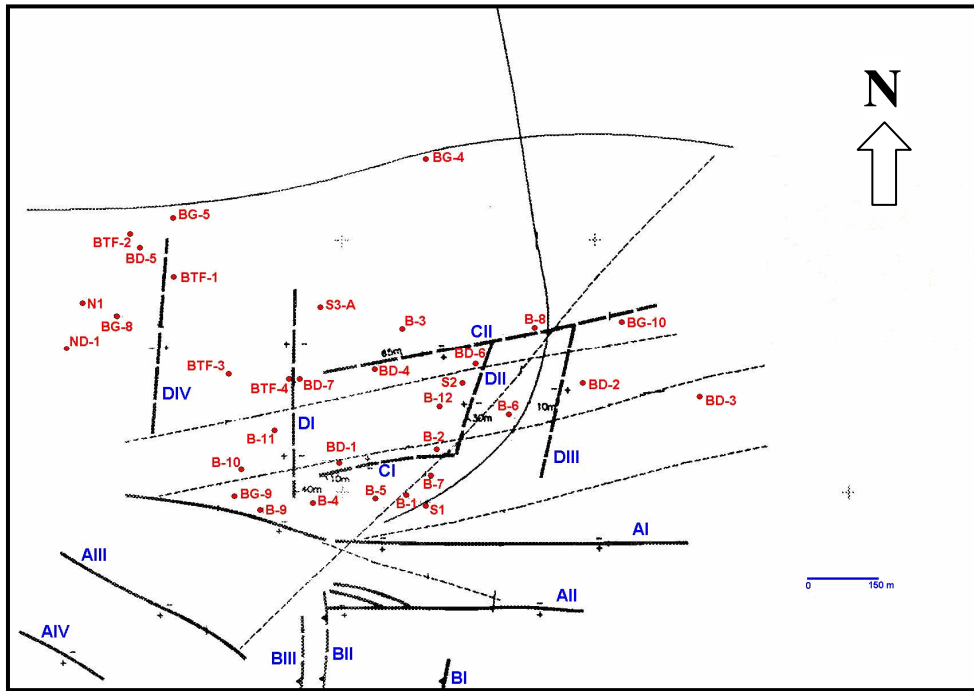


Figure 2.4- Fault systems and well location of Balçova geothermal field (Satman et al., 2001).

The third structural map of the field is shown in Figure 1.2. In that map, possible faults are represented by dashed lines. The following observations are made by comparison of Figure 1.2 and Figure 2.4.

- There are no faults in Figure 1.2 that stand for the faults DI, DIII and DIV that are shown in Figure 2.4.
- The fault (AG-II) that locates close to B-1 and B-12 wells in Figure 1.2 probably stand for the fault DII of Figure 2.4.
- AG-III fault shown in Figure 1.2 probably stands for the fault CII of Figure 2.4. It is longer than CII fault and extends up to BTF-3 well. The dip of it is 70° .
- AG-I fault shown in Figure 1.2 is extended and reaches ND-1 well at west and BD-12 well at east. While the west part of the AG-I fault is straight in Figure 1.2, it has a break point and an angle in Figure 2.4. The dip of the AG-I fault is 65° .

- The locations of the faults south of AG-I fault are completely different in those maps.

2.3. Temperature Structure

Initial pressure and temperature distributions as well as the changes in reservoir pressure and temperature in response to production and injection practices should be evaluated while constructing the model of the field. Thus, significant information such as the location of permeable zones, initial temperatures of different zones, location of the feeding zone(s) and whether there exists a zone where surface water intrusion occurs, the location of it, how system reacts for different injection and production procedures can be gained.

So far, 16 deep and 31 shallow wells have been drilled in Balçova geothermal field. Among these wells some of them were abandoned because of technical difficulties. Some of the wells that were used for the utilization of geothermal energy in Balçova field are listed in Table 2.1 which also includes information about lithology, final drilled depths, casing properties and mud loss intervals.

Evaluating the initial temperature distribution of wells (Figures 2.5 and 2.6), it can be said that, in wells B-4, B-7 and B-10, 110-120 °C water flows below the depth 30 m (Figure 2.6). The temperature profiles of the wells B-2, B-3, B-6 and B-8 do not indicate any hot water zones as there exists continuous temperature increase with depth. Deep wells can be grouped into two according to their initial temperatures (Figure 2.5). While permeable zones of the wells BD-1, BD-2, BD-3 and BD-4 have temperatures between 130-140 °C, permeable zones of the wells BD-5 and ND-1 locating in the west of the field have temperatures lower than 120 °C.

Temperature profiles indicate fractured permeable zone between 300-420 m in well BD-1. Mud losses occurred at the depth of 363 m and increase in drilling rate at the depths 360-365 m and 400-415 m confirm this observation. There are permeable zones between the depths 350 and 450 m in well BD-2. Mud losses encountered below the depth of 420 m. The well BD-3 has permeable zone between the depths 415 and 590 m. During the drilling process of BD-3 mud losses occurred below the depth of 420 m and there was increase in drilling rate at the depths 410-450 m and 500-560 m. Temperature profile of the well BD-4 indicates

permeable zone between the depth 520 m and 620 m. Observed increase in drilling rate at the depth 590 m confirms that permeable zone.

The temperature profile of BD-5 shows two different permeable zones. These permeable zones locate at 300-400 m and 600-900 m. Mud loss and increase in rate during the drilling process confirm those permeable zones. The well BD-7 has permeable zone between 425 m and 600 m. Mud loss happened between 450 m and 550 m. The well ND-1 has permeable zone between 50-150 m and the temperature is around 95 °C (Satman et al., 2001).

Table 2.1- Properties of the wells in Balçova geothermal field (Çetiner, 1999, Çetiner, 2004, Yilmazer et al., 1998, Yilmazer et al., 1999, Aksoy, 2001).

Well Name	Total Depth (m)	Lithology		Casing		Mud Loss Interval (m)
		Interval (m)	Lithology	Interval (m)	Type and Diameter (in)	
B-4	125	0 - 68	Alluvium	20 - 86	Casing, 8 5/8	80 - 90
		68 - 125	Flysch	86 - 114	Perforated Liner, 8 5/8	
B-9	48	0 - 33	Alluvium	18.5 - 40.5	Casing, 14	33 - 48
		33 - 48	Flysch	40.5 - 46.5	Perforated Liner, 14	
B-10	125	0 - 30	Alluvium	0 - 125	Casing, 13 3/8	
		30 - 125	Flysch	-	-	
B-11	125	0 - 24	Alluvium	0 - 125	Casing, 13 3/8	
		24 - 125	Flysch	-	-	
BD-2	677	0 - 38	Alluvium	0 - 360	Casing, 9 5/8	400 - 560
		38 - 677	Flysch	360 - 677	Perforated Liner, 8 1/2	
BD-3	750	0 - 60	Talus	0 - 350	Casing, 9 5/8	420 - 750
		60 - 750	Flysch	350 - 750	Perforated Liner, 8 1/2	
BD-4	624	0 - 40	Alluvium	0 - 315.88	Casing, 9 5/8	430 - 650
		40 - 624	Flysch	306.89 - 624	Perforated Liner, 7	
BD-5	1100	0 - 116	Alluvium	0 - 595.46	Casing, 9 5/8	655 - 1050
		116-1100	Flysch	585.54 - 1100	Perforated Liner, 7	
BD-6	606	0 - 22	Alluvium	0 - 295	Casing, 9 5/8	400 - 570
		22 - 606	Flysch	280.97 - 606	Perforated Liner, 7	
BD-7	700	0 - 98	Alluvium	0 - 331.91	Casing, 9 5/8	440 - 560
		98 - 700	Flysch	322.46 - 700	Perforated Liner, 7	
BD-8	630	-	Alluvium	0 - 285	Casing, 13 3/8	500 - 630
		0 - 630	Flysch	281 - 629	Perforated Liner, 9 5/8	
BD-9	772	0 - 18	Talus	0 - 312	Casing, 13 3/8	
		18 - 772	Flysch	307.62 - 772	Perforated Liner, 9 5/8	
BD-14	371	0 - 40	Talus	0 - 126.5	Casing, 13 3/8	232 - 370
		40 - 371	Flysch	114 - 370	Perforated Liner, 9 5/8	
BD-15	472	0 - 30	Alluvium	0 - 186.40	Casing, 13 3/8	293 - 449
		30 - 472	Flysch	184 - 472	Perforated Liner, 9 5/8	

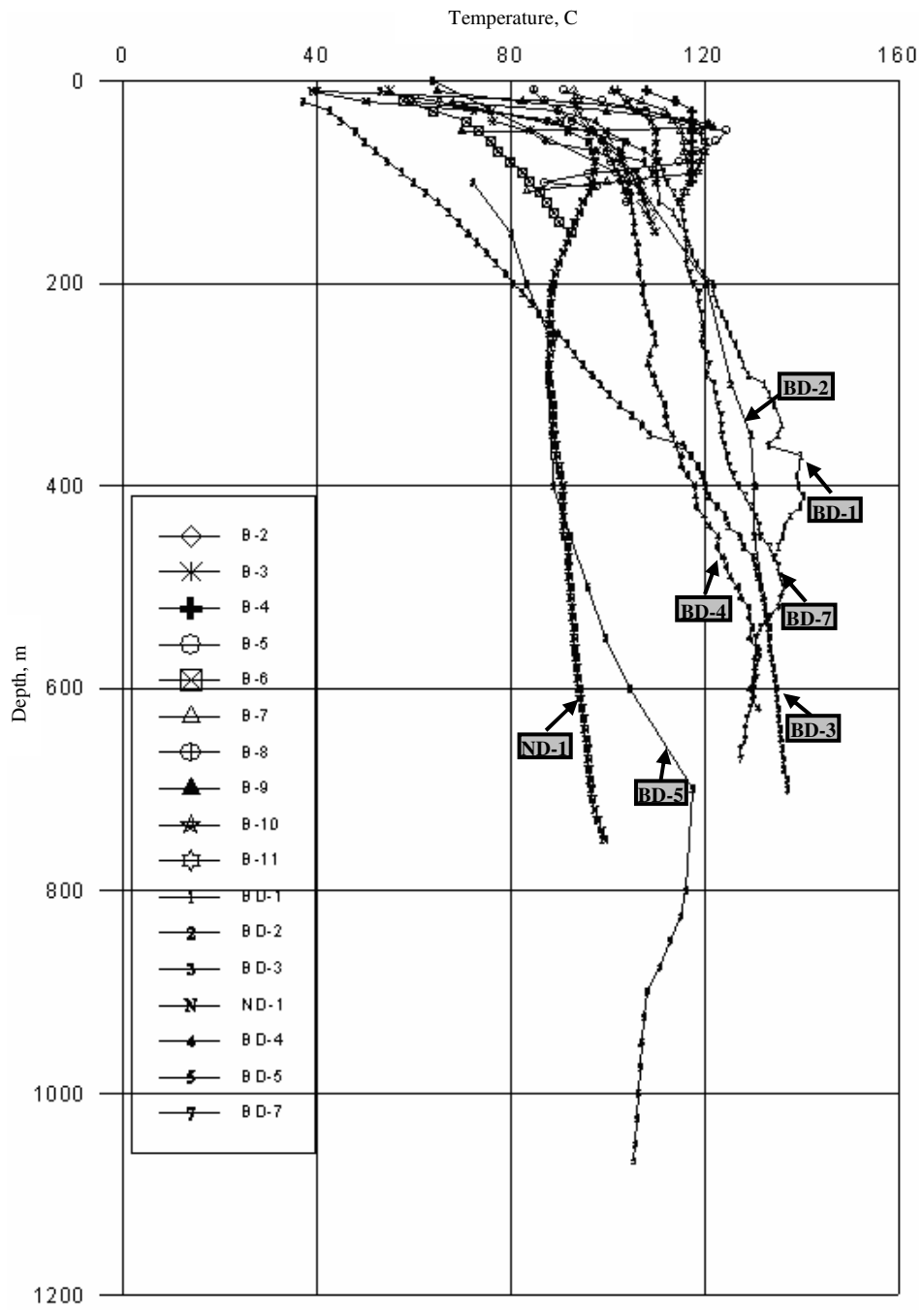


Figure 2.5- Temperature profiles of deep wells (Satman et al., 2001).

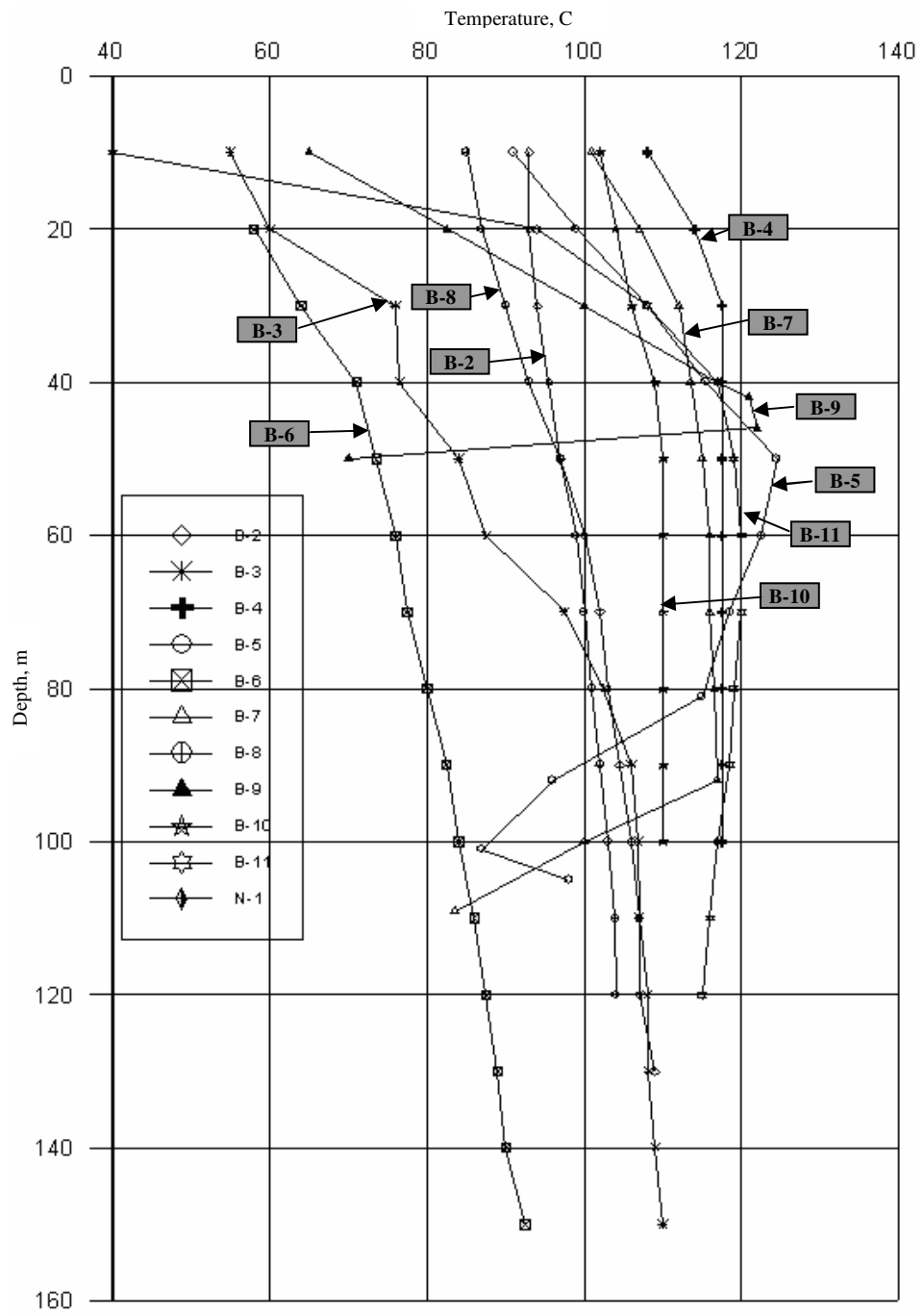


Figure 2.6- Temperature profiles of shallow wells (Satman et al., 2001).

Figures 2.7 to 2.9 show the temperature recordings of each well of the field as function of time. Analysis of the change in the temperature of wells with time can give valuable information on the possible effects of production-injection practices carried out in the field. In year 2000, injection was done through the wells B2, B9, B12, BD-1 and BD-3. In that year most injection was done into the shallow wells, around 60 % of water was injected into the well B-9. It can be seen from the Figure 2.9 that decrease in temperature existing in shallow wells could not be recovered during the summer time- peak value of temperatures of shallow wells in year 2000 is lower than the peak value of temperatures in year 1999. In year 2001 there was no injection to deep wells and most injection was done through the well B-9 (around 60 %). Again in that year the temperature of shallow wells did not reach to their value that exists in summer time of previous year indicating that there is a continuous temperature drop in shallow wells. This situation can also be observed for deep wells but decrease in temperature exists in very small amounts. In year 2002 injection rate to shallow wells was decreased and half of the water used for injection purpose was sent to the well BD-8. It can be observed that there is temperature increase in both shallow and deep wells in the summer time of that year compared to temperature values in the summer time of the previous year. This increment is clearer in shallow wells, which indicates the effect of deep well injection especially to BD-8. In year 2003 all injection was done through the well BD-8. Though common expectation that the temperature values of wells would decrease due to injection of cold water during the winter time, increase in temperature in both shallow and deep wells during the winter time of the year 2003 occurred. This situation again shows the importance of injection of water to the deep well BD-8.

In the time period that includes end of the year 2003 and start of 2004, and in the time period that includes the end of the year 2004 and the start of 2005 a sharp decrease in pressure can be observed in both shallow and deep wells (Figure 2.10 and Figure 2.11). Static water level information from the deep wells ND-1 and BD-2 indicates that pressure at the start of the year 2005 is lower than the pressure at the start of the year 2004. It is clear that if the injection and production procedure continues like that lower pressure values will exist in the field. The same situation also exists for shallow part of the field. The static level information from wells B-11 and B-12 shows that the pressure declines in the shallow part as if it does in the deep portion of the field. At the time period that includes the end of the year 2004 and the start of 2005 a sharp decrease in temperature can be observed in both shallow and deep wells. There is also such a drop in shallow wells in the time

period that includes the end of the year 2003 and the start of 2004. This sharp decline in temperature may be the result of intrusion of cold surface water. As pressure declines, more surface water will enter the field and cause the temperature of the field to decline. For later years, more injection was performed and as a result pressure increased in both shallow and deep parts of the field, which can be observed from the static water level information obtained from the wells, B-11, B-2 and ND-1. As a result of this process, sharp decreases in temperature were avoided and shallow wells recover to its temperature which was at the year 2000. There is a small temperature decrease in deep wells. It is clearer in well BD-2. This decline may contribute the deep injection of water. Most water, around 80 %, was injected through the well BD-8, which is located far away from wells BD-4 and BD-6 so that its contribution in temperature decline is less for these wells.

From the temperature variations in shallow and deep wells, it can be stated that injection of water to well B-9 mostly affects the region in which the wells B-9, B-4 and B-10 locate. This region constitutes the west part of the field. Injection of water to well B-9 resulted in lower temperature decrease in the eastern region consisting of BD-3, BD-2 and BD-7 and B-5 wells compared western part. This may relate to natural recharge which blocks the water coming from B-9 well as it ascends in the fault and flows through the alluvium to the north.

To avoid surface water entering the field, pressure of the field must be increased, which can be actually done by injecting more water to the field. However, this procedure will also result in temperature decline in the field. Whether injecting more water or allowing surface water to enter the field is a better way depends on many cases, for example, the distance of the well that is used for injection purpose to the production wells, the pressure of the surface water.

Production from the wells, BD-9, BD-11 and BD-12 were increased as injection to deep wells was increased. This will allow cold water to locate in the region between the well BD-8 and BD-9 and where no production occurs and so prevents the cold water totally flows to the west region where most of the production occurs.

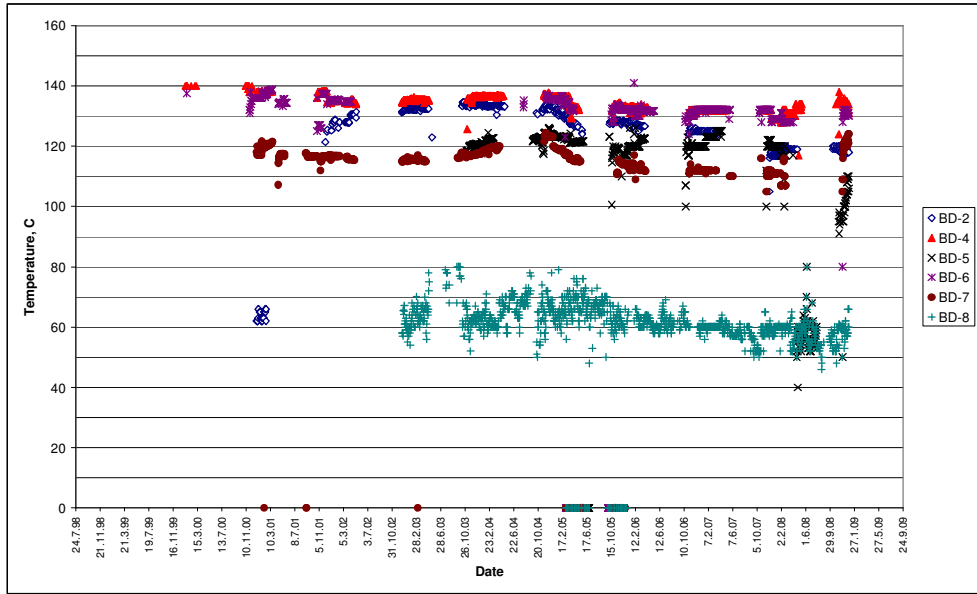


Figure 2.7- Temperature of deep wells (BD-2, BD-4, BD-5, BD-6, BD-7, BD-8) with respect to time.

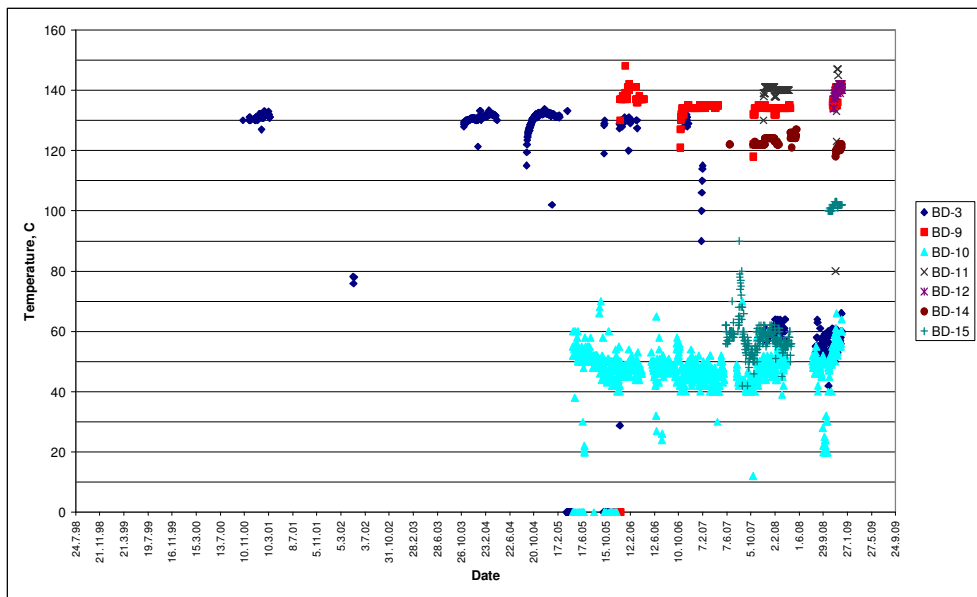


Figure 2.8- Temperature of deep wells (BD-3, BD-9, BD-10, BD-11, BD-12, BD-14, BD-15) with respect to time.

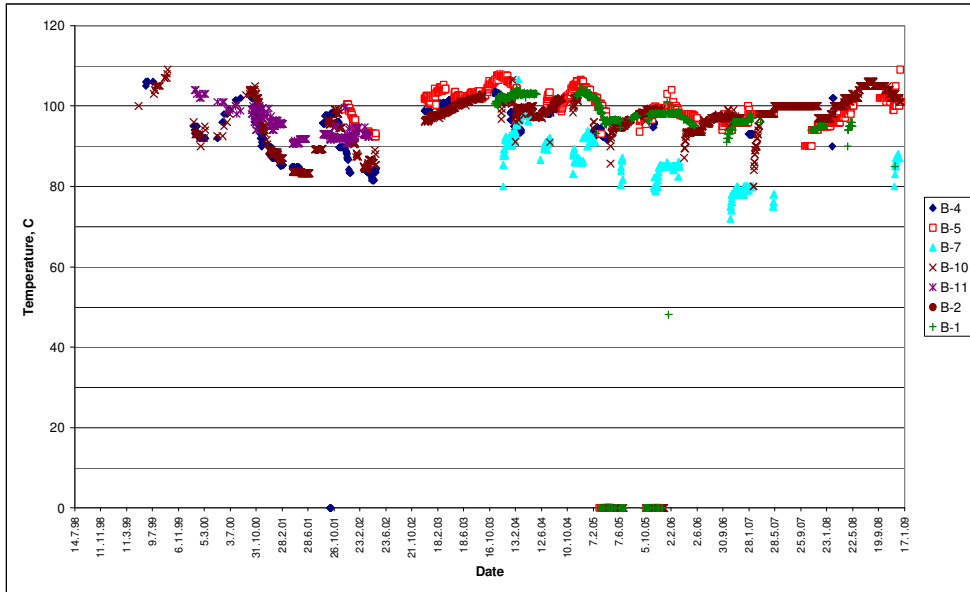


Figure 2.9- Temperature of shallow wells with respect to time.

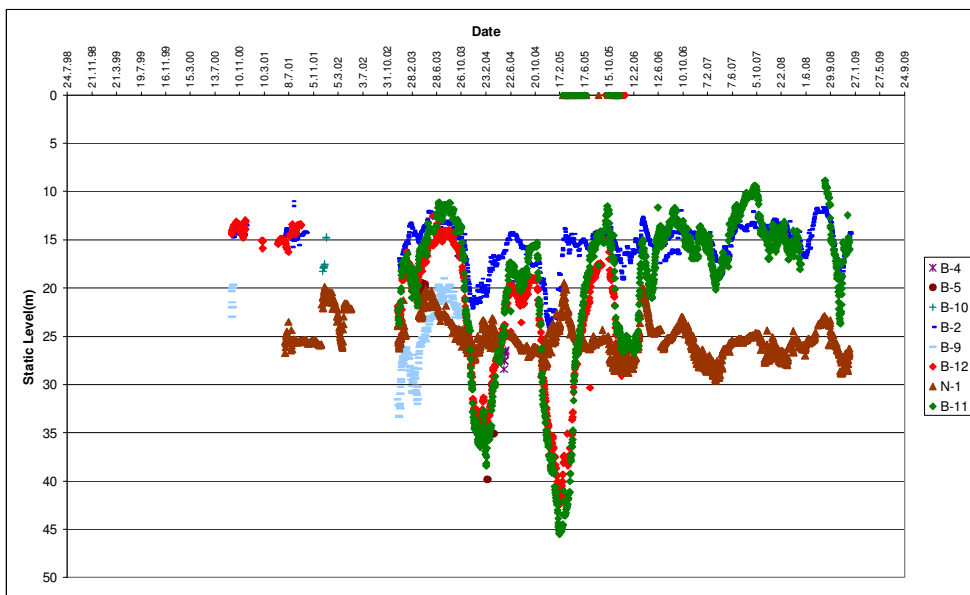


Figure 2.10- Static water level of shallow wells with respect to time.

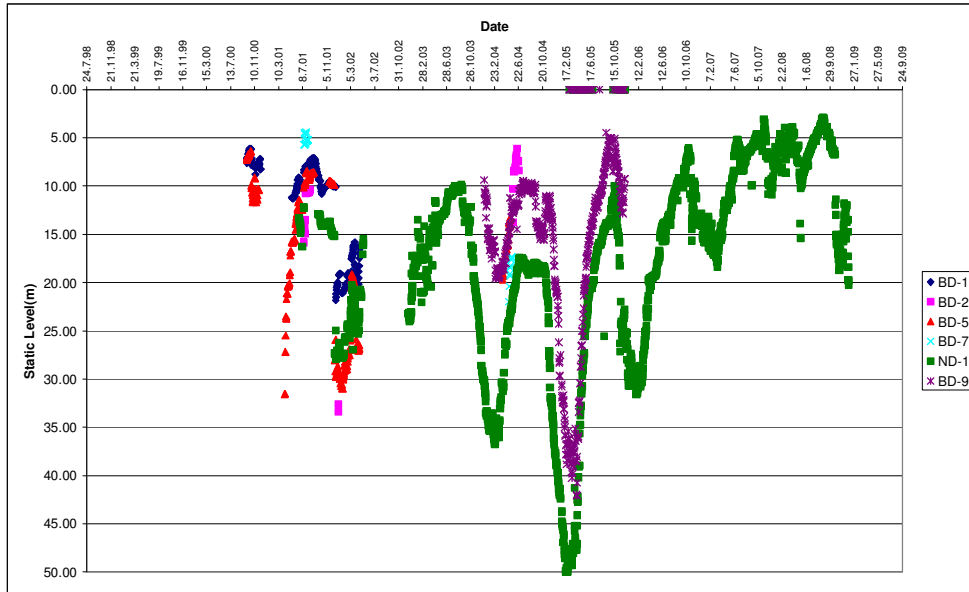


Figure 2.11- Static water level of deep wells with respect to time.

2.4. Hydrologic Balance

In the region south of AG-I fault, three important basins take place. In that region water flows through Alionbaşı, Ilıca and Hacıahmet streams (Figure 2.12). Ilıca basin having 35 km² area comprises most of the region. Balçova dam locating north of Seferihisar horst prevents water to flow through Ilıca stream. 8.5 *10⁶ m³ water flows to the dam and 5*10⁶ m³ water passes through Alionbaşı stream per year (İZSU, 1997). Hacıahmet basin comprises 6 km² area. How much water flows through Hacıahmet stream is not known. However, the flowrate of water in that stream is very small compared to Alionbaşı and Ilıca stream may be assumed as 2*10⁶ m³ per year considering the likeness with nearby basins. It can be assumed that totaly, 15.5*10⁶ m³ water flows through those streams per year (Aksoy, 2001).

According to the data recorded at the İzmir Güzelyalı meteorological station, situated a few km east of the Balçova field, the mean annual precipitation rate is 686 mm per year and average temperature in a year is 17.7 °C. These values are recorded near sea level but the elevations of recharge areas of Ilıca stream and other streams are higher than 900 m.

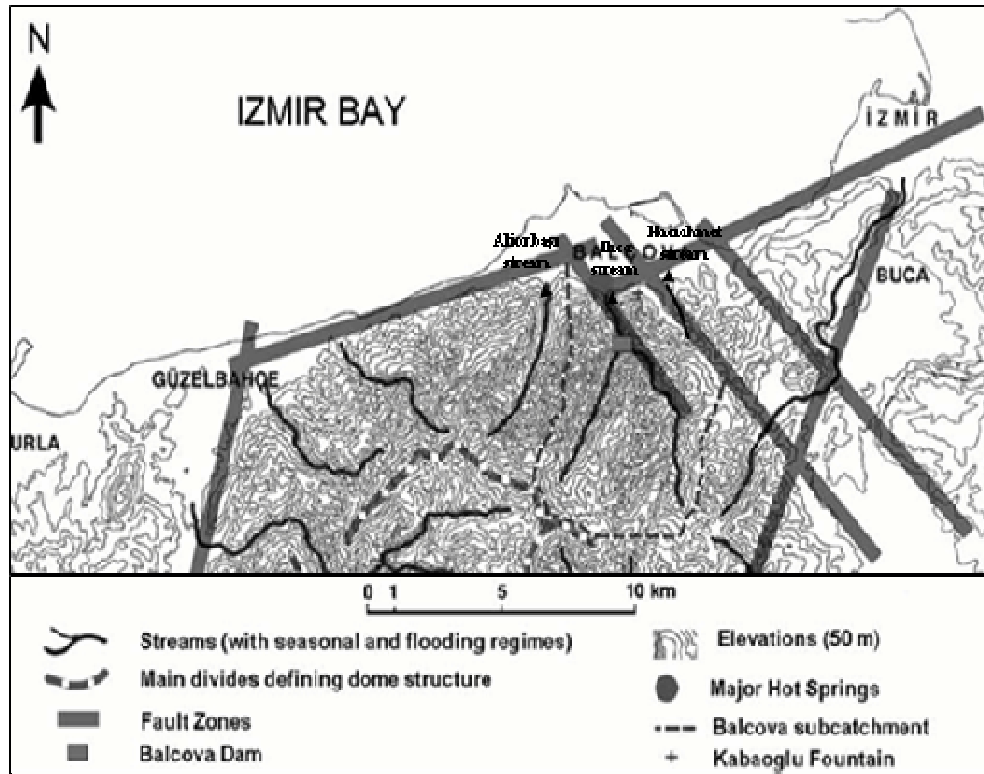


Figure 2.12- Streams and fault zones of the area around Balçova field (Serpen and Kayan, 2001).

The precipitation rates increase with altitude, probably as much as 40-50 mm/100m in Turkey (Erinc, 1969) and temperature decreases with altitude and the temperature gradient is 0.5 °C/100 m (Serpen and Kayan, 2001). Thus, these information must be considered while calculating evapotranspiration rate.

Assuming average 500 m altitude and that the precipitation gradient is 40 mm/100m and temperature gradient is 0.5°C/100 m, it is calculated that $10.6 \cdot 10^6$ m³/y (336 l/s) water infiltrates through underground at the 55 km² region. However, how much of this infiltrated water reaches the main feeding area around Agamemnon-1 fault is difficult to estimate.

If the precipitation gradient is taken as 50 mm/100m and temperature is taken as 15 °C, the rate of water infiltrating through underground at the 55 km² region is calculated as 446 l/s.

Not using the gradients, assuming P is equal to 686 mm/y and T is equal to 17.7 °C, the result shows that no water infiltrates through underground.

2.5. Chemical and Isotopic Characteristics of Balçova Waters

Geothermal waters generally have high amounts of dissolved chemical matter. Dissolution of elements is related to water and mineral balance. The amount of element is the characteristic feature of temperature and environment where it is found. The data from water chemistry can be used for determining temperature of geothermal system, feeding zone and the ratio of mixture with surface water. Measurements on water samples obtained from the field can give clue about some characteristics of the formation. Moreover, the information about non condensable gas and dissolved solid concentration can be gained by making such measurements. Thus, correct decision of which equation of state to be used in the model can be made.

Chemical analysis of water samples from Balçova wells as well as surface water samples are listed in Table 2.2 (Aksoy, 2001).

Geothermal waters generally have Na/K ratio higher than 10. If Na/K ratio is smaller than 15, it is an indication that ascending rate of the fluid is high. On the other hand, higher Na/K ratio indicates lateral flows and conductive cooling. In regard to this information, it can be stated that ascending rate of water in Balçova geothermal field is high as the ratio of Na with respect to K is around 11 in water taken from the field.

In geothermal waters, the amount of Mg generally changes between 0.01 and 0.1 ppm. Higher concentrations indicate the mixture of hot water with water close to surface. The concentration of Mg changes between 10-24 mg/l in waters taken from Balçova field, which indicates that hot water in the field mixes with cold water from the surface.

In geothermal systems, high amount of NH_4 is result of water heated by vapor close to surface. Water coming from deep sedimentary rocks also contains high amounts of NH_4 . The amount of NH_4 in Balçova waters is around 1 mg/l. From this information it may be stated that water is not heated by vapor close to surface nor comes from deep sedimentary rocks.

Table 2.2- Results of analysis of waters in Balçova region (Aksoy, 2001).

	Date	T	Na+	K+	Na/K	Mg2+	NH4+	Cl-	TDS(1)	TDS(2)
		C	mg/l	mg/l		mg/l	mg/l	mg/l	mg/l	mg/l
B-4	17.11.2000	96	371	31	11.97	13	1.15	206	1627	1210
B-4	06.04.2001	94	407	36	11.31	14		186	1694	
B-10	17.11.2000	99	379	32	11.84	14	0.85	190	1610	1370
B-10	06.04.2001	93	425	39	10.90	12		193	1777	
B-11	17.11.2000	100	367	30	12.23	24	1.01	208	1583	
B-11	06.04.2001	93	411	34	12.09	13		194	1730	
BTF-3	17.11.2000	103	364	31	11.74	21	0.66	198	1584	1190
BTF-3	06.04.2001	96	403	36	11.19	16		198	1679	
BD-3	17.11.2000	127	401	35	11.46	17	0.98	211	1696	1310
BD-3	10.02.2001	127	439	38	11.55	18	0.64	216	1723	
BD-3	06.04.2001	130	431	39	11.05	10		232	1719	
BD-4	17.11.2000	136	388	34	11.41	16	1.21	205	1676	1350
BD-4	10.02.2001	136	415	35	11.86	18	0.46	218	1700	
BD-4	06.04.2001	138	438	42	10.43	9		212	1778	
BD-6	17.11.2000	132	395	35	11.29	17	0.88	231	1677	1000
BD-6	10.02.2001	135	400	36	11.11	18	0.43	228	1686	
BD-6	06.04.2001	136	453	40	11.33	9		223	1807	
BD-7	25.12.2000	119	391	30	13.03	12	1.51	205	1616	1270
BD-7	10.02.2001	121	390	31	12.58	18	0.68	203	1683	
BD-7	06.01.2001	118	352	35	10.06	13		159	1576	
Emek	24.11.2000	60	242	23	10.52	44	0.01	166	1347	1070
Ilca	24.11.2000	73	361	31	11.65	26	0.75	190	1558	1110
İzmir Sport	24.11.2000	34	258	24	10.75	35	0.19	207	1242	1010
İşletme K.	25.12.2000	36	433	24	18.04	38	0.56	260	1883	1510
Dam Lake	02.12.2000	12	11	2	5.50	39	0.04	40	414	210
Kabaoğlu F.	17.11.2000	18	17	2	8.50	41	0.94	25	378	160
Deniz S	03.12.2000	15	11472	1040	11.03	2470	3.26	23000	41002	40080
BH-1	10.02.2001	80	380	31	12.26	21	0.47	280	1740	
Car Wash.	10.02.2001	40	345	30	11.50	27	0.01	184	1542	
BD_2 Renj	10.02.2001	62	395	29	13.62	21	0.45	209	1646	

High amounts of chloride indicate that geothermal water having high rates directly feeds the field. Chloride map is used for determination of high temperature regions and direction of surface water entering into the system. This direction is indicated by regions containing low concentration of chloride.

The increase in chloride concentration towards to east and also observed temperature increase towards to east indicates that hot water that feeds the field comes mainly from the eastern part of the field. Decrease in chloride towards the

west is a evidence of surface water intrusion to the field (Figure 2.13) (Aksoy et al., 2007).

In the ternary diagram of Cl, SO₄, HCO₃ it is seen that balçova waters are in the class of bicarbonate waters (Figure 2.14) (Serpen, 2003).

In the ternary diagram of Na, K, Mg, Balçova waters plot in the immature region (Figure 2.15) (Aksoy et al., 2007).

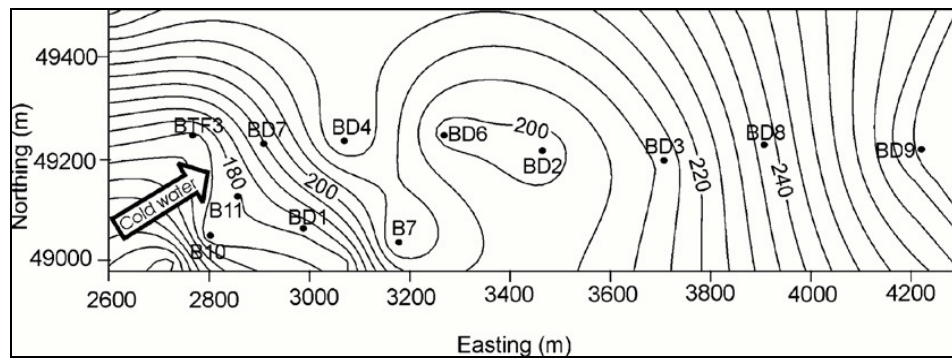


Figure 2.13- Chloride distribution (in mg/kg) in the Balçova geothermal field (Aksoy et al., 2007).

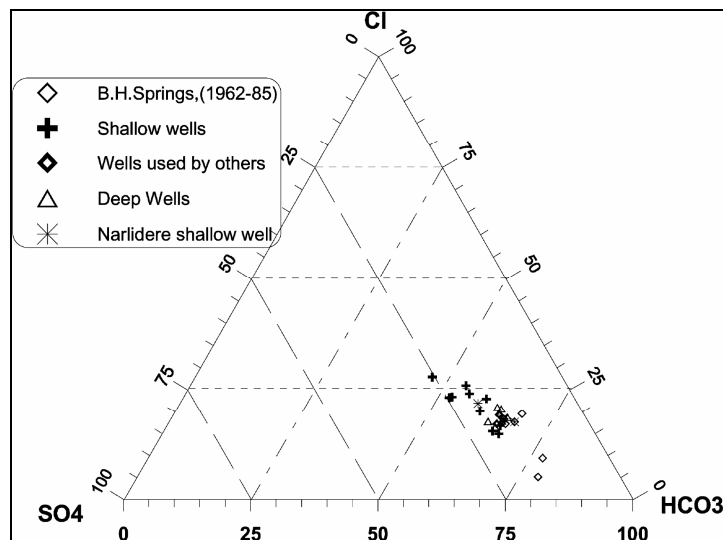


Figure 2.14- Ternary diagram of Cl, SO₄ and HCO₃ (Serpen, 2003).

Different geothermometers can be used to estimate the temperature of the reservoir rock in geothermal fields. They use the assumption that mineral concentration only depends on the relation between water and rock, the reaction is continuous, minerals exist in enough amounts and reaction between rock and water reaches equilibrium. Which geothermometer should be selected depends on many factors, such as the temperature of water, amount of CO₂, Mg, pH of the water, etc.

It was observed that Na-K geothermometer gave value 189±11 °C and Na-K-Ca geothermometer gave value 179±18 °C for the temperature of the reservoir rock (Aksoy, 2001).

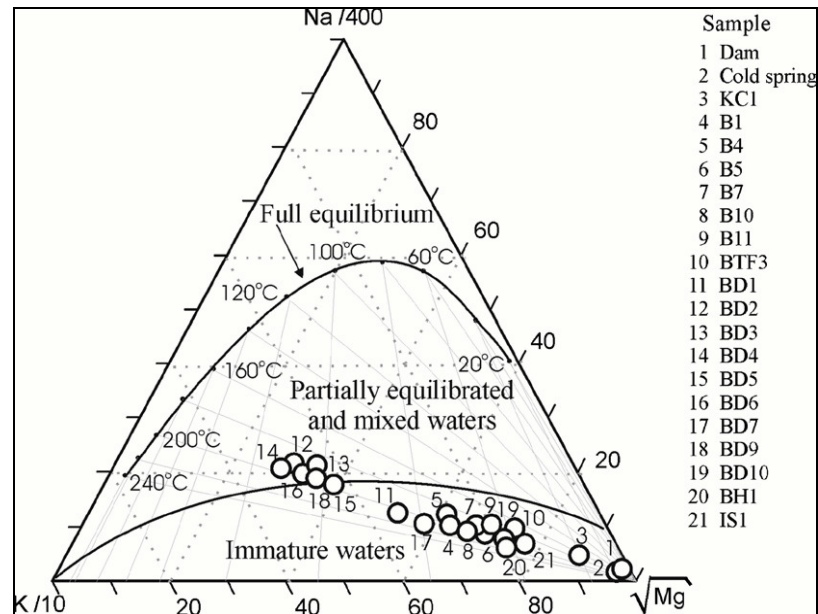


Figure 2.15- Ternary diagram of Na, K, Mg (Aksoy et al., 2007).

The altitude of the recharge area is calculated to be about 500 m on the basis of the δD values (Aksoy, 2001).

Cold water intrusion from the surface changes tritium amount in the field. Increase in tritium amount that happened in the field is another evidence of surface water intrusion to the field (Table 2.3).

Balçova geothermal waters can be classified as immature, bicarbonate waters. The amount of dissolved solids does not exceed 2000 ppm and the amount of non-condensable gas content is lower than 1000 ppm. All waters taken from the field have nearly neutral pH.

Table 2.3- Isotopic composition of balçova area waters (Aksoy, 2001).

Well	Date	O18(‰)	D(‰)	T(TU)
B-4	05.06.2000	-7.97	-47.44	2
B-10	05.06.2000	-8.08	-45.83	1.45
B-11	05.06.2000	-7.77	-43.9	1.25
BTF-3	05.06.2000	-8.1	-42.51	0.9
BTF-3	06.04.2001	-5.93	-39.98	2.3
BD-3	17.02.2000	-5.35	-37.1	0.68
BD-3	06.04.2001	-5.69	-42.22	1.1
BD-4	17.02.2000	-5.19	-37.6	0.13
BD-4	05.06.2000	-8.07	-46.55	1.05
BD-4	06.04.2001	-5.69	-39.54	4.2
BD-6	06.07.2000	-5.66	-41.9	1.8
BD-6	06.04.2001	-5.54	-38.25	2.05
BD-7	06.04.2001	-5.89	-38.61	1.3
Dam Lake	05.06.2000	-6.41	-39.79	4.7
Kabaoğlu F.	05.06.2000	-6.1	-35.8	6.9
Sea Water	06.07.2000	2.54	12.22	3.7

As Balçova waters have low dissolved solids and very low non condensable gas content (approx. 0.08% CO₂ by weight) equation of state-1 (EOS-1) which includes water with steam was selected to be used in the simulation and necessary adjustments were made to take into account of effect of surface water intrusion since it changes the temperature and pressure distributions as it enters to the field.

2.6. Conceptual Model

Conceptual model of Balçova Geothermal field will be discussed in this section.

The main production zone is the AG-I fault. Nearly all deep wells cross this fault or have a connection with this fault through faults and joints.

Meteoric waters penetrate deep into formation through faults, fractures, joints, and permeable zones if there exist. Then this water is heated by an undefined heat source and ascends to the upper parts due to buoyancy and pressure difference. This ascending water connects with AG-I fault from the east and deep portion of it and moves to the surface. After reaching the alluvium formation which has some permeability that can easily transmit flowing water it then flows to the north where alluvium formation connects to the sea. This hot water also flows into lower part of flysch formation having good permeability caused by faults, fractures and joints. Figure 2.16 shows the conceptual model of Balçova Geothermal field prepared by Aksoy et al., (2007).

According to the studies conducted on water samples, it can be stated that water penetrates to the AG-I fault mostly from deeper and eastern parts. That the temperature in the AG-I fault increases to the east and chloride distribution confirms the idea that the hot water penetrates to the AG-I fault from the eastern part of it. With the help of modeling studies conducted for the field, for natural state condition, the temperature of the penetrating hot water was assumed as about 160°C and the rate of it was assumed as about 50 kg/s. This results in 33 MWt energy entering the system.

Because of its higher permeability compared to other zones of the field, the main flow of water occurs in the AG-I fault. There are some faults considered to be located near AG-I fault but these faults are categorized as possible faults. Permeable zones created by small fractures and joints may exist instead of these faults.

Because of its low porosity keeping capacity of flysch formation is too low, so this support the phenomena that flowing hot water is fed from the faults, fractures and joints which causes rapid movement of water and so less cooling of hot water due to their high permeability.

Alluvium has a narrow structure in the place where it connects with AG-I fault and become wider to the northern parts. Narrow structure causes high pressures at the connection point and the rest of the AG-I fault.

Types of the heat source, location of it, conductivity of it are all unknown. However, temperature of the reservoir rock (around 190°C) could be estimated by analyzing the water samples taken from the field.

It can be assumed that heating of the field by means of conduction has negligible effect compared to convective heating if the heat source locates deep enough and far away. That conductive heating has negligible effect compared to convective heating in Balçova field was confirmed with modeling studies.

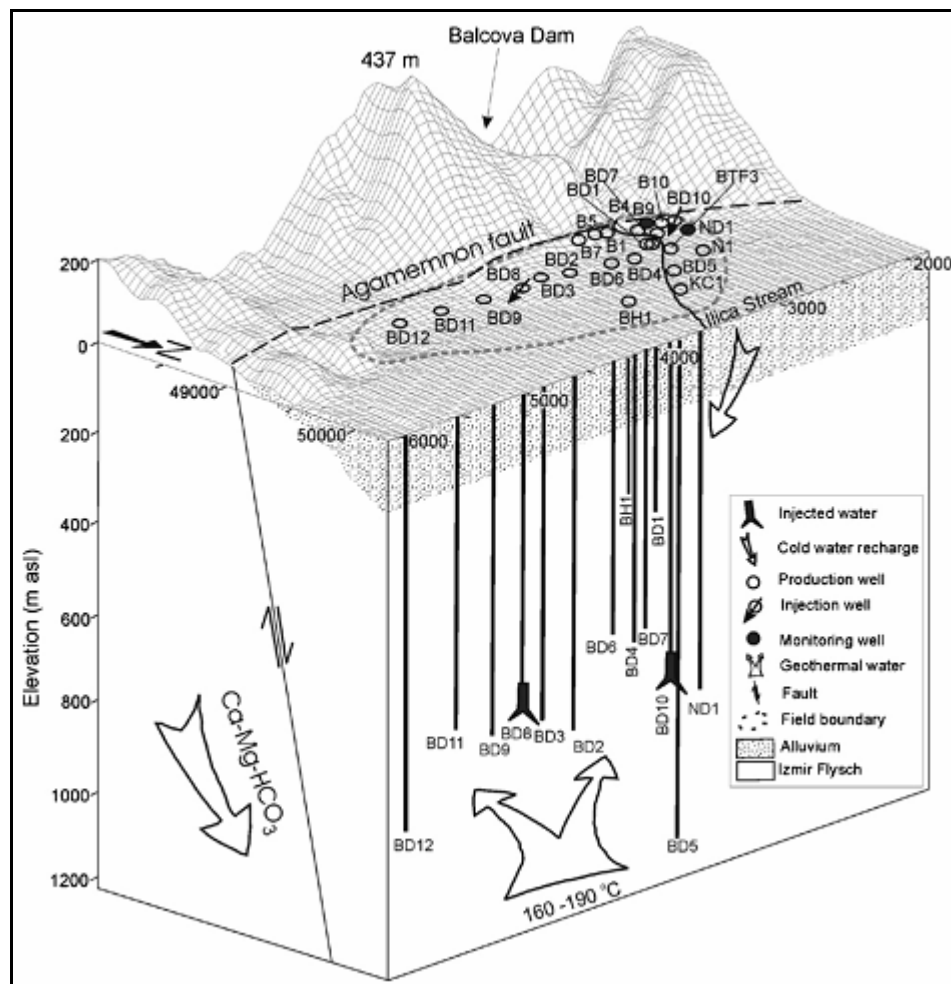


Figure 2.16- Conceptual model of the Balçova geothermal field (Aksoy et al., 2007).

The thickness of the permeable zone in the upper part of the field is about 40 m and in some place it decreases to about 10 m or no more exists which is confirmed by temperature distributions in the field.

That 140°C temperature value at 700 m decreases to 120°C close to surface can be contributed to cooling effect of the atmosphere and the rocks locating out of the heating zone. As going deeper cooling resulting from atmosphere has negligible effects.

Cold water intrusion also happens in the field and it penetrates into the field mainly from the southwestern part of the AG-I fault.

CHAPTER 3

RESERVOIR SIMULATION AND FLOW IN FRACTURED MEDIA

3.1. Reservoir Simulation

“The area reservoir simulation applies the concepts and techniques of mathematical modeling to the analysis of the behavior of reservoir systems. In a narrower sense the term reservoir simulation refers only to the hydrodynamics of flow within the reservoir, but in a larger sense it can and more often does refer to the total system which includes the reservoir, the surface facilities, and any interrelated significant activity. The basic flow model consists of the partial differential equations which govern the unsteady-state flow of all fluid phases in the reservoir medium. Incorporated into the model are all the algorithms needed to solve these equations. The simulator is then a collection of computer programs which implement the mathematical model on a particular digital machine.

3.1.1. The Need for Reservoir Simulation

The need for reservoir simulation stems from the requirement for petroleum engineers to obtain accurate performance predictions for a reservoir under different operating conditions. This need arises from the fact that in a recovery-project which may involve a capital investment of hundreds of millions of dollars, the risk associated with the selected plan must be assessed and minimized. Factors contributing to this risk include complexity of the reservoir because of heterogeneous and anisotropic rock properties; regional variations of fluid properties and relative permeability characteristics; the complexity of the recovery mechanisms; and the applicability of other predictive methods with limitations that may make them inappropriate. The first three factors are beyond the engineer's control; they are taken into consideration in reservoir simulation through the generality of input data built into reservoir-simulation models and the availability of simulators for various recovery techniques. The fourth factor can be controlled through proper use of sound engineering practices and judicious use of reservoir simulation.

3.1.2. The Modeling Approach

Models are basically of two types; in a very pedestrian way they are simply the ones you can touch and the ones you cannot. The former are physical models, the latter mathematical models.

1. Physical models are essentially scaled-down reproductions of the original, as evidenced in pilot plants, prototypes, and like, or models constructed to duplicate a process which is physically similar to the original although it may operate under a different set of physical laws. The best example of this is the potentiometric model used to predict reservoir flow by capitalizing on the one-to-one correspondence between flow in porous media and the flow of ions in an electric potential field.
2. Mathematical models are systems of mathematical equations describing the physical behaviour of the process under investigation. In a reservoir work, these equations are generally very complicated partial differential equations, but they could be rather easy equations system in other fields. Because of the size and the complexity of these mathematical models, a computer is required to solve the system.

Simulator's formulation and development require substantial background in mathematics and the applied sciences. The use of it, however, requires only good engineering skills and common sense. There is a feedback loop in mathematical modeling. The simulator operates in a computer environment, and everything else operates in an engineering setting. The process begins with the input provided by the engineer; this is processed by the simulator and the output is obtained. At this point the information is analyzed for the effects of previous changes on the operating characteristics, and if modifications are needed, they are made and the process repeated. As the engineer cycles through this loop, his/her input, by virtue of his expertise, continuously upgrades the results, and as more and better information becomes available as time passes, he/she can produce an efficient and reasonably accurate predictive tool for his/her process.

3.1.3. Numerical Models

Numerical models utilize digital machines to solve the mathematical equations which govern the behavior of the fluids in porous media. They provide a generalized

approach using a gridded format which can accommodate any reservoir description just by a reordering of the indices of the grids. The numerical models originated in the middle 1950s have evolved extremely rapidly to the point where almost every conceivable reservoir behavior pattern can be simulated. The procedure involved consists of discretizing the reservoir into blocks and performing mass and energy balances on all these blocks simultaneously. This gridding of cells allows a more realistic representation of rock and fluid properties which can vary in any manner.

3.1.4. Reservoir-Simulation Application

Reservoir simulation is generally performed in several steps.

1. Set the study objectives: The first step of any successful simulation study is to set clear, achievable objectives. These objectives must be compatible with available data and production history. Objectives are used to set goals, define basic strategy, identify available resources, and determine what is to be learned from the study.
2. Acquire and validate all reservoir data: Once the study objectives have been defined, reservoir and production data are gathered. Only the data required to meet the objectives of the study should be incorporated into the simulation model. Incorporating additional detail that does not add to understanding the objectives leads to overkill.

The data itself are usually in a form not directly applicable to a computer solution, and some preprocessing must be undertaken to produce the data in usable form. There are usually several sources of the same data information, and the engineer must exercise his judgment in differentiating and selecting the best data available. Sometimes there are no data available for a particular case; in a situation like this the engineer must determine some alternate means of obtaining the same information.

The groups of data generally required in making a simulation run are as follows:

Fluid data

Rock data

Production data

Flow rate data

Mechanical and operational data

Economic data

Miscellaneous data

3. Construct the reservoir model: After the data have been gathered and validated, the simulation model is built. In this step the reservoir is divided into grid blocks. Formation properties, such as porosity, directional permeabilities, and net-pay thickness, are assigned to these grid cells. The different grid cells can have different reservoir properties; however, reservoir properties are assumed to be homogeneous within a grid cell. Because different cells can have different properties, areal and vertical trends in data can be incorporated into the model. At this stage of the study, all data must be properly scaled for the simulation grid.
4. History match the reservoir model: Once the simulation model has been built it must be tuned, or history matched, with available production data because much of the data in a typical simulation model is not known for certain but is the result of engineers and geologists interpretations. Although these interpretations are generally the best representation of available data, they are still subjective and may require modifications.
5. Run prediction cases: The final step in the simulation process is the prediction phase, in which various production schemes are evaluated and sensitivity analyses of various production and reservoir parameters are performed.

The main objective of any simulation study is to gain knowledge of the subject reservoir. In most simulation studies, most of the knowledge is gained during the data-gathering, history matching, and prediction phases. During the data-gathering and history-matching phases, all relevant reservoir data are collected, validated, and synthesized into coherent field model. This process will inevitably yield information about the reservoir that was unknown before the study. During the prediction phase, questions concerning the subject reservoir can be addressed and most of the study objectives are met.

3.1.5. Benefits of Simulation

The engineer knows he/she has a single opportunity to produce the reservoir; any mistakes made in the process will be around forever. However, the simulation study can be made several times and the alternatives examined. When the simulation study is used as a management tool, the efficient utilization of available energy within the reservoir can lead to greater ultimate production and certainly a more economical operation. In the more complex systems- for example, layered heterogeneous reservoirs with commingled production- it has been previously impossible to handle all these variables; today the engineer can examine such systems without undue difficulty to predict their behavior. One benefit of simulation which in reality was not designed into the process at the start but has evolved as a fruitful by-product is the presence now of a common ground between companies and regulatory bodies and other agencies which deal with petroleum resources. This commonality is the knowledge that all these groups are now using simulators to determine reservoir performance, and the differences between two opposing groups can be narrowed down to the data used rather than to the calculation procedure itself. The calculation procedure do not differ by very much, and if need be a standardized approach can be used in which the data can be run by a third-party system for comparison purposes. Finally, it can be said in a rather laconic way that even if the results of the simulator study were inconclusive, the mechanics of simulation have compiled all the data pertinent to that reservoir into one compact data base which is probably now in better shape than it ever was before” (Henry, 1977).

3.2. Flow in Fractured Media

Most geothermal reservoirs consist of fractured rocks. Global fluid flow occurs primarily through a network of highly permeable interconnected fractures. Rocks having low permeability provide conductive heat supply, and may conduct some liquid. Interpretation of well tests in fractured reservoirs, analysis of heat sweep during cold water injection (heat transfer from matrix rocks to fluids flowing in the fractures), and design and analysis of tracer tests are typical tasks for reservoir engineers that deal with fractured reservoirs. Physical characteristics of the reservoir (parameters such as fracture spacing and connectivity, permeability of the matrix rocks), flow process to be modeled (fluid production, injection, tracer migration), available data and objectives of the study effects the selection of the process to be used.

“Effective continuum method” or ECM in which the reservoir is modeled as a single porous medium and the aim is to determine reservoir parameters that represent the properties of the fractured porous medium is the simplest approach used in modeling studies.

Explicit modeling of fractures is another method that can be used in modeling of fractured reservoir. In this approach, fractures are represented by defining a region of large areal extent but small width. This process is not applicable to situations where fractures are too numerous. However, if a major fracture or fault zone is to be dealt, an explicit modeling may be a suitable process.

The most widely used approach is the double porosity concept which was first proposed by Barenblatt et al. (1960) and popularized by Warren and Root (1963). In this approach global flow occurs through interconnected fractured. Rock matrix and fractures can exchange fluid. This is known as interporosity flow. Interporosity flow depends on the pressure differences between matrix and fractures and can be approximated as being quasisteady in some situations.

The quasi-steady approximation is applicable to systems that includes isothermal single-phase flow, fluids that have small compressibility and large pressure diffusivities resulting in a phenomena in which pressure changes in fractures penetrate quickly deep into the matrix blocks. This approximation is not applicable for multiphase flows, or coupled fluid and heat flows since the transient periods for interporosity flow can be very long. The necessity of resolving the driving pressure, temperature, and mass fraction gradients at the matrix/fracture interface is evident for these situations. To achieve the resolution of these gradients, method of “multiple interacting continua” (MINC) is used. In MINC method, it is assumed that changes in fluid pressures, temperatures, phase compositions, etc. propagate rapidly through the fracture system but slowly in the matrix system. With this assumption, it can be stated that changes in parameters relating to matrix are controlled by the distance from the fractures (Pruess, 2002).

CHAPTER 4

TOUGH2

4.1. General Concepts in TOUGH2

“TOUGH2 is a numerical simulation program designed for multi-dimensional fluid and heat flows of multiphase, multicomponent fluid mixtures in porous and fractured media. It is used in different areas, such as geothermal reservoir engineering, nuclear waste isolation studies, environmental assessment and remediation, flow and transport in variably saturated media and aquifers.

TOUGH2 utilizes different equation of states (EOS). These are EOS1 (water, water with tracer), EOS2 (water, CO₂), EOS3 (water, air), EOS4 (water, air, with vapor pressure lowering capability), EOS5 (water, hydrogen), EOS7 (water, brine, air), EOS7R (water, brine, radionuclide 1, radionuclide 2, air), EOS8 (water, air, oil), EOS9 (saturated-unsaturated flow), EWASG (water, NaCl, non-condensable gas).

TOUGH2 solves mass and energy balance equations. Fluid advection is represented by Darcy’s law. Moreover, TOUGH2 utilizes equations for diffusive mass transport. TOUGH2 uses necessary equations to define real cases where heat flow occurs by both conduction and convection (Appendix C). It uses the assumption that there exists thermodynamic equilibrium in all grid blocks at all times.

“Integral finite difference” method (IFPM) is used for space and time discretization. Time is discretized fully implicitly (Appendix C). With the integral finite difference method, TOUGH2 has the advantage of being applicable to regular and irregular discretization. Moreover, double and multiple-porosity methods can be used for fractured media.

Space and time discretization results in strongly coupled nonlinear algebraic equations. Newton-Raphson iteration is used for solving these equations. Matrix including primary thermodynamic variables to be calculated, secondary variables functions of primary thermodynamic variables are formed at each iteration. The

matrix is solved using one of the linear equation solvers: direct solver, bi-conjugate gradient solver, Lanczos-type bi-conjugate gradient solver, generalized minimum residual solver, stabilized bi-conjugate gradient solver. Automatic time step adjustment in which the aim is to use the highest time step size without exceeding certain number of iterations is a recommended option to be used in the program” (Pruess et al., 1999).

4.2. Equation of State Modules

Different equation of states (EOS) can be used in TOUGH2.

“EOS1 is used for pure water in its liquid, vapor, and two phase states. Water properties such as, density, specific enthalpy, viscosity, saturated vapor pressure are calculated using steam table equations prepared by International Formulation Committee. Utilizing these equations, density and internal energy can be calculated within experimental accuracy and viscosity and steam are represented to within 2.5 % by correlations given in the same reference. Neglecting the effects of capillary and adsorption on vapor pressure lowering, vapor pressure of water is made to be equal to saturated vapor pressure when two-phase conditions exist.

Two waters including different trace constituents but having identical physical properties can be represented with EOS1. For situations in which two waters exist all thermophysical properties are assumed to be independent of component mixture. It is also assumed that concentrations of trace constituents are low enough so that they do not appreciably affect the thermophysical properties.

Pressure and temperature are used as primary variables for single phase conditions. For two phase conditions either gas pressure-gas saturation or temperature-gas saturation are used as primary variables. If two waters containing different trace constituents and having identical physical properties are to be used, X which is mass fraction of water 2 is used as the third primary variable.

EOS2 that includes water and CO₂, accounts for non-ideal behavior of gaseous CO₂, and dissolution of CO₂ in the aqueous phase with heat solution effects. The partial pressure of non-condensable gas is a function of mole fraction of the dissolved non-condensable gas in the aqueous phase and Henry’s law coefficient which is strongly dependent on temperature. Primary variables are pressure,

temperature, CO₂ partial pressure for single-phase condition, and gas phase pressure, gas saturation, CO₂ partial pressure for two phase condition.

EOS3 is capable of handling of water and air. It is assumed that air behaves as an ideal gas. Partial pressures of air and vapor are added to obtain gas phase pressure. Since change in Henry's constant with respect to temperature is very small, it is kept constant. Primary variables are pressure, air mass fraction and temperature for single phase condition gas phase pressure, gas saturation plus 10 and temperature. 10 is added to gas saturation to make a distinction between single and two-phase conditions.

EOS4 is capable of handling with water, air and includes vapor pressure lowering capability. Vapor pressure is not only function of temperature but also capillary pressure which is a function of saturation. Primary variables are pressure, temperature, air partial pressure for single-phase condition and gas phase pressure, gas saturation and air partial pressure for two-phase condition.

In EOS5 water and hydrogen is used. Density of the gaseous hydrogen is computed from the ideal gas law. A table is used to obtain interpolated data for viscosity and water solubility of hydrogen. The primary variables are same as they are in EOS3.

In EOS7 water, brine and air is used. Being different from EOS3, EOS7 represents the aqueous phase as a mixture of pure water and brine. It is important for salinity not to reach saturated levels as non-physical results may be obtained. It is assumed that fluid volume is conserved when water and brine are mixed and compressibility and expansivity of water is equal to that of brine. That salinity effects the air solubility is taken into account in EOS7. Primary variables are pressure, brine mass fraction, air mass fraction and temperature for single-phase condition gas phase pressure, brine mass fraction, gas saturation plus ten, temperature for two phase conditions. 10 is added to gas saturation to make a distinction between single and two-phase conditions.

In EOS8, water, air and oil is used. Oil is referred as dead oil, meaning non-aqueous phase liquid that has no volatile or soluble components. The oil phase has intermediate wettability. Capillary pressure of oil phase is neglected. Low order polynomials functions of pressure and temperature are used to calculate viscosity, density, and specific enthalpy of the oil phase. Pressure, air mass fraction, oil phase saturation and temperature are used as primary variables for two phase

conditions in which gas-oil or aqueous-oil take place. Gas phase pressure, gas saturation plus 10, oil phase saturation and temperature are used as primary variables for three-phase conditions.

In EWASG water, NaCl, non-condensable gas (NCG) components are used. Being immobile, relative permeability of the NaCl is taken as zero. Precipitation of salt in the pore space results in reduction in pore volume available for fluid phases and so reduction in the permeability of the medium. The coefficients used in Henry's law depend not only on temperature but also on salinity. That density, enthalpy, viscosity, and vapor pressure of water depends on salinity is considered in EWASG. The primary variables are pressure, salt mass fraction or solid saturation plus 10, NCG mass fraction, temperature for single fluid phase and pressure, salt mass fraction or solid saturation plus 10, gas phase saturation plus 10, temperature are for two fluid phases. 10 is added to solid saturation to determine whether or not a precipitated phase is present from the numerical range of the second primary variable.

In EOS7R water, brine, radionuclide 1, radionuclide 2 and air are included. Radionuclides which can undergo decay with user-specified half life are considered water soluble and volatile, but are not allowed to form a separate non-aqueous fluid phase. Stable components can also be used instead of radionuclides setting half life of them to very large values. Henry's law is used to partition radionuclides between aqueous and gaseous phases. Radionuclide concentrations do not affect the thermophysical properties of the aqueous phase. Pressure, brine mass fraction, mass fraction of Rn1, mass fraction of Rn2, air mass fraction, temperature are used for single-phase conditions and gas phase pressure, brine mass fraction, mass fraction of Rn1, mass fraction of Rn2, gas saturation plus ten, temperature are used for two-phase conditions" (Pruess et al., 1999).

4.3. Petrasim

"Petrasim is a graphical interface for the TOUGH2 family of simulators that have been applied multi-phase, multi-component problems in one, two and three-dimensional porous and fractured media. Petrasim interface helps guide the user through the steps of an analysis (Appendix D). These include:

- Selecting an EOS.
- Defining the problem boundaries and creating a mesh.
- Selecting the global options to be used in the analysis.
- Specifying the material properties.
- Defining the default initial conditions for the model, either directly or by loading the results of a previous analysis.
- Using the grid editor to define cell-specific data, such as material, sources, sinks, and initial conditions.
- Setting the solution and output option.
- Solving the problem.
- Post-processing of results using contour and time history plots” (Thunderhead Engineering, 2009).

CHAPTER 5

STATEMENT OF THE PROBLEM

There is a continuous increase in demand to space heating applications in Balçova geothermal field. As a result, both produced and injected volumes of geothermal water for heating have been increasing. Higher production/injection practices in any geothermal field should be studied carefully not to harm the reservoir characteristics of the field, such as decline in reservoir pressure due to high production but not sufficient injection, or decline in temperature due to excess injection and early breakthrough.

Balçova District Heating system was started in 1996 and continuously expanded as a result of increasing demand. Yet, there exists capacity of the field for further expansion the response of the field to the expected increase in volumes of produced and injected geothermal water should be studied carefully for the possible effects of the additional volumes. The most common practice to study such problems is the modeling studies through reservoir simulation applications.

This study is aimed to construct a reservoir simulation model for Balçova geothermal reservoir by utilizing TOUGH2, a numerical simulation program designed for multi-dimensional fluid and heat flows of multiphase, multi component fluid mixtures in porous and fractured media. Natural state modeling, history matching of the production/injection practices and different scenarios for performance predictions of the Balçova geothermal field will be achieved.

CHAPTER 6

RESULTS AND DISCUSSION

6.1. Methodology

Any reservoir simulation study includes several steps allowing various aspects of model components to be modified as required to match the measured and calculated data. The conceptual model forms the basis of model components, such as permeability distribution, sources of fluid and heat, boundary conditions. In that respect the required data is gathered and validated.

The steps that any reservoir simulation study includes are:

1. Development of grid model. Material properties such as permeability, porosity, heat conductivity any injection or production values are assigned to each grid block.
2. Natural State Modeling in which the aim is to determine the initial temperature and pressure distributions is performed. The model data is matched with measured data and necessary adjustments on material properties, enthalpy of water were made to increase the quality of the match.
3. Using the results obtained from natural state modeling, history matching in which the aim is to match the model pressure and temperature with measured values for production and injection period is performed.
4. The final step is to predict the future performance of the field under different injection and production scenarios.

TOUGH2 which is a numerical simulation program designed for multi-dimensional fluid and heat flows of multiphase, multi component fluid mixtures in porous and fractured media was used for modeling the Balçova geothermal field.

As Balçova waters have low dissolved solids (1000 ppm to 1800 ppm) and very low non condensable gas content (approximately 0.08% CO₂ by weight) equation of state-1 (EOS-1) which includes water with steam was selected to be used in the program.

In the model, it is assumed that İzmir flysch in which Agamemnon-I fault locates is impermeable. The system is considered to be heated by the hot water that ascends in Agamemnon-I fault. Hot water whose enthalpy is 6.6E5 J/kg (corresponding to water temperature close to 160 °C) enters the reservoir from east and ascends in Agamemnon-I fault and also flows laterally to western part of the field. The flow also happens in the permeable zone that is close to surface and thought to be related to Alluvium formation. The hot water in this layer flows towards north. Cold water intrusion from surface is also taken into effect with fixed state option. Thus, more cold water introduces into the system as pressure decreases due to the production.

6.2. Model Creation

In the grid model, there are 39168 blocks in total. The number of blocks in x direction is 34, in y direction is 32 and in z direction is 36. The surface covers an area of 4.89 km². The dimensions of the system are 3029 m×1614 m×2550 m in x, y and z directions, respectively. Thus total volume is around 12.5 km³. From surface to the depth of 100 m, thickness of the blocks is 10 m. With those small thicknesses, it is possible to separate different formations, permeable zones and impermeable zones at nearly exact depths and thus the throws of faults can be represented in the model. The thickness of the deeper blocks are larger compared to blocks in shallow sections. The area of the blocks in the region where most of the production is done is smaller than the area of the blocks that are far from the current production region. This application makes it possible to place each well into a single block that is small enough.

The Agamemnon-I (AG-I) fault is represented by thin sections, which results in an increase in the number of grid blocks. Although, increase in the number of blocks may result with difficulties in the simulation process, using larger volumes to

represent the faults is not recommended if permeability difference between the matrix and the fault is large.

Table 6.1 lists different materials used in simulation model. In the simulation model AG-I fault having a 2000 md is represented by thin columns having 5 m wide and described as material FAULT. The material ROCK2 having 100 md permeability was assigned to cells near the AG-I fault. The extension of ROCK2 in x-y coordinate or y-z coordinate was determined by matching calculated temperature values obtained after the model was run with the measured temperature values. AG-I fault connects with alluvium formation close to the surface. In the model, Alluvium formation is also represented with the material ROCK2. To match the calculated temperature values with measured temperature values in wells BD-5 and ND-1, the permeability of the west of the AG-I fault should have been made higher than the rest of the fault. As a result, the permeability of the western section of the fault was estimated about 6000 md (material FAU2). The material ROCK3 having a permeability of 300 md was assigned to cells north of the western section of the AG-I fault. The cells to which the material ROCK3 are assigned may correspond to region occupied with the fault D-IV. The material ROCK1 was assigned for the rest of the model.

The air on the surface is generally represented with the material AIR having zero porosity, zero permeability but 0.3 W/m-°C wet heat conductivity, 1000 J/kg-°C specific heat and density 1.205 kg/m³. These wet heat conductivity, specific heat and density values are used for air at 20 °C.

Assigned values for density, wet heat conductivity and specific heat are the same for all materials except AIR and AIR2. These are averaged values used for rocks and are also default values used in TOUGH2. Here, the value of density and specific heat are close to values used in resource assessment of Balçova Geothermal Field (Arkan and Parlaktuna, 2005). On the other hand, porosity and permeability are estimated by using the measurements obtained from literature. Porosity and permeability estimation studies are presented in Appendix A and Appendix B, respectively.

Created grid model dimensions are shown in Figure 6.1 and distributions of each material in different cross-sections are presented in Figures 6.2 - 6.7. The coloring of material in grid model is given in Table 6.2.

Table 6.1- Properties of the materials used in the program.

Name:	ROCK1	ROCK2	ROCK3	AIR
Density-(kg/m³):	2600	2600	2600	1.205
Porosity:	0.03	0.1	0.1	0
X Permeability (m²):	0	1.00E-13	3.00E-13	0
Y Permeability (m²):	0	1.00E-13	3.00E-13	0
Z Permeability (m²):	0	1.00E-13	3.00E-13	0
Wet Heat Conductivity- (W/m-C):	2	2	2	0.3
Specific Heat - (J/kg - C):	1000	1000	1000	1000
Name:	FAULT	FAU2	AIR2	
Density-(kg/m³):	2600	2600	1.205	
Porosity:	0.1	0.1	0	
X Permeability (m²):	2.00E-12	6.00E-12	0	
Y Permeability (m²):	2.00E-12	6.00E-12	0	
Z Permeability (m²):	2.00E-12	6.00E-12	0	
Wet Heat Conductivity- (W/m-C):	2	2	0.1	
Specific Heat - (J/kg - C):	1000	1000	1000	

Table 6.2- Coloring of materials used in grid model.

MATERIAL	COLOR
ROCK1	Blue
ROCK2	Light blue
ROCK3	Lime
FAULT	Aqua
FAU2	Light green
AIR	Bright green
AIR2	Brown

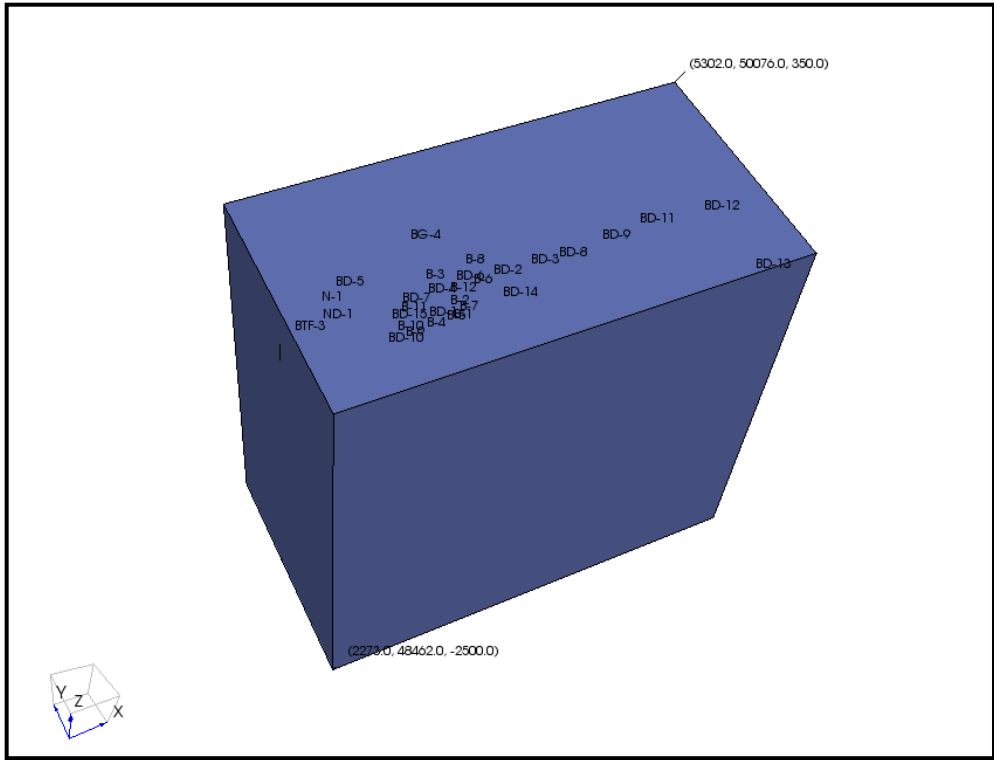


Figure 6.1- Dimensions of grid model of Balçova geothermal field.

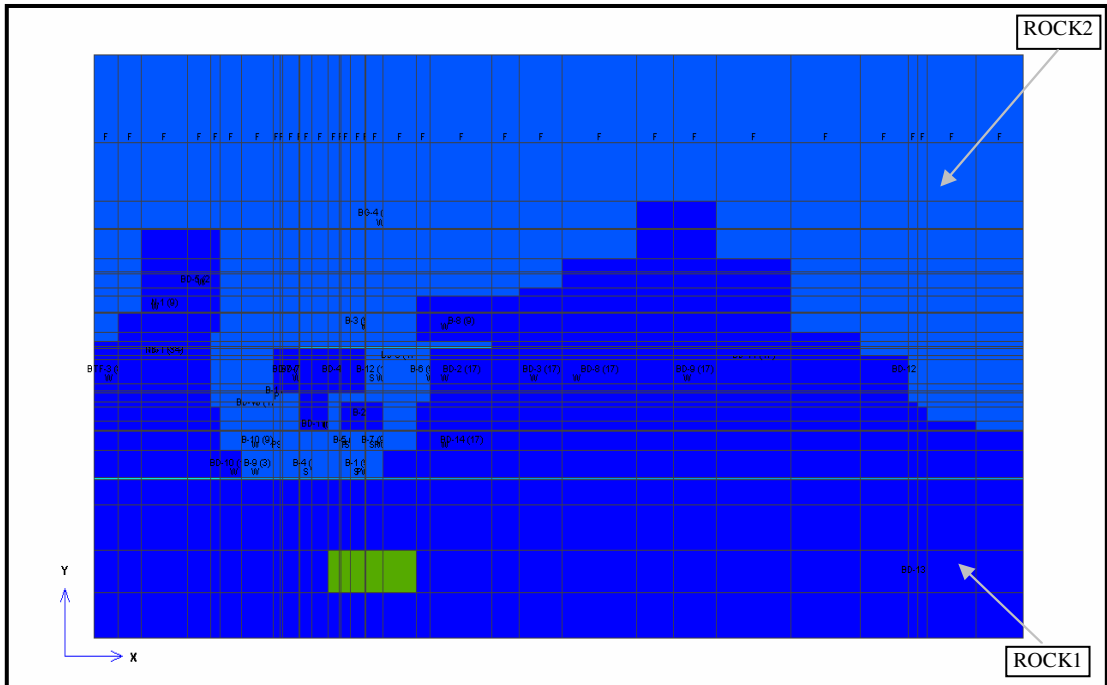


Figure 6.2- Material distribution for the cross-section Z=-15.

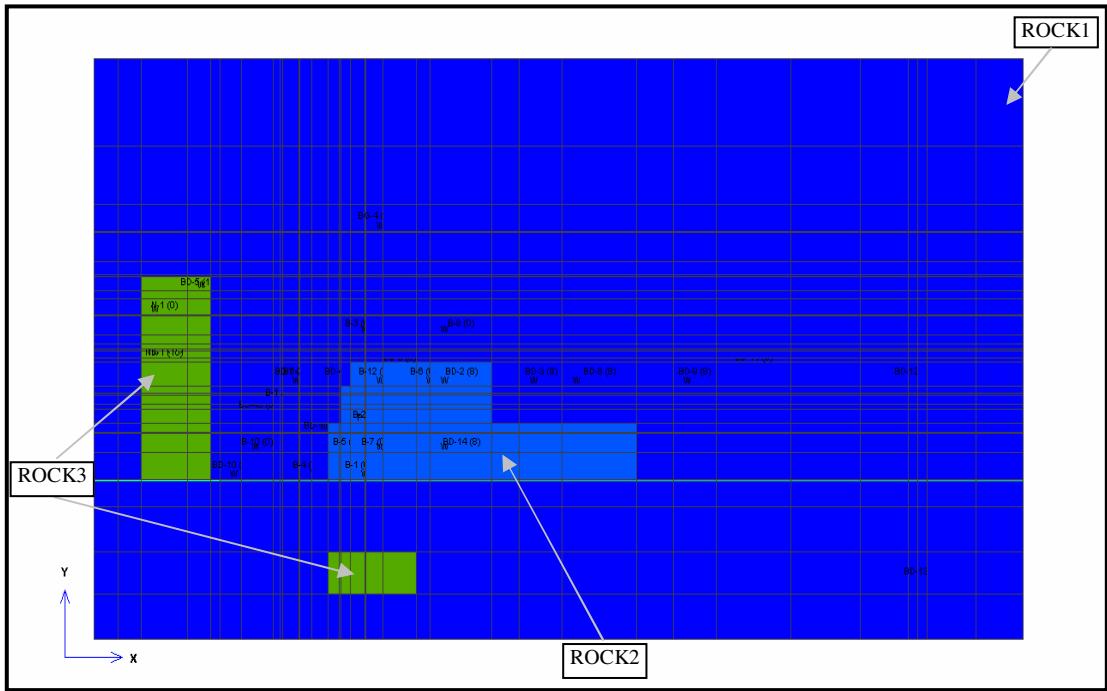


Figure 6.3- Material distribution for the cross-section Z=-150.

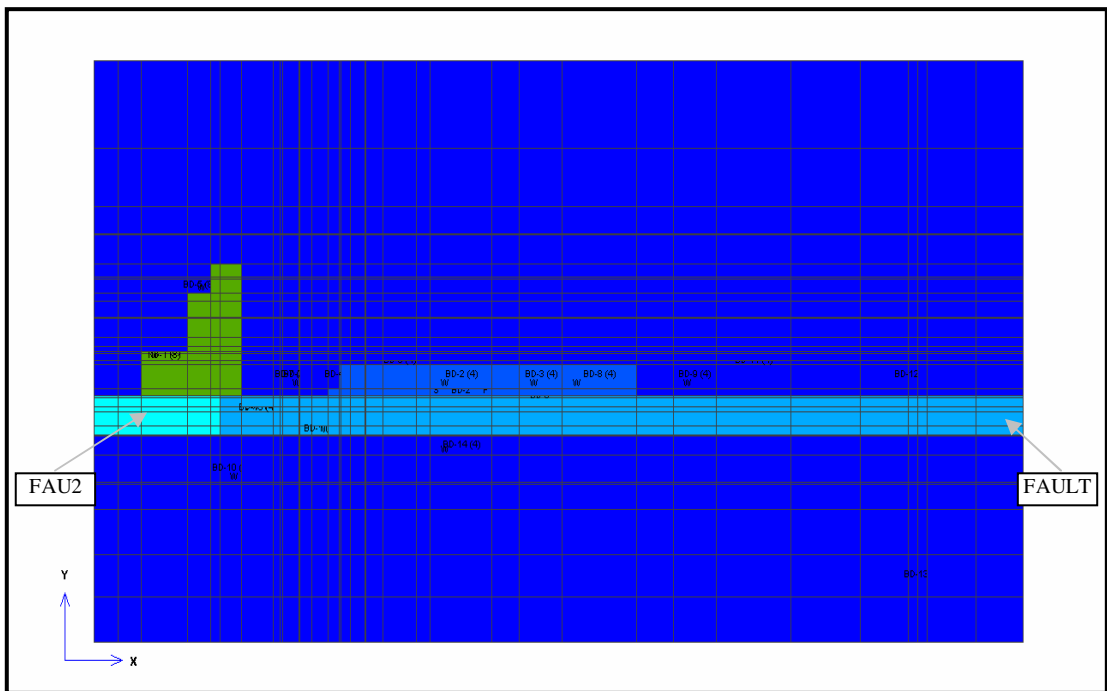


Figure 6.4- Material distribution for the cross-section Z=-400.

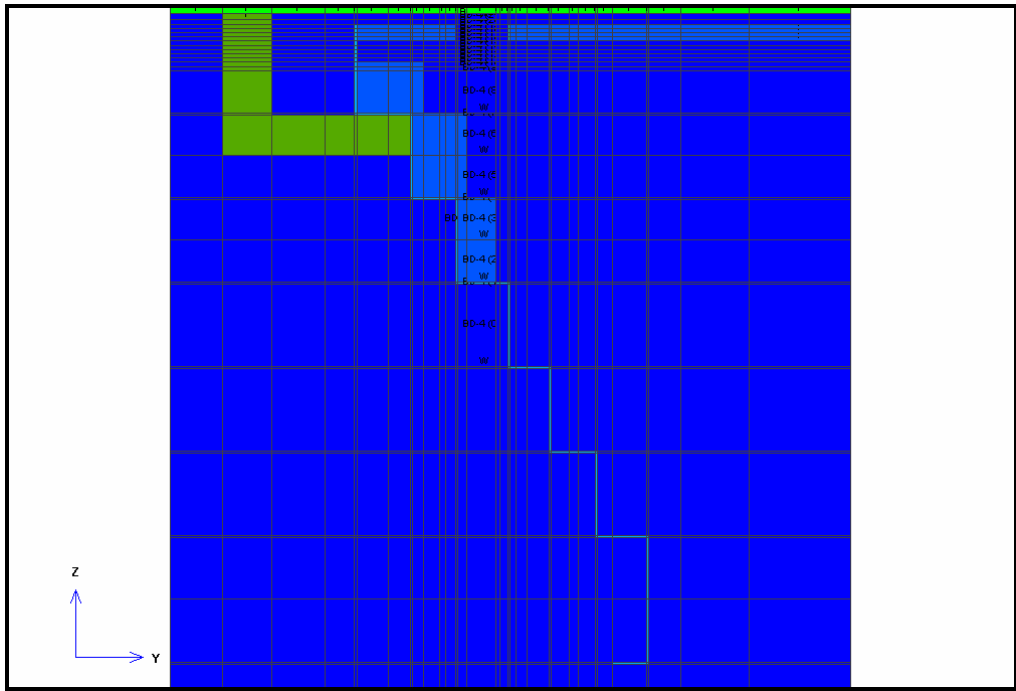


Figure 6.5- Material distribution for the cross-section X=3075.

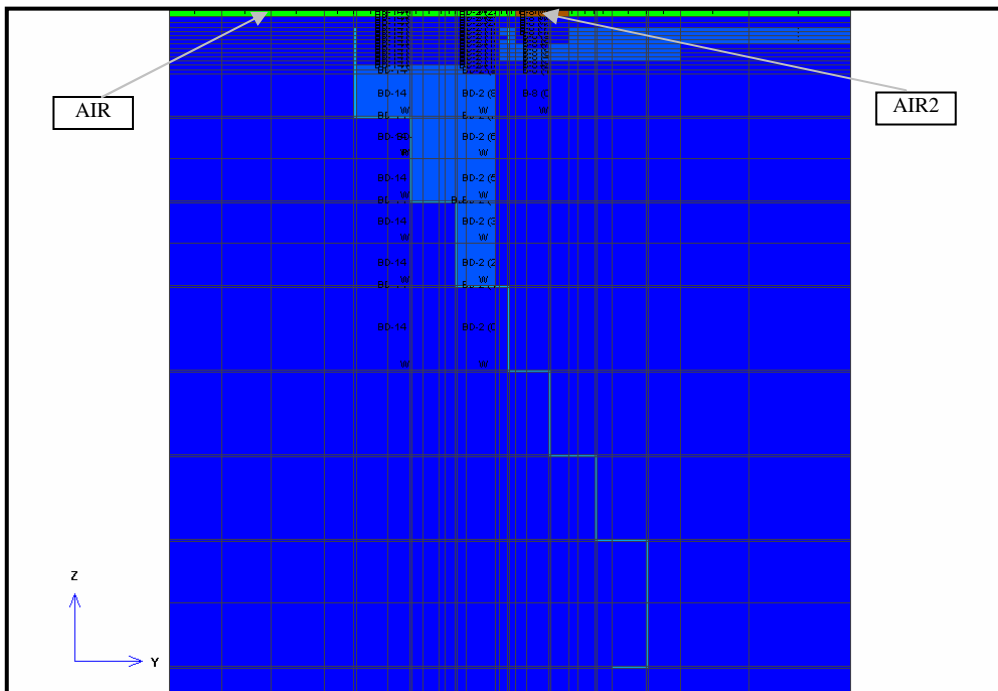


Figure 6.6- Material distribution for the cross-section X=3470.

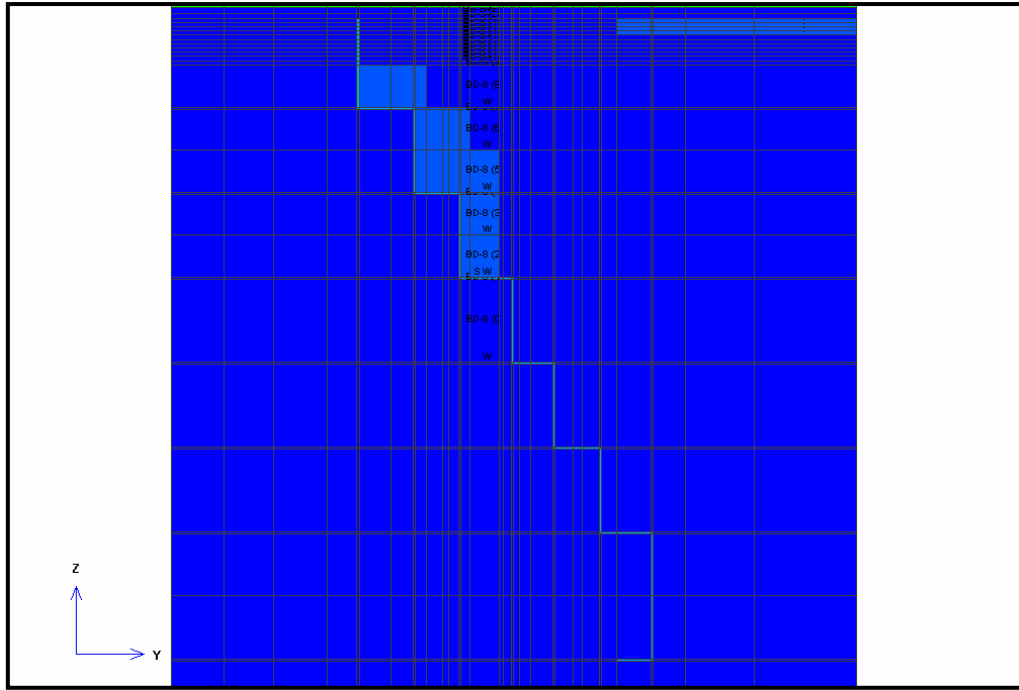


Figure 6.7- Material distribution for the cross-section X=3920.

6.3. Natural State Modeling

Natural State Modeling is the stage of geothermal reservoir modeling in which the state of the field before its exploitation is modeled. It is known that geothermal reservoirs evolve over geological time. The rate of change of thermodynamic properties during geological time (natural state) is minimal compared to changes resulted from exploitation of reservoir. It is therefore concluded that the geothermal reservoirs in their natural state can be considered in pseudo-steady state conditions. It is a common practice in geothermal reservoir simulation studies to run the model with no production/injection conditions to reach the pseudo-steady state.

The following boundary conditions were applied during the Natural State Modeling of Balçova Geothermal Field:

1. The hot water is fed into the reservoir through the AG-I fault with a mass flow rate of 50 kg/s and enthalpy of 6.6E5 J/kg.

2. The location of the hot water entry into the reservoir is at the eastern part of the AG-I fault at the depth 1500 m and extends 1140 m in x direction.
3. The cells locating on the northern part of the alluvium formation are in fixed state and in that region pressure is around $5E5$ pascal, which is actually the hydrostatic pressure at that level.
4. The cells locating on the surface are in fixed state. These cells have temperatures of 20°C , nil porosity and permeability and have heat conductivity, specific heat and density values that are used for air at that temperature. Thus, with these applications, cooling effect of atmosphere could be taken into effect.
5. The region around the model is in no-flow condition. Neither fluid flow nor heat flow occurs in that region and between the cells in the model and that region.

Figures 6.8 - 6.18 give comparisons of temperature profiles of different wellbores obtained from natural state modeling with measured temperature profiles. In these figures, bold continuous line represents model data and circles represent measured data. It is seen that there is a good match of model results with measured data. The goodness of fit is quantified in Figure 6.19 where the observed and calculated temperatures are plotted. It is observed that they are all accumulated around the 45° line. Average values of the differences between observed and calculated temperatures represented with root mean square deviation (RMSD) which is the square root of the average of the squares of the differences between observed and predicted values are shown in Table 6.3.

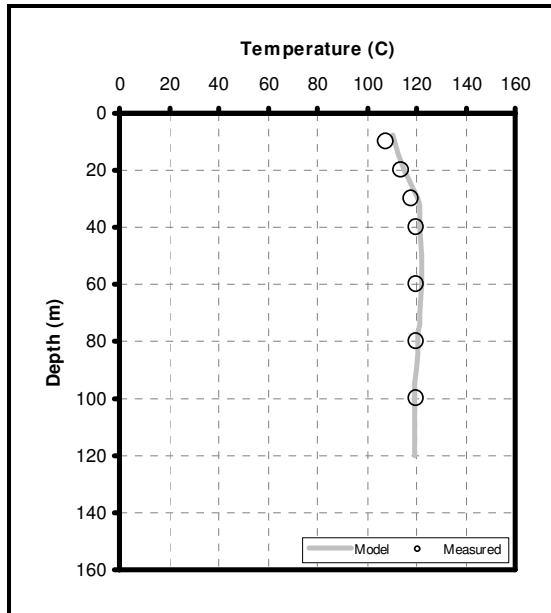


Figure 6.8- Temperature vs. depth profiles for the shallow well B-4.

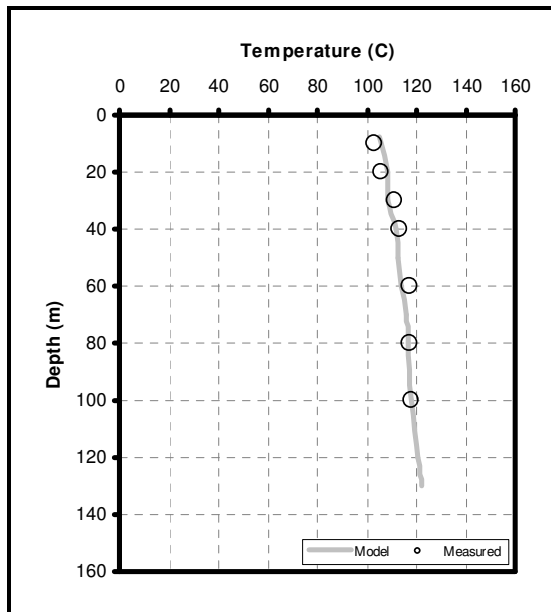


Figure 6.9- Temperature vs. depth profiles for the shallow well B-7.

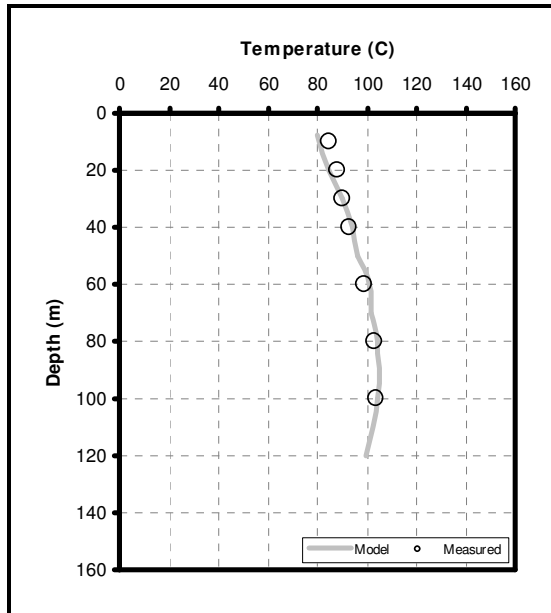


Figure 6.10- Temperature vs. depth profiles for the shallow well B-8.

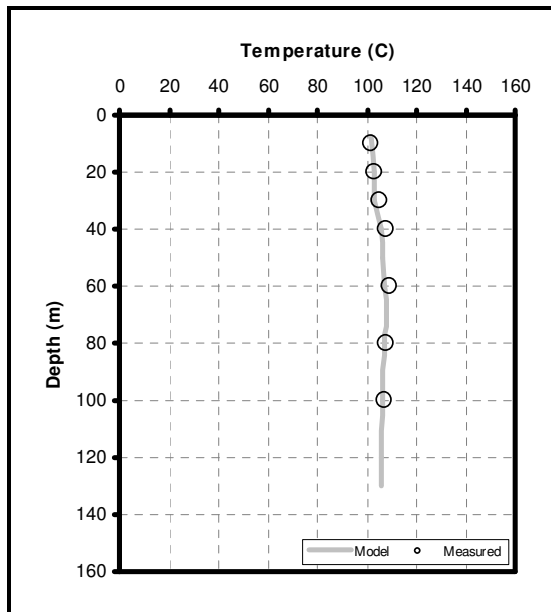


Figure 6.11- Temperature vs. depth profiles for the shallow well B-10.

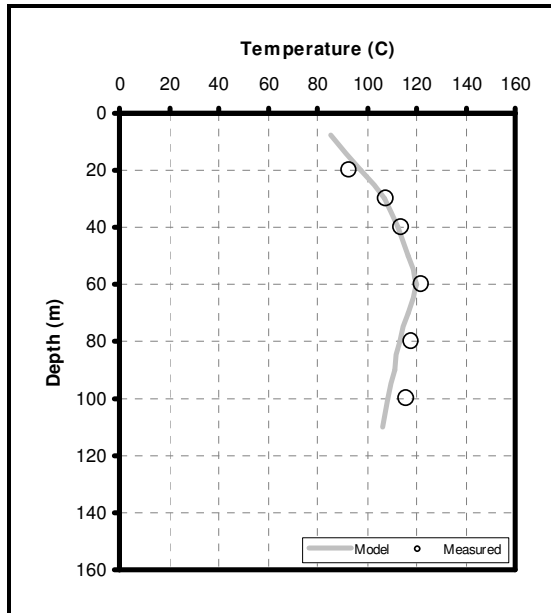


Figure 6.12- Temperature vs. depth profiles for the shallow well B-11.

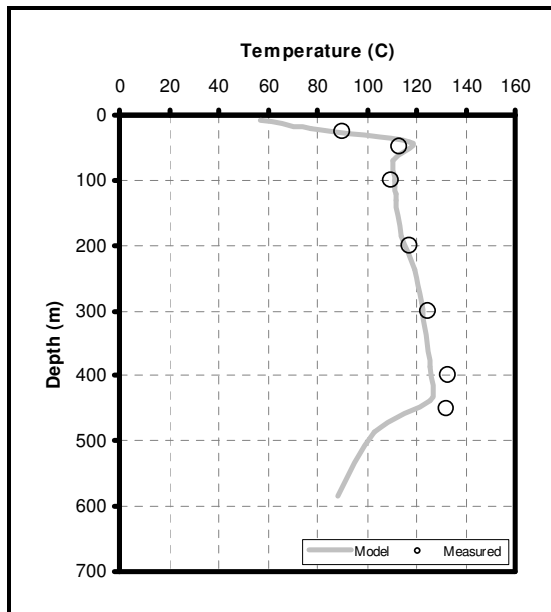


Figure 6.13- Temperature vs. depth profiles for the deep well BD-1.

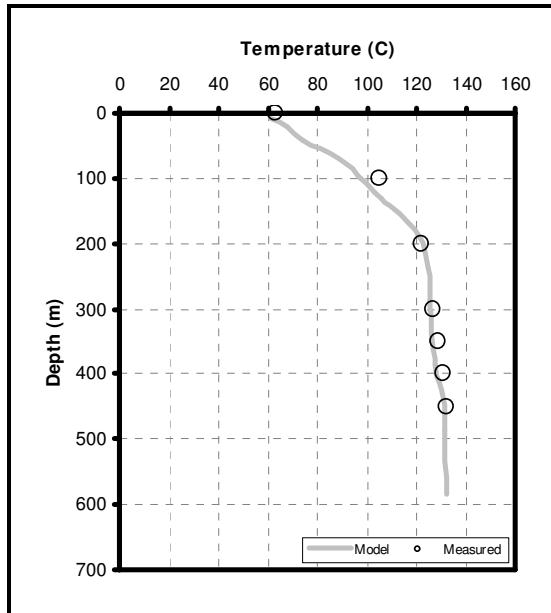


Figure 6.14- Temperature vs. depth profiles for the deep well BD-2.

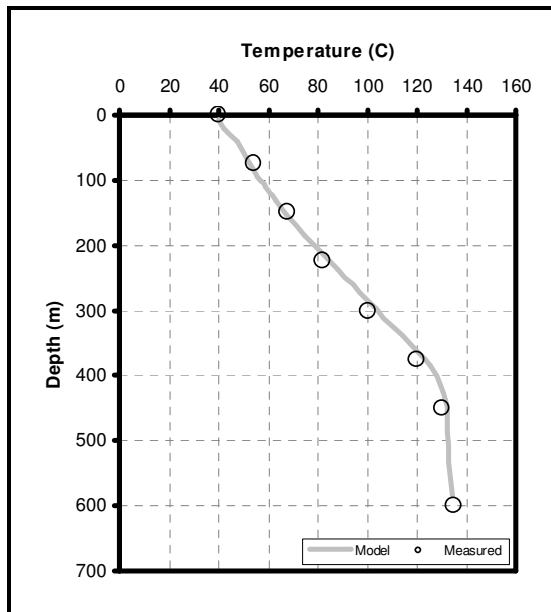


Figure 6.15- Temperature vs. depth profiles for the deep well BD-3.

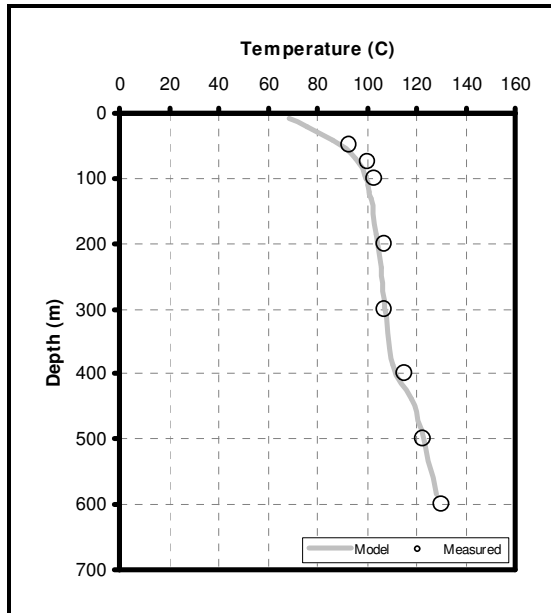


Figure 6.16- Temperature vs. depth profiles for the deep well BD-4.

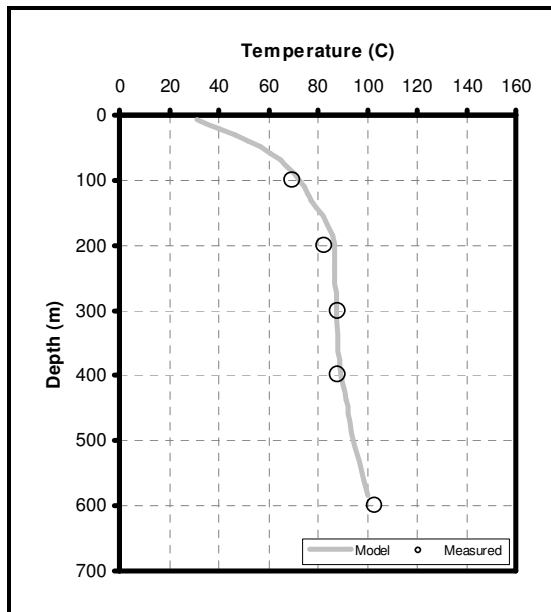


Figure 6.17- Temperature vs. depth profiles for the deep well BD-5.

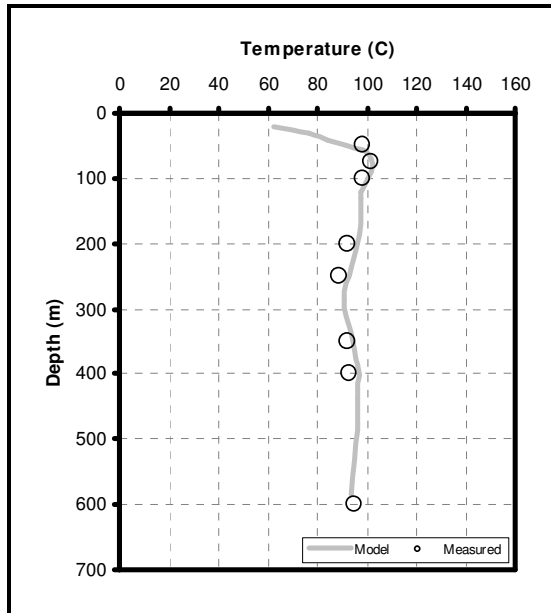


Figure 6.18- Temperature vs. depth profiles for the deep well ND-1.

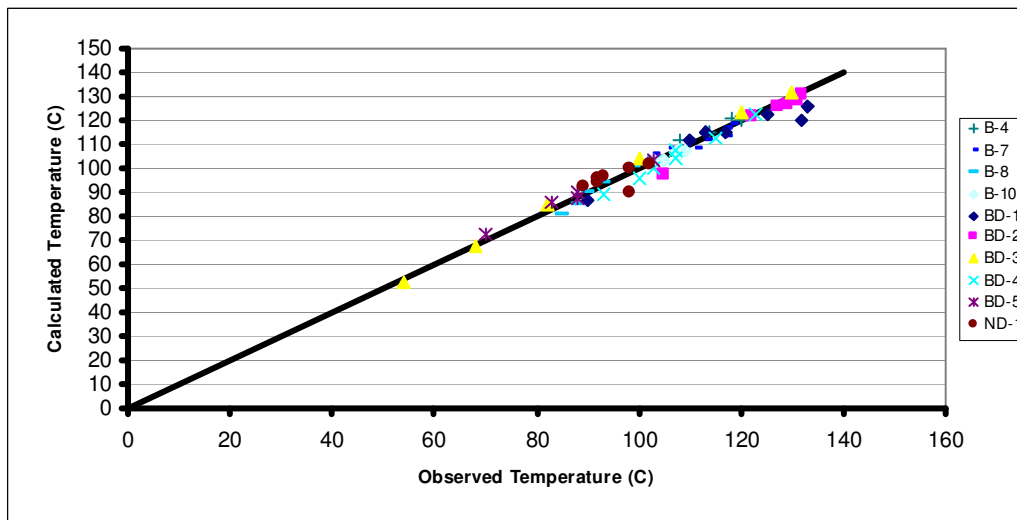


Figure 6.19- A comparison of the observed and calculated temperatures for initial condition.

Table 6.3- RMSD values of temperatures for different wells at initial condition.

Well	RMSD
B-4	2.00
B-7	2.18
B-8	2.17
B-10	1.33
BD-1	5.65
BD-2	3.29
BD-3	2.59
BD-4	2.74
BD-5	1.92
ND-1	4.10

Temperature distributions on cross sections at different locations in X coordinate and areal distributions at different depths obtained from natural state modeling are presented in Figures 6.20 – 6.24. The cross sections were taken from the coordinates of $x = 2800$, $x = 3000$, $x = 3700$, $x = 4400$. Areal distributions, on the other hand, are representing $z = 0$, $z = -15$, $z = -85$, $z = -350$, $z = -550$.

Analysis of X direction cross sections (Figures 6.20 and 6.21) indicate that the hottest section of the cross section at $x = 4400$ is at a deeper location and occupy smaller area compared to the cross section at $x = 3700$. The same observation is valid in between $x = 3700$, $x = 3000$ and $x = 3000$, $x = 2800$ pairs. Such a behavior is in agreement with the conceptual model that the hot water enters the field from deep and eastern part and loses some of its energy as flowing to the western part. Along the cross sections at x directions, the coldest part belongs to the cross section at $x = 2800$. This is compatible with initial measured temperature distribution.

From areal temperature distributions (at $z = 0$, $z = -15$, $z = -85$, $z = -350$ and $z = -550$), it can be observed that the hot water loses some of its energy as flowing upwards. The temperature distributions at $z = 0$ and $z = -15$ is compatible with the surface map prepared for Balçova field (Figure 2.4). The hottest place on those cross sections is near the impermeable zone locating at the center.

It was shown that both shallow and deep wells have a unique pressure gradient of 9.86 kPa/m (Serpen, 2003). Figure 6.25 shows natural state modeling results as the change in pressures of the blocks representing AG-I fault with depth. The

location where the pressures were taken is the region that is at the same x direction with BD-1 well. The pressure gradient from natural state modeling (9.4 kPa/m) is compatible with the gradient obtained from measurements of the wells.

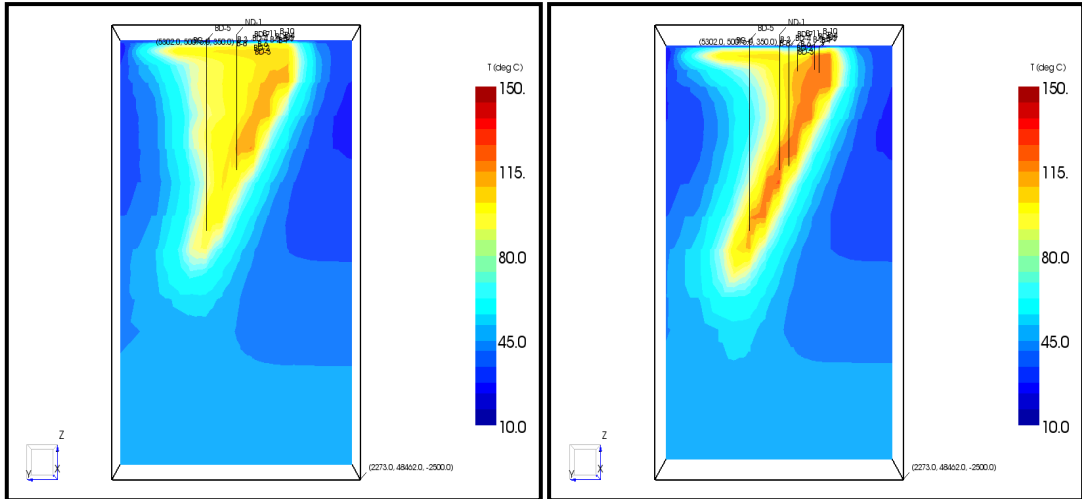


Figure 6.20- Initial temperature distributions for cross-sections x=2800 and x=3000.

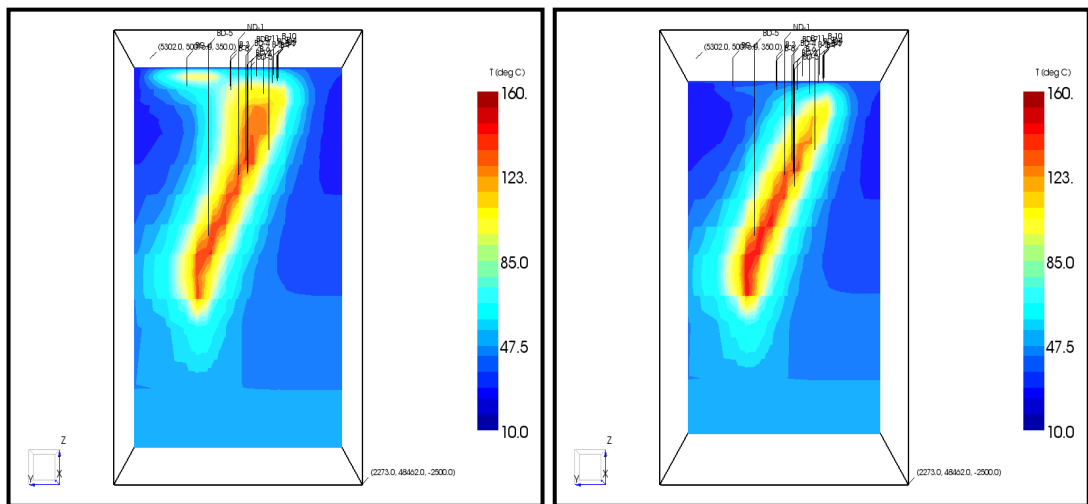


Figure 6.21- Initial temperature distributions for cross-sections X=3700 and X=4400.

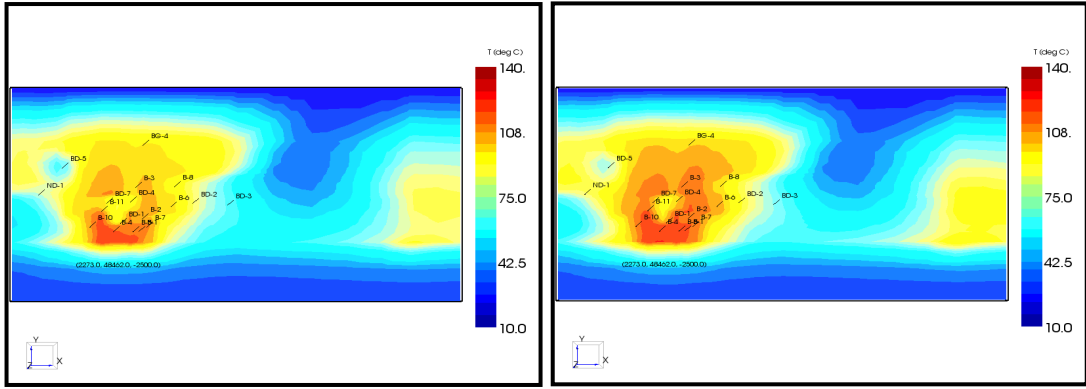


Figure 6.22- Initial temperature distributions for cross-sections Z=0 and Z=-15.

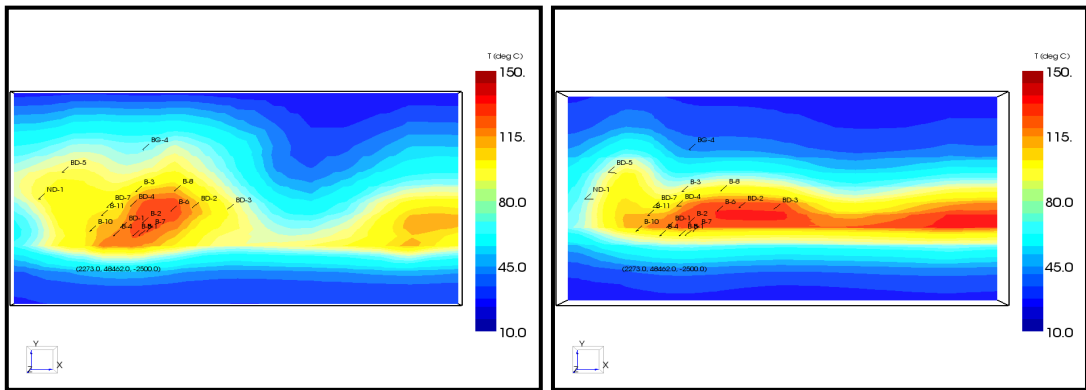


Figure 6.23- Initial temperature distributions for cross-sections Z=-85 and Z=-350.

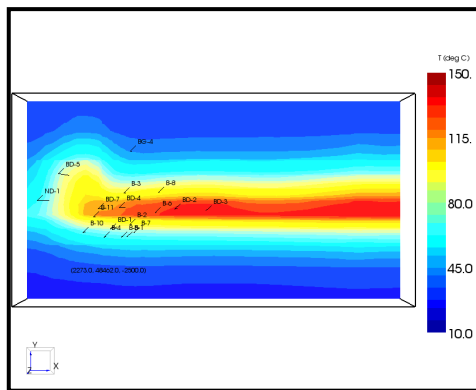


Figure 6.24- Initial temperature distribution for cross-section Z=-550.

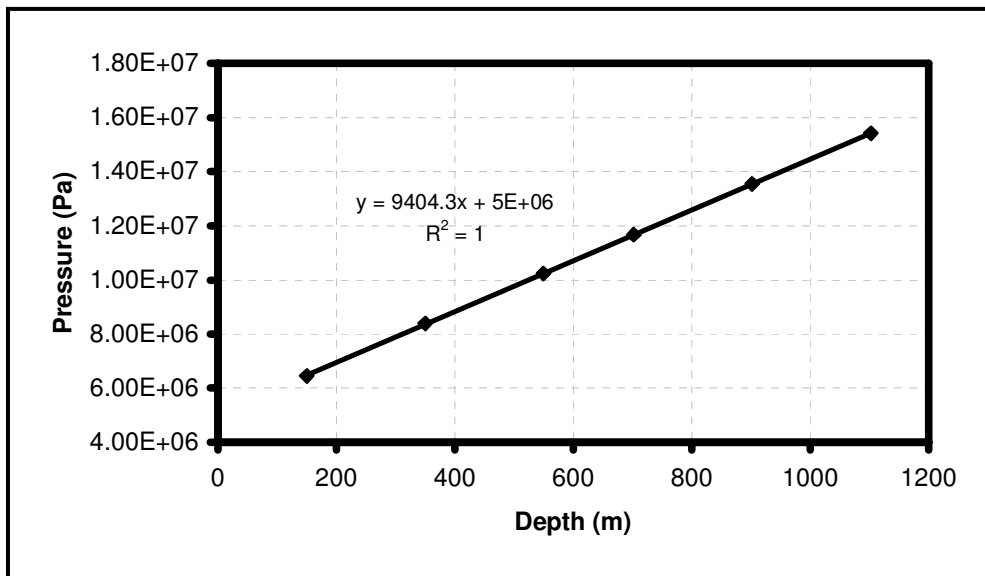


Figure 6.25- Model pressure vs. depth profile for initial condition.

6.4. History Matching

After completing the initial state modeling studies, history matching studies were carried out. The rate of hot water entering the AG-I fault was estimated as 50 kg/s in natural state modeling, but it was found from the initial runs of history matching that this rate is not enough to sustain the high rate of fluid production of the field. Therefore, the boundary condition was changed to a fixed state option for the cells in which there was injection of hot water in natural state modeling. Thus, increase in hot water rate entering the AG-I fault due to pressure decline caused by production was taken into account. Also, cold water recharge to the shallow depths was carried into effect in history matching studies. The cold water enters to the geothermal system from the surface south of the AG-I and ends at the depth of 250 m where cold water crosses AG-I fault. Early production and shallow injection trials into B-9 resulted with temperature decline in B-10. On the other hand there was decline in temperatures of B-1 and B-7 which are not tied to injection from B-9. This behavior was attributed to the cold water invasion because of the pressure decline in the area due to heavy production. The region where cold water flows is denoted with the material ROCK3. The intrusion of cold water was adjusted using fixed state option for the cells located at the surface. The temperature of the fixed

state cells is 10 °C and pressure is 6.2E6 Pa. The pressure of the fault during natural state modeling at the depth where cold water enters is much higher than the pressure of the fixed state cell. This information may indicate that no cold water or little amount of it enters the field during natural state condition. To observe cooling in well B-11 another fault which may correspond to the fault D1 (Figure 2.4) and starts near well B-4 and continues near well B-11 was created. The material Fau2 was assigned to this fault.

There are deep and shallow wells drilled in Balçova Geothermal Field both for production and injection purposes. Generally, deep wells are represented with letters BD and shallow wells are named with letter B. There are 15 wells named as BD. Among these, BD-8 and BD-10 wells have been used for only injection purposes. BD-1, BD-3, BD-5 and BD-15 wells have been used for both production and injection. All other deep wells named as BD have had contribution to total production. The number of wells named as B is 12. B-3, B-6, B-8 wells have never been used thus abandoned. B-9, B-2 and B-12 wells were used as injection wells initially and abandoned after 2003 as deep injection started. Other wells have been used for production. Most of the production coming from shallow wells has been obtained from B-5 and B-10 wells and injection has mainly done through the well BD-8 (Around %80).

Yearly production – injection statistics and the contribution of each well (per cent of yearly totals) for the period of 2004 – 2008 are presented in Table 6.4. BD-4, BD-9, B-5 and B-10 are the main producers of the field having at least 10 % share each. Among these wells, B-10 has the highest production contribution with an increasing share from 17.2 % in 2004 to 29.6 % in 2008. On the other hand, 6 wells were utilized for injection in the period of 2004 – 2008. BD-8 is the flagship of injection with a decreasing trend of 99.2 % in 2004 to 70.4 % in 2008. There is an increasing trend in the yearly injection of the field. The number of injection wells increases with the increase in yearly injection and the contribution of new injection wells increase also.

Table 6.4- Total production and injection (m³) of the wells and their share (%) between 2004 and 2008.

PRODUCTION										
	2004		2005		2006		2007		2008	
Production Wells	Production (m ³)	%	Production (m ³)	%	Production (m ³)	%	Production (m ³)	%	Production (m ³)	%
BD-1	168,562	4.6	76,860	1.8	49,600	1.1	64,763	1.4	60,421	1.2
BD-2	400,366	11.0	475,490	11.3	242,008	5.3	182,680	4.0	293,607	6.0
BD-3	381,521	10.5	83,822	2.0	111,835	2.4	13,114	0.3	0	0.0
BD-4	595,676	16.4	679,270	16.1	467,503	10.2	664,899	14.4	467,642	9.6
BD-5	275,336	7.6	323,622	7.7	265,984	5.8	212,419	4.6	71,378	1.5
BD-6	106,867	2.9	475,099	11.3	580,858	12.7	626,405	13.6	199,675	4.1
BD-7	226,378	6.2	295,035	7.0	215,373	4.7	147,536	3.2	55,017	1.1
BD-9	0	0.0	89,990	2.1	801,366	17.5	740,049	16.0	676,570	13.9
BD-11	0	0.0	11,763	0.3	0	0.0	110,557	2.4	414,558	8.5
BD-12	0	0.0	2,473	0.1	0	0.0	0	0.0	104,849	2.2
BD-14	0	0.0	6,600	0.2	0	0.0	130,645	2.8	163,485	3.4
BD-15	0	0.0	1,091	0.0	0	0.0	0	0.0	423,138	8.7
B-1	162,679	4.5	317,394	7.5	197,019	4.3	62,522	1.4	28,506	0.6
B-4	102,921	2.8	58,688	1.4	0	0.0	6,392	0.1	3,103	0.1
B-5	370,231	10.2	388,378	9.2	520,072	11.4	382,261	8.3	451,989	9.3
B-7	227,307	6.2	91,102	2.2	92,787	2.0	39,837	0.9	4,902	0.1
B-10	625,133	17.2	831,007	19.7	1,028,419	22.5	1,231,518	26.7	1,438,374	29.6
TOTAL	3,642,977		4,207,715		4,572,823		4,615,598		4,857,215	
INJECTION										
	2004		2005		2006		2007		2008	
Injection Wells	Injection(m ³)	%	Injection(m ³)	%	Injection(m ³)	%	Injection(m ³)	%	Injection(m ³)	%
BD-1	0	0.0	0	0.0	0	0.0	0	0.0	11,639	0.3
BD-3	12,240	0.8	0	0.0	0	0.0	26,639	0.8	674,132	17.8
BD-5	0	0.0	0	0.0	0	0.0	0	0.0	33,121	0.9
BD-8	1,498,396	99.2	1,537,647	82.4	2,036,191	79.9	2,749,047	81.9	2,665,153	70.4
BD-10	0	0.0	328,524	17.6	511,533	20.1	352,799	10.5	243,768	6.4
BD-15	0	0.0	0	0.0	0	0.0	226,693	6.8	157,146	4.2
TOTAL	1,510,636		1,866,171		2,547,723		3,355,178		3,784,959	

Using the temperature and pressure values obtained from natural state modeling and production and injection data recorded between 1996 and 2009 in the model, the simulation was performed for 13 years. Bottomhole temperature values obtained from the simulation study were matched with values that were measured during the period 1996-2009 (Figure 6.26 - 6.39). Except for BD-3 well, it can be said that an acceptable match exists between the measured and model data. After year 2003, most of the injection was performed through the well BD-8. Examining the effect of BD-8 well on BD-2 well it may be said that such a drop in temperature of BD-3 well is an expected result since BD-3 well is closer to BD-8. Although model data is compatible with measured data for the well BD-6 in the time period

2007-2008, there is a small temperature difference between measured and model data after 2008. Temperatures obtained from the model decrease more sharply. This may be an expected result since more injection is performed in that year and there is a little difference in production amount for those years. The goodness of the match is quantified in Figure 6.47 where the observed and calculated temperatures are plotted. It is observed that they are all accumulated around the 45° line. Average values of the differences between observed and calculated temperatures represented with root mean square deviation (RMSD) are shown in Table 6.5.

Since there is no recorded bottomhole pressure values for production wells, measured water level in different wells were matched with pressure values obtained from the model for those wells (Figure 6.40 – 6.46). Bold continuous line represents model data and points represent measured data. There is a good agreement between the model data and measured water level.

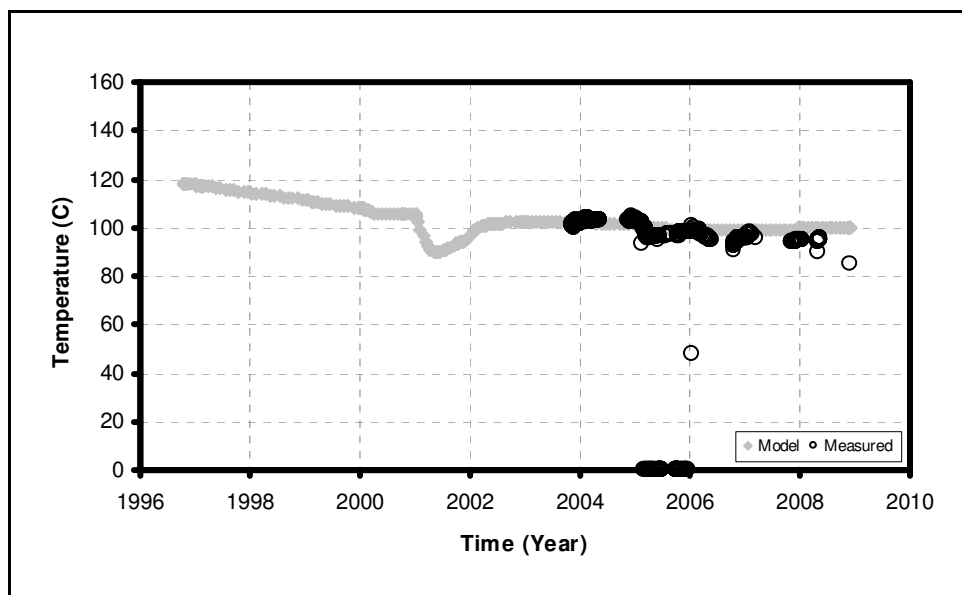


Figure 6.26- A comparison of the simulated and measured temperatures for well B-1.

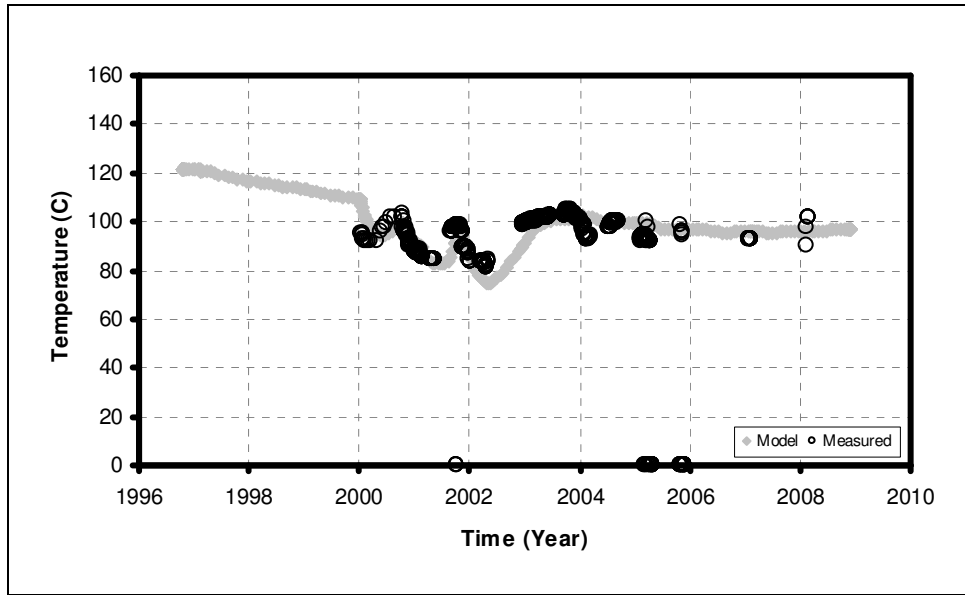


Figure 6.27- A comparison of the simulated and measured temperatures for well B-4.

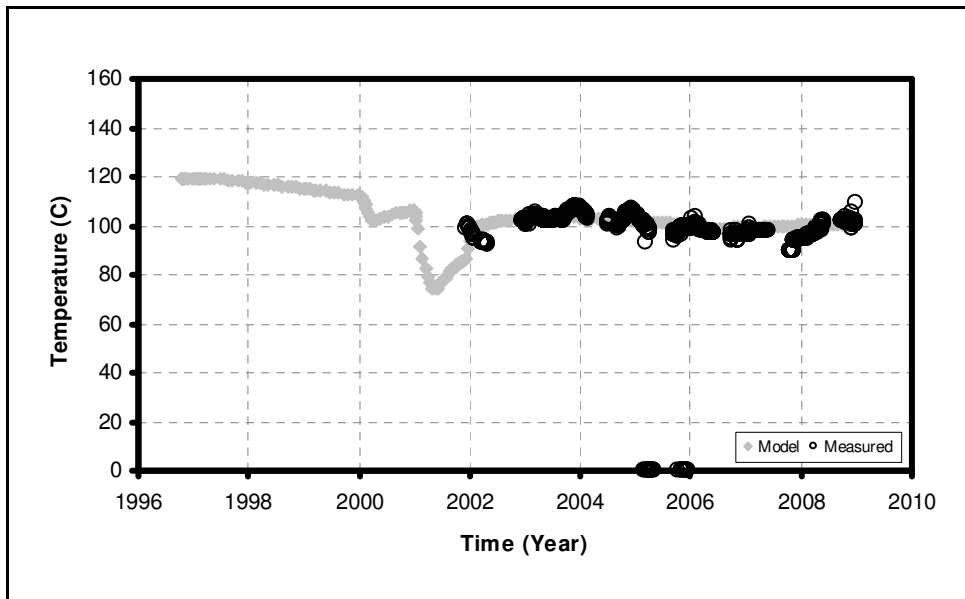


Figure 6.28- A comparison of the simulated and measured temperatures for well B-5.

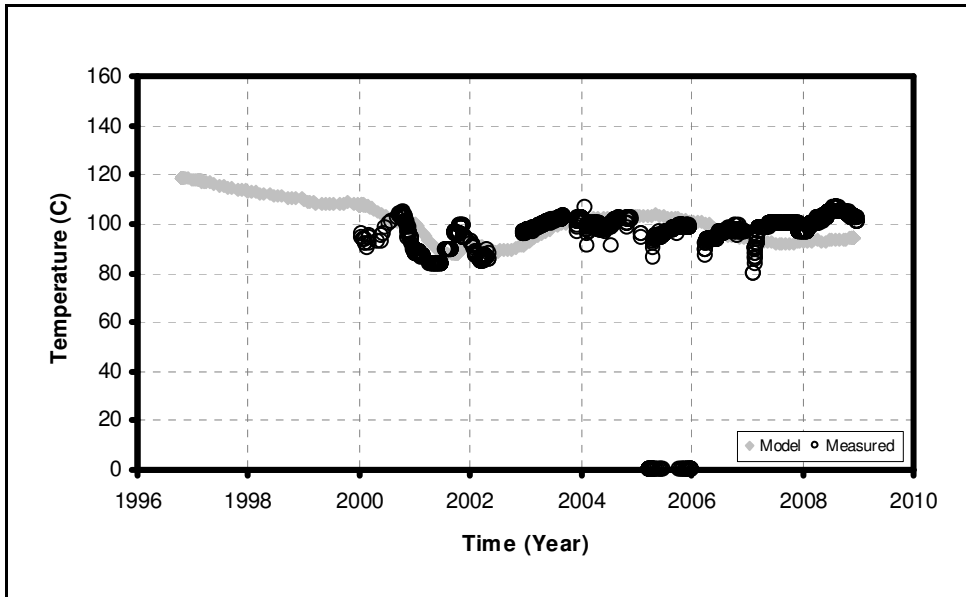


Figure 6.29- A comparison of the simulated and measured temperatures for well B-10.

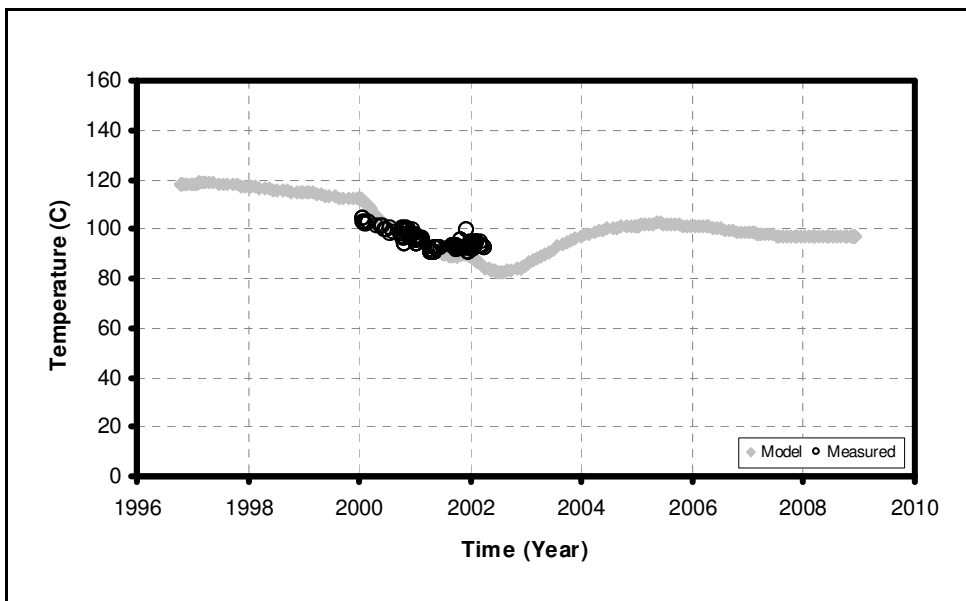


Figure 6.30- A comparison of the simulated and measured temperatures for well B-11.

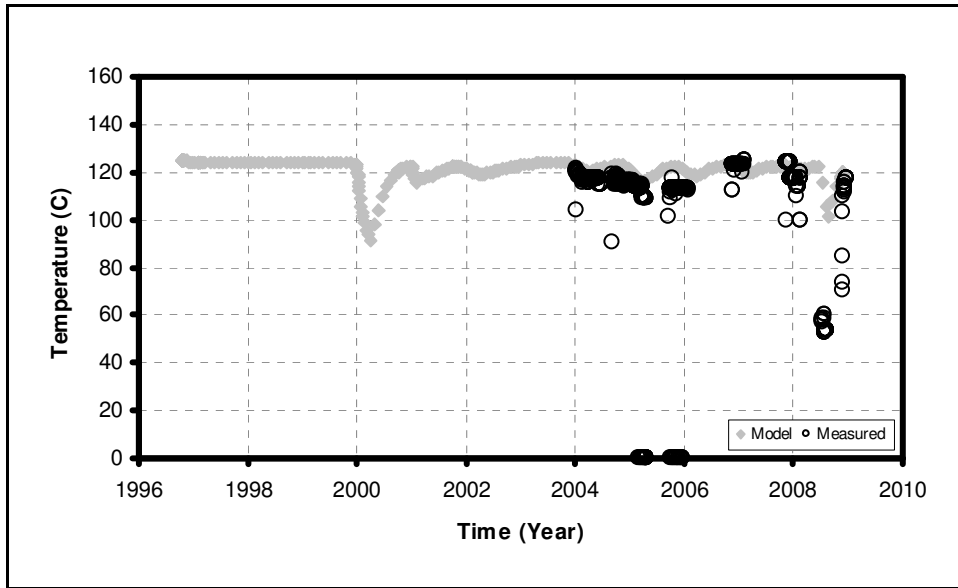


Figure 6.31- A comparison of the simulated and measured temperatures for well BD-1.

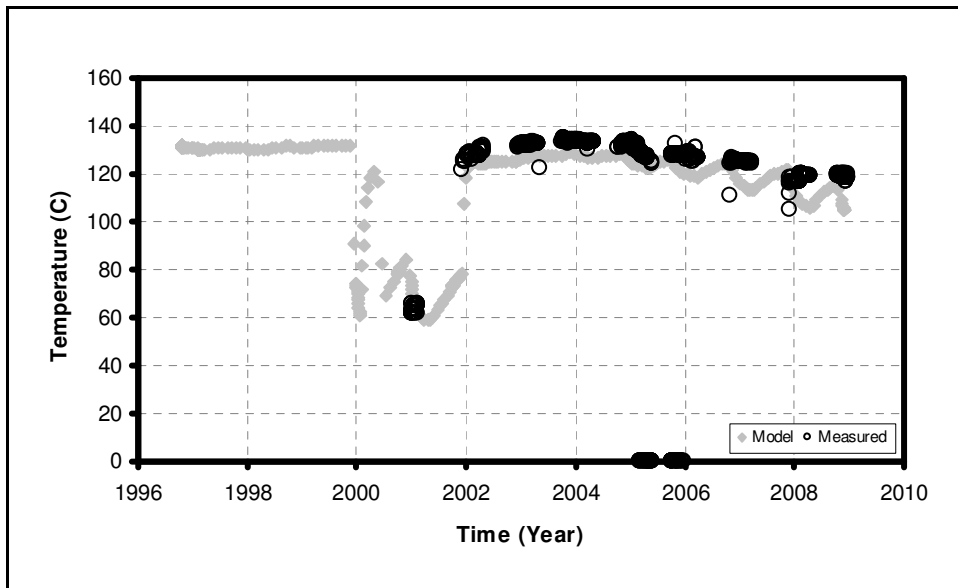


Figure 6.32- A comparison of the simulated and measured temperatures for well BD-2.

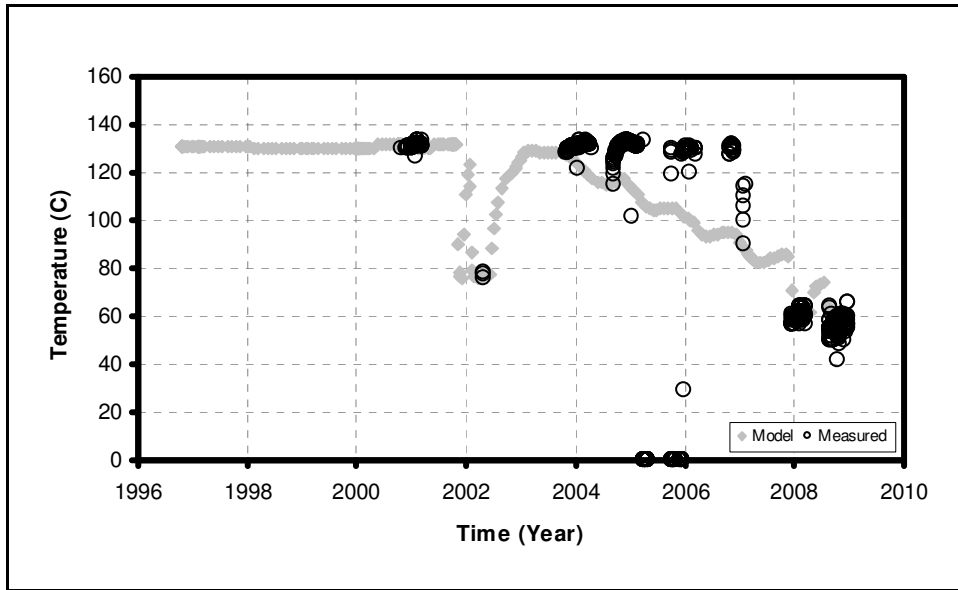


Figure 6.33- A comparison of the simulated and measured temperatures for well BD-3.

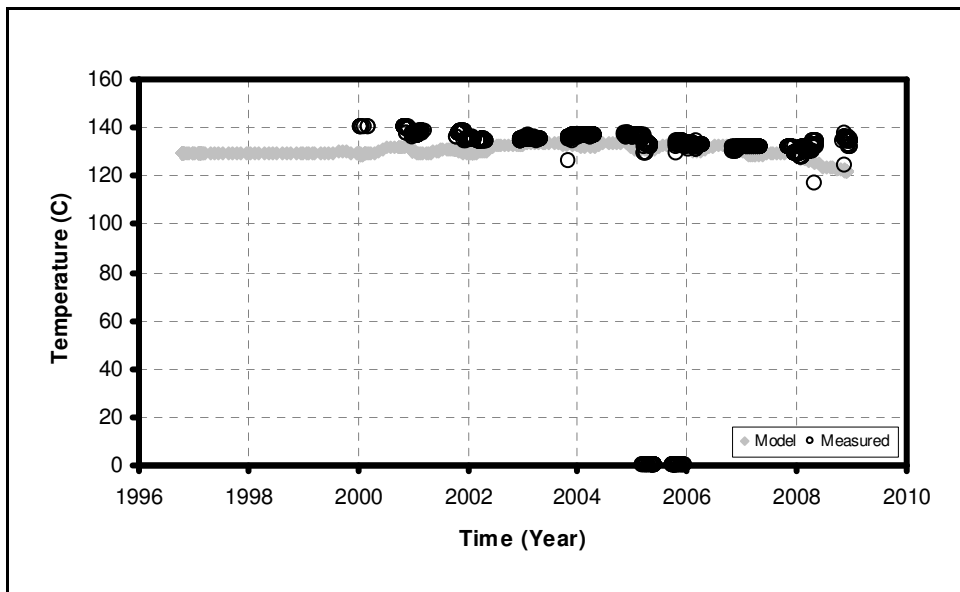


Figure 6.34- A comparison of the simulated and measured temperatures for well BD-4.

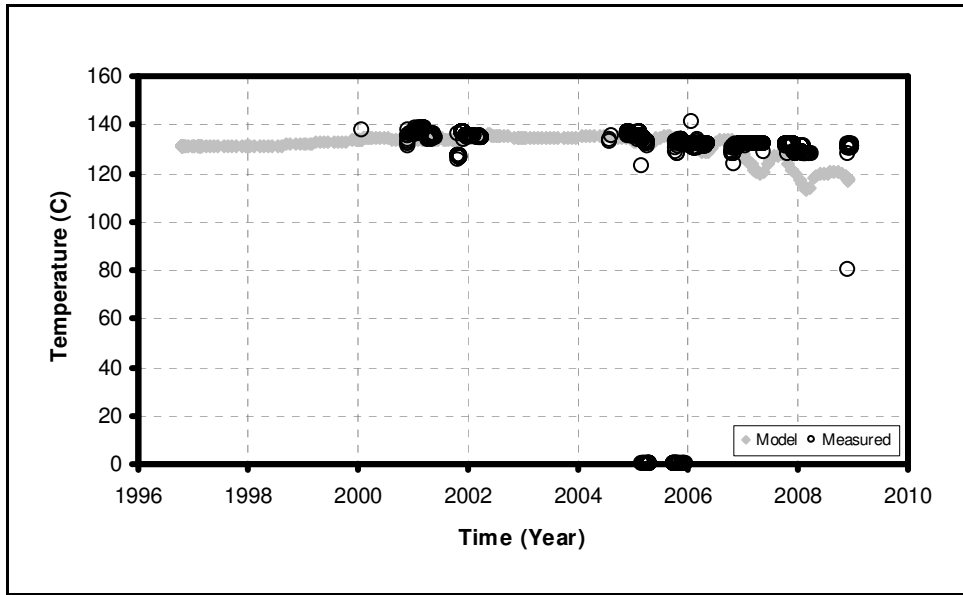


Figure 6.35- A comparison of the simulated and measured temperatures for well BD-6.

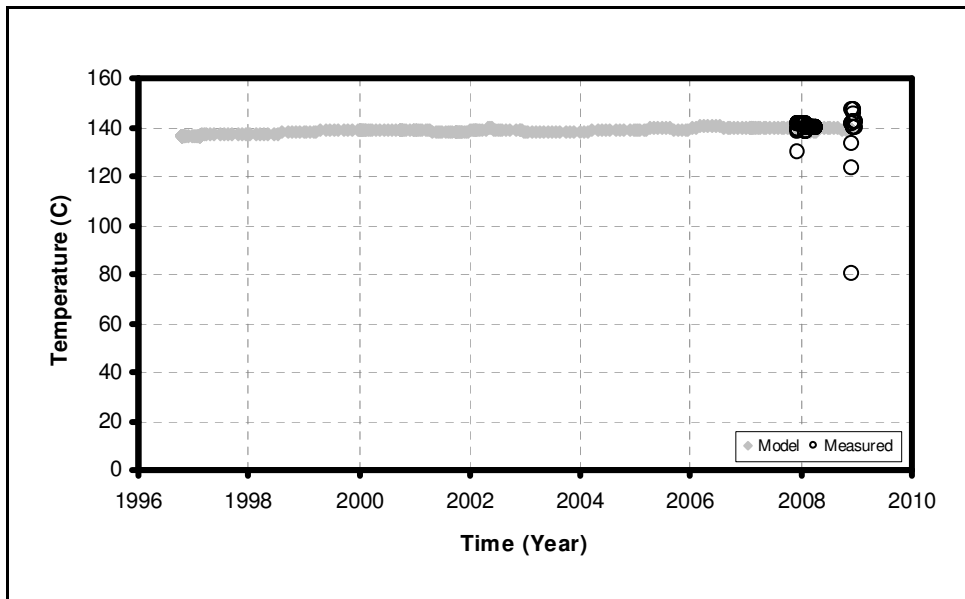


Figure 6.36- A comparison of the simulated and measured temperatures for well BD-11.

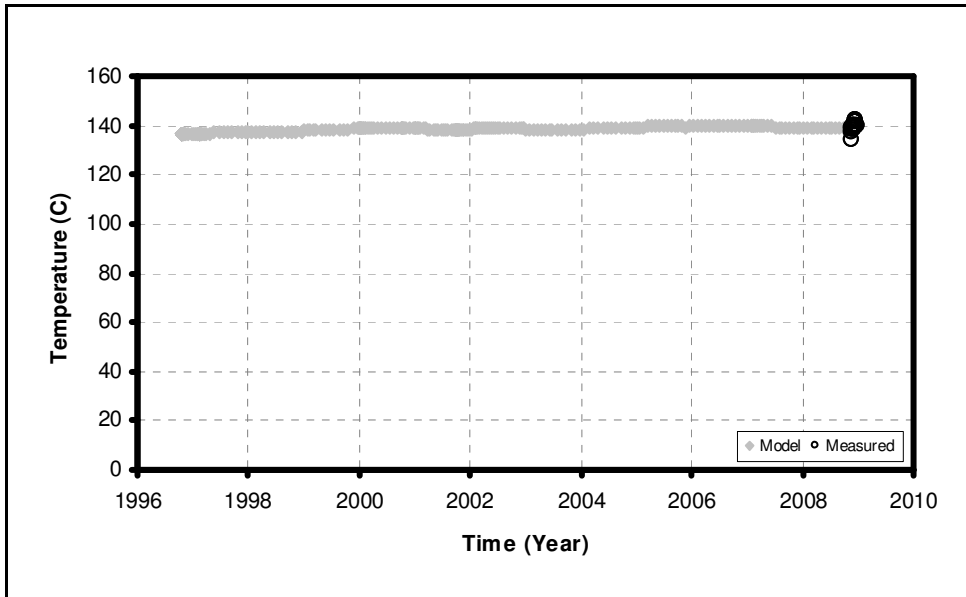


Figure 6.37- A comparison of the simulated and measured temperatures for well BD-12.

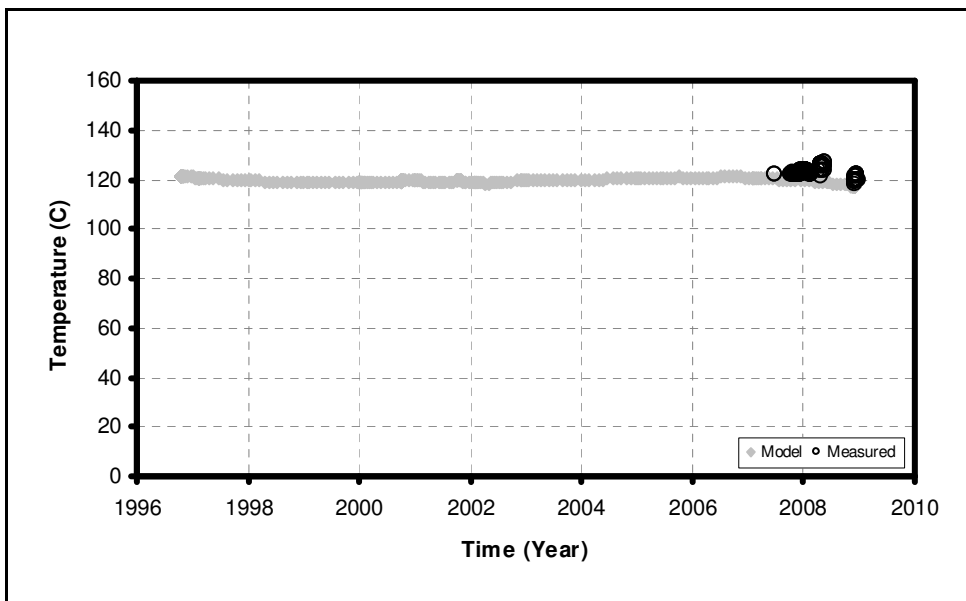


Figure 6.38- A comparison of the simulated and measured temperatures for well BD-14.

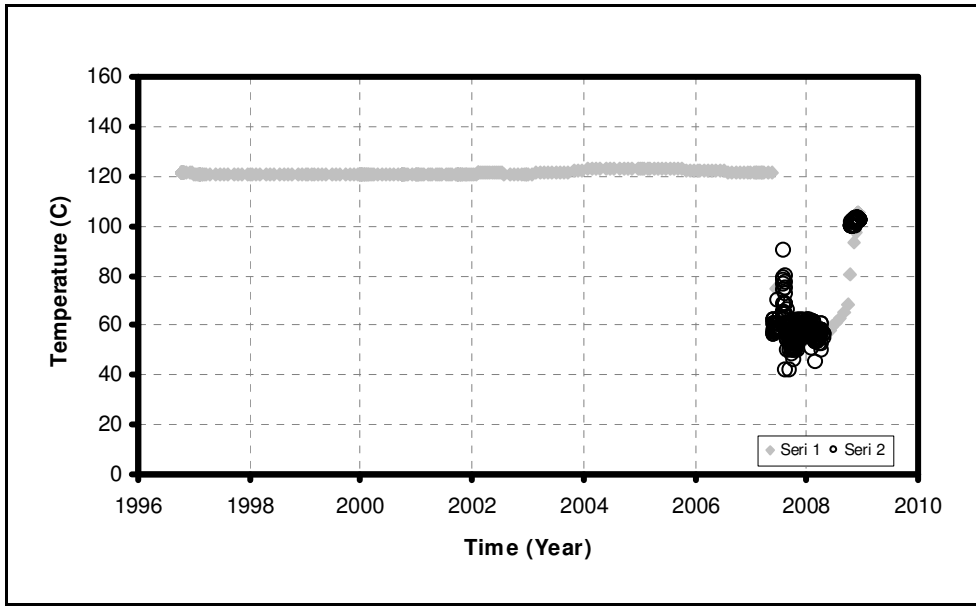


Figure 6.39- A comparison of the simulated and measured temperatures for well BD-15.

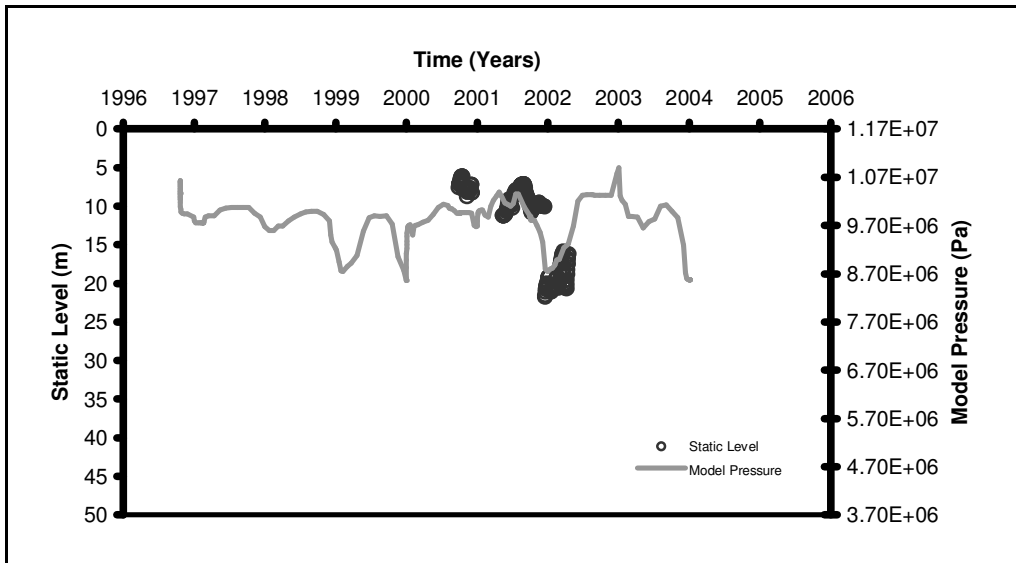


Figure 6.40- A comparison of the model pressure and measured water level at well BD-1.

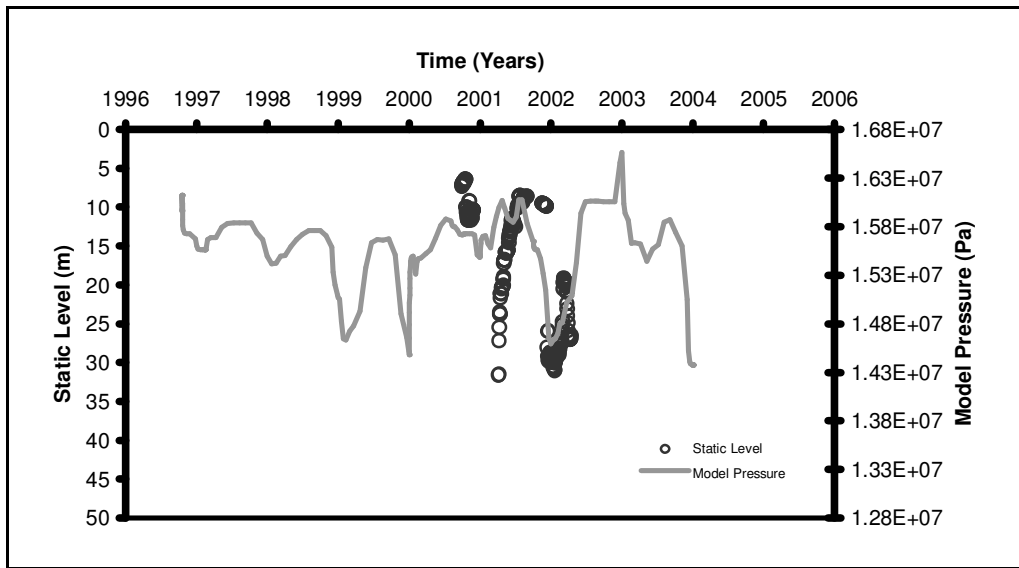


Figure 6.41- A comparison of the model pressure and measured water level at well BD-5.

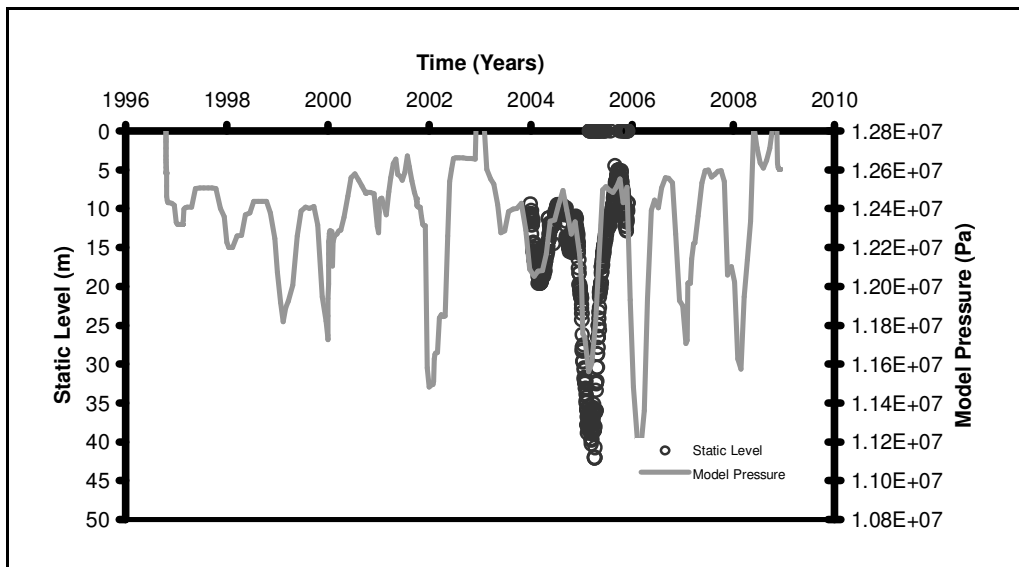


Figure 6.42- A comparison of the model pressure and measured water level at well BD-9.

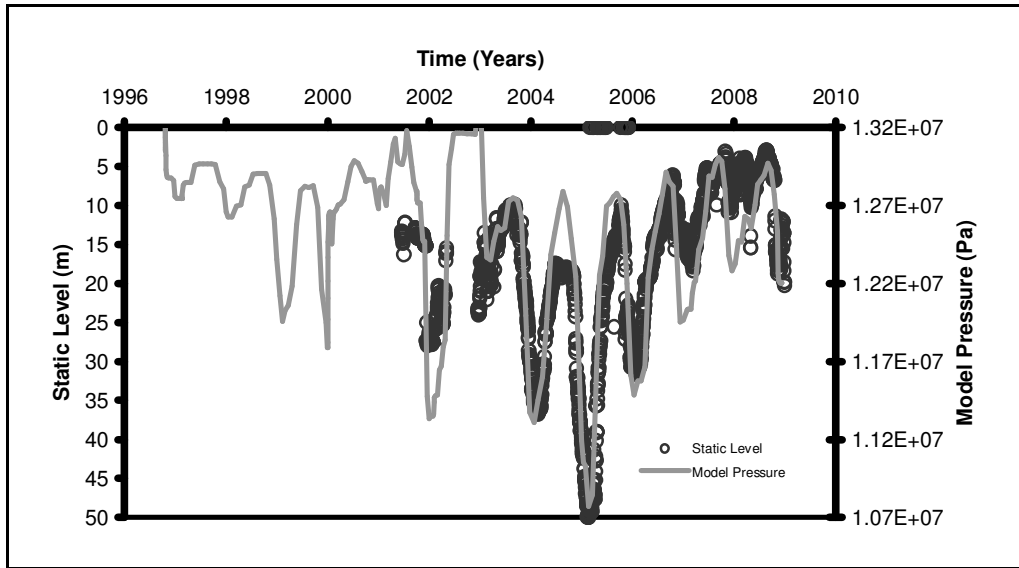


Figure 6.43- A comparison of the model pressure and measured water level at well ND-1.

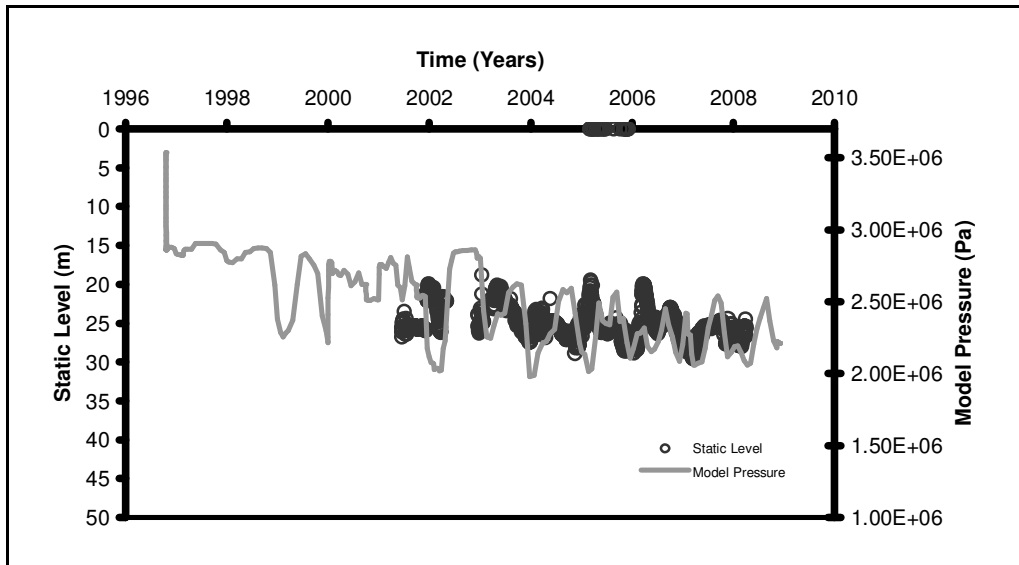


Figure 6.44- A comparison of the model pressure and measured water level at well N-1.

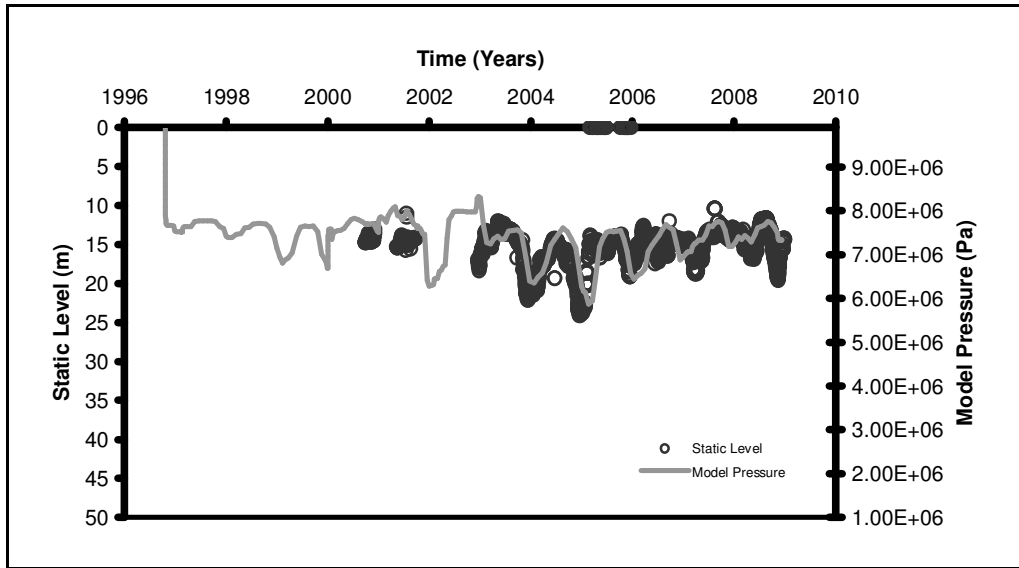


Figure 6.45- A comparison of the model pressure and measured water level at well B-2.

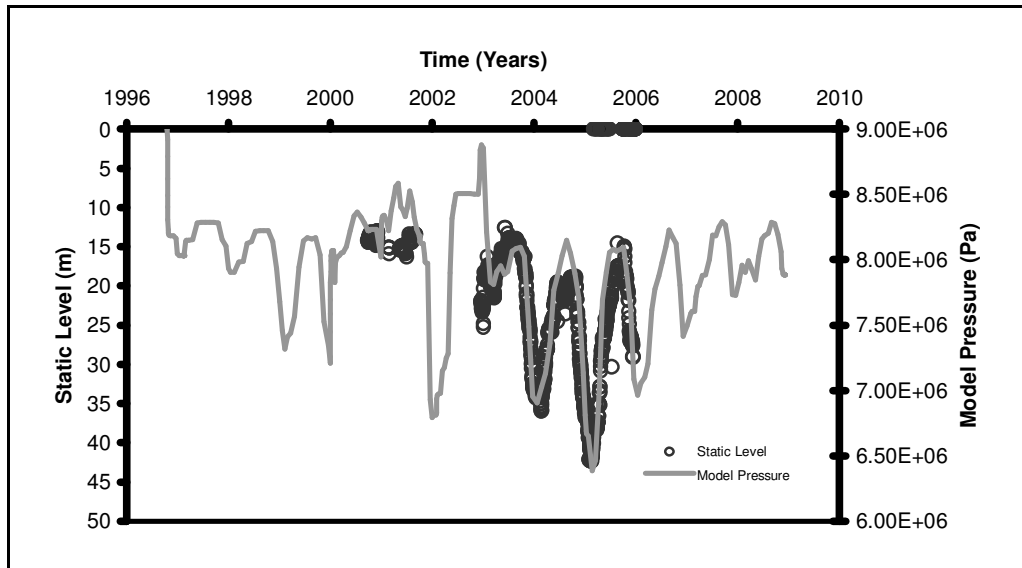


Figure 6.46- A comparison of the model pressure and measured water level at well B-12.

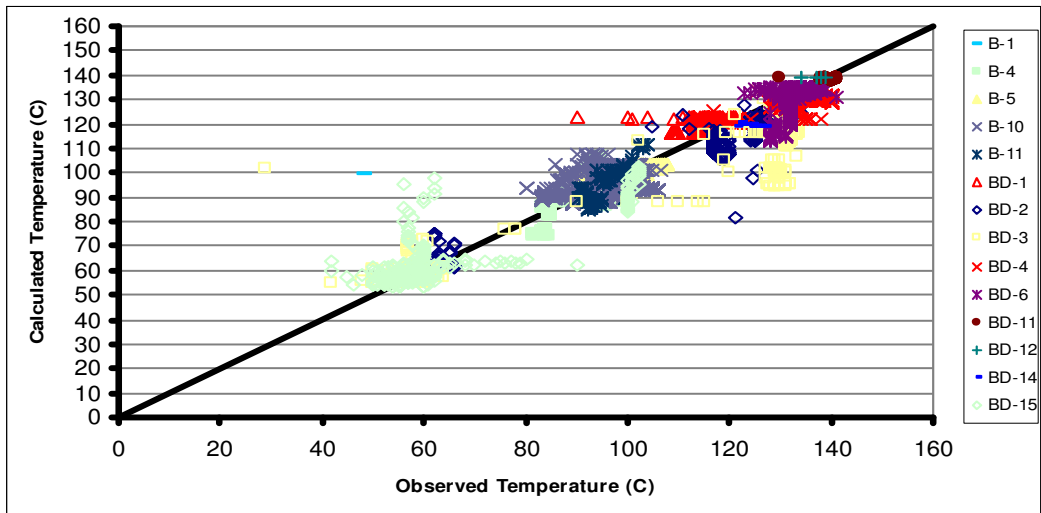


Figure 6.47- A comparison of the observed and calculated temperatures for the production and injection period.

Table 6.5- RMSD values of temperatures for different wells for the injection and production period.

Well	RMSD
B-1	3.40
B-4	4.71
B-5	3.22
B-10	6.36
B-11	3.82
BD-1	6.05
BD-2	7.35
BD-3	14.80
BD-4	4.61
BD-6	6.42
BD-11	2.26
BD-12	2.92
BD-14	3.84
BD-15	7.91

6.5. Future Forecasting

Future forecasting of Balçova geothermal field was carried out by using three different production / injection Scenarios.

- Scenario-1: Production and injection rates in year 2008 were repeated for 20 years. For initial condition, pressure and temperature values obtained at the end of 2008 were used. Although BD-1, BD-5 and BD-15 wells were used for both production and injection in year 2008, they were used only for production in Scenario-1 since they were utilized as production wells at the end of 2008 and the amount of water injected through those wells in that year constitute only 4% of the total injection. In year 2008, total injection constitutes the % 80 of total production. It is important to notice that injection was mainly performed through BD-8 well (% 80 of total injection in 2008). Removing the water amount that was injected through BD-1, BD-5 and BD-15, total injection constitutes around % 75 of total production. Figure 6.46 show the locations of wells used in Scenario-1.
- Scenario-2: The simulation was run for 15 years and production and injection rates in year 2008 were repeated for 3 years, then production rates were increased by 10 % every three years and injection rates were increased by 17 % every 3 years. As production increases, injection to production ratio was needed to be increased not to come across with problems about pressures. In last year injection amount was almost equal to production amount. Some time later, more water will have to be injected than what is produced, which is unrealistic. This 15 years time period is the limit as the amount of injected water becomes larger than the amount of production after that time. Although BD-1, BD-5 and BD-15 wells were used for both production and injection in year 2008, they were used only for production in Scenario-2 since they were utilized as production wells at the end of 2008 and the amount of water injected through those wells in that year constitute only 4% of the total injection. For initial condition pressure and temperature values obtained at the end of 2008 were used. Locations of wells that were used in Scenario-2 are given in Figure 6.47.
- Scenario-3: A well that is assumed to be drilled to 1000 m depth at the location of BT-1 well is added for injecting water. In first three years, injection rates of BD-3 and BD-10 in year 2008 were repeated. 57 % of what

is injected through BD-8 removed from that well and transformed to the new well. Injection rates in the new well are same for all years and maximum injection rate in that well is 400 m³/h. Other injection rates were increased as production increased. The production Scenario is same as that of second Scenario; production rates in year 2008 were repeated for 3 years, then they were increased by 10 % every three years. Injection rates of BD-3, BD-8 and BD-10 were increased by 25 % every three years. Simulation run continued up to 2022 as injection amount needed to balance the production exceeds the production amount after that time. For initial condition pressure and temperature values obtained at the end of 2008 were used. Figure 6.48 is the map showing the locations of wells used in Scenario-3.

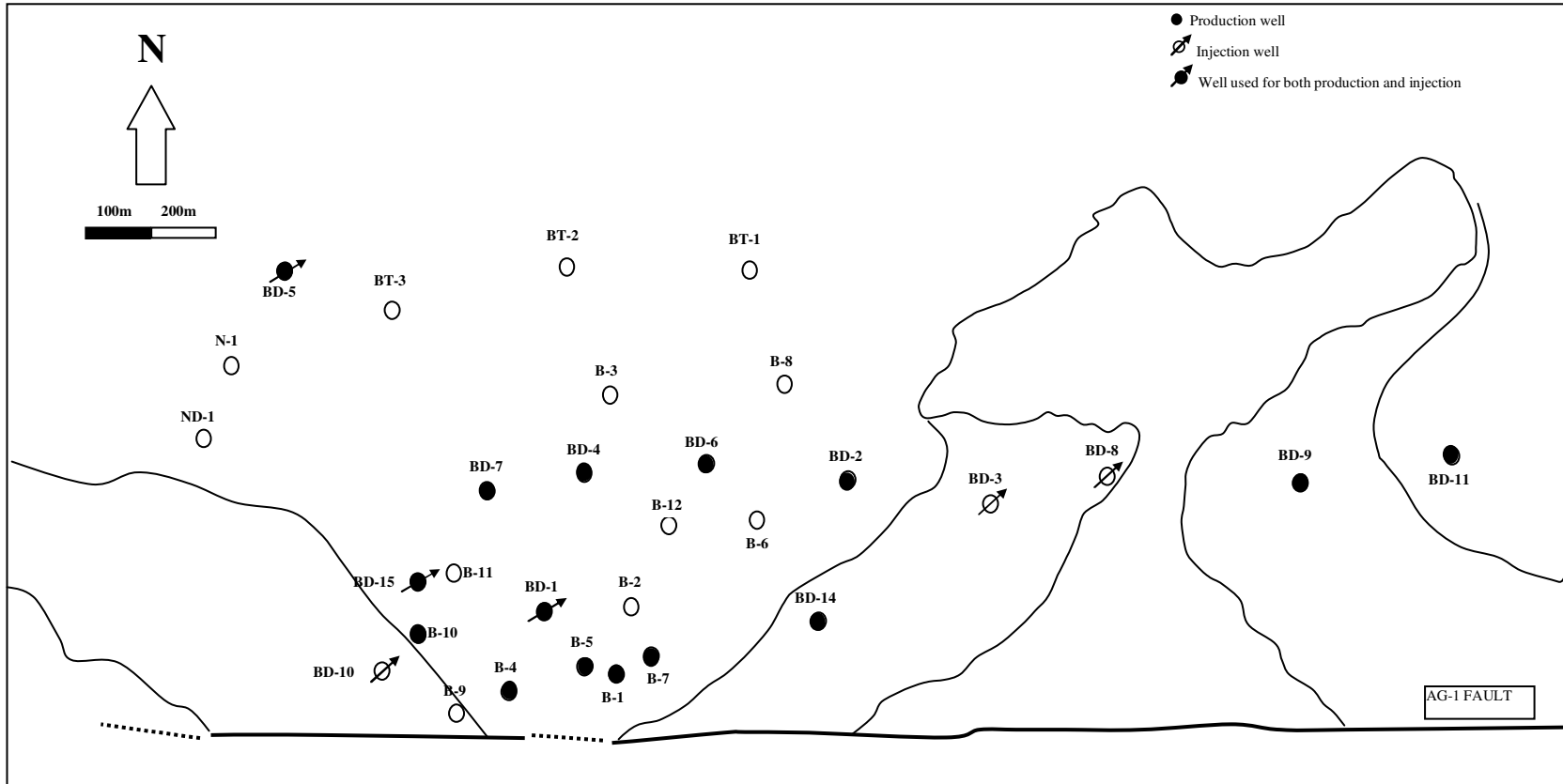


Figure 6.48- Production and injection wells used in Scenario-1.

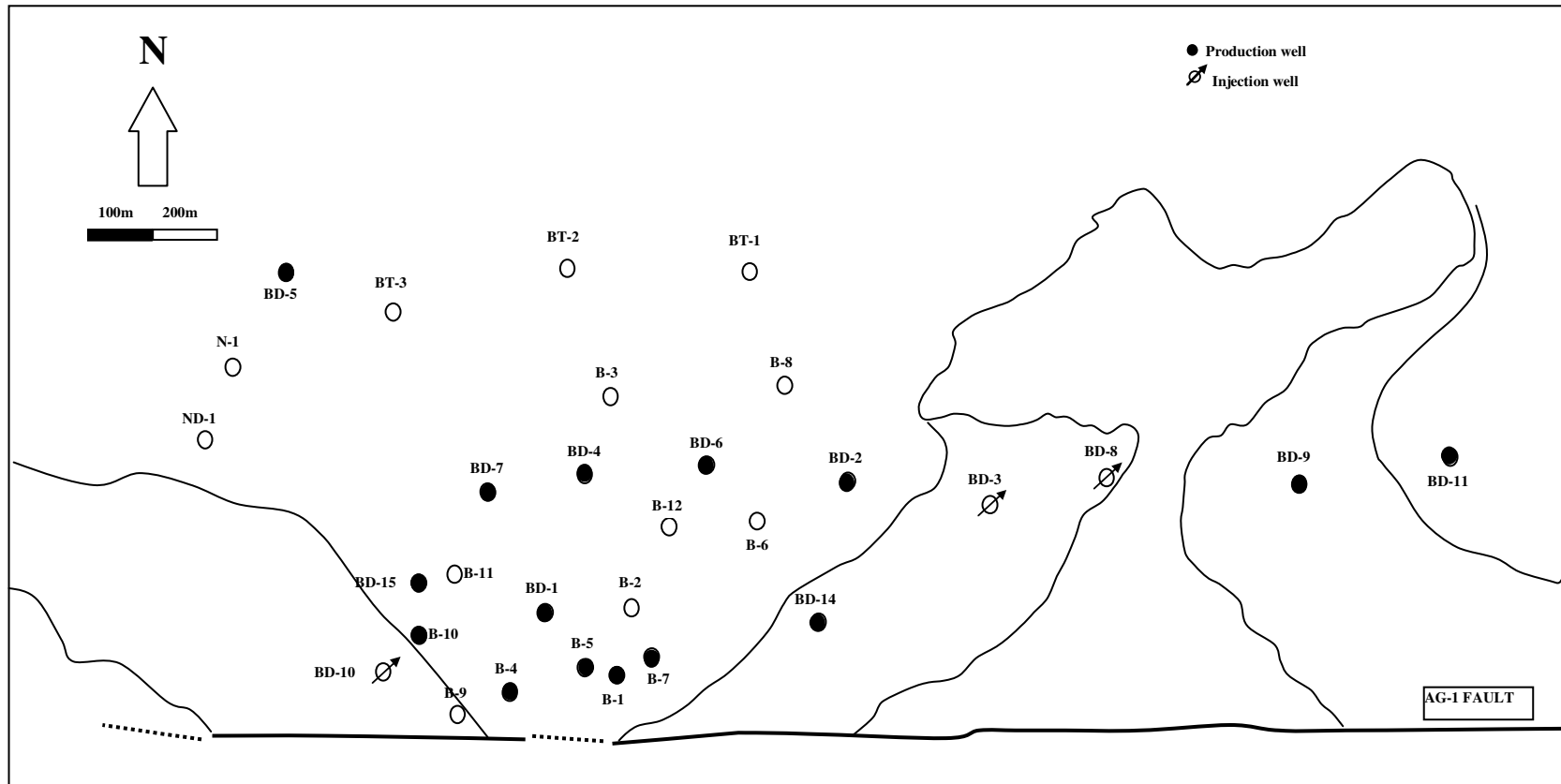


Figure 6.49- Production and injection wells used in Scenario-2.

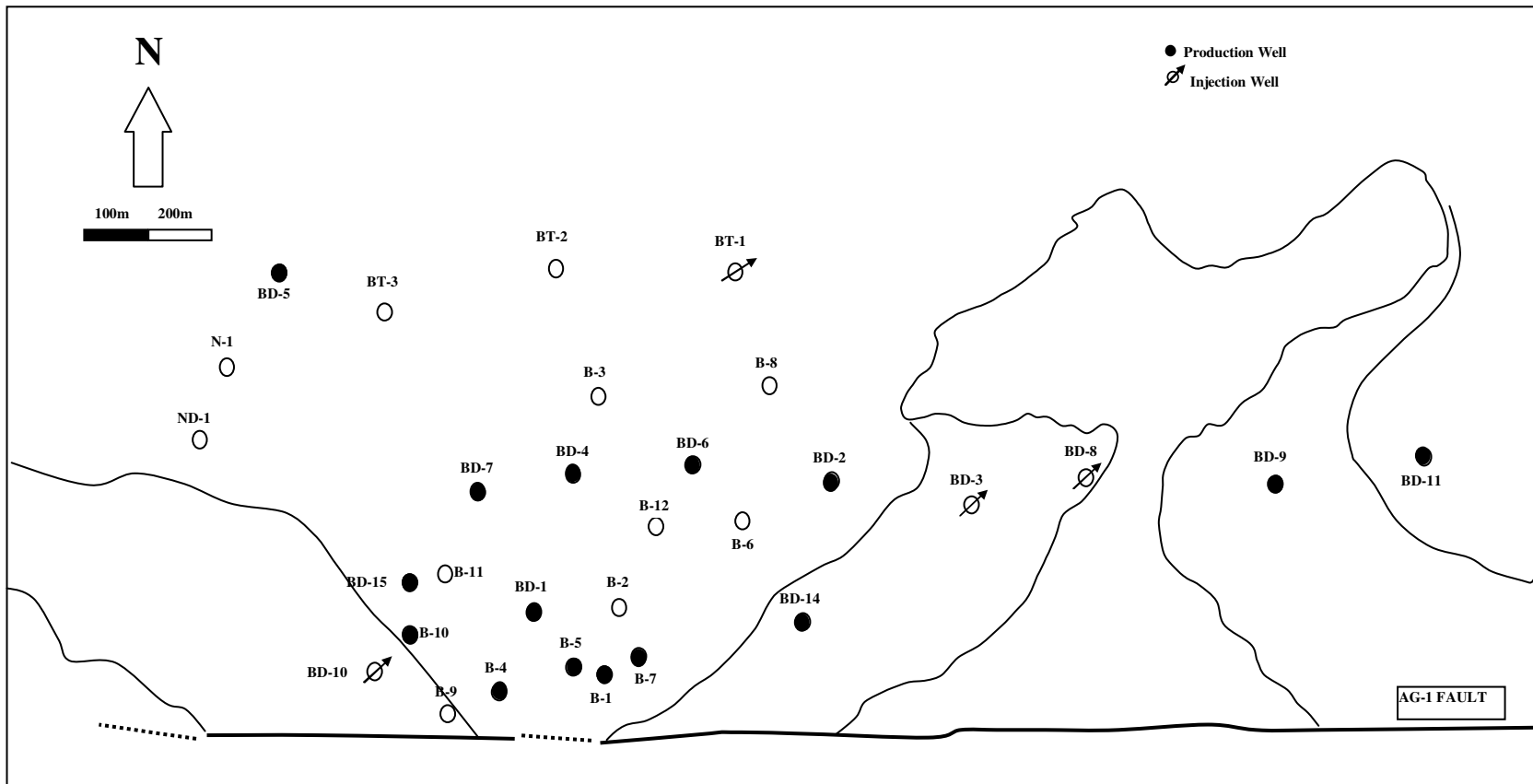


Figure 6.50- Production and injection wells used in Scenario-3.

In Scenario-1, areal temperature distributions at $z=0$, -15 , -85 , -350 , -550 and temperature distributions on cross-sections at $x=2500$, 2800 , 3000 , 3700 , 4400 were examined for years 2009, 2014, 2019, 2024 and 2029 (Figure 6.51 – 6.80). The following interpretations were made by analyzing the temperature distributions.

At cross-section of $x=2500$, continuous increase in temperature can be observed from 2009 to 2029. Increase in temperature starts from deeper parts and finally reaches to shallow parts. At layer $x=2800$, decrease in temperature in the region where most of the production carried out can be seen. Decrease in temperature at that region can be more observable at layer $x=3000$ and $x=3700$. The shallow part of layer $x=3700$ has temperature of around $70\text{ }^{\circ}\text{C}$.

At layers $z=0$ and $z= -15$, continuous decrease in temperature can be observed with time. The northern parts are hotter than the southern parts although opposite situation exists at initial condition. At layer $z=-85$, continuous decrease in temperature again can be seen. The hottest part takes place at the region where the wells B-5 and B-1 locate. Temperature decrease caused by injection of cold water can easily be observed at layers $z=-350$ and $z=-550$. It is clear that cold water that is mainly injected through BD-8 penetrates more to the western part. Increase in temperature observed at layer $x=2500$ can also seen at the west of these layers. As time passes, cold region extends to west and east part of the field but extends more to the west part where the most of the production is performed and as time passes the west part where ND-1 and BD-5 wells locate gets hotter.

Examination of temperature distribution in Scenario-1 gives the result that in such an injection and production scenario the water that is mainly injected through BD-8 and some of which is injected through BD-3 well directly flows through the production region and blocks some portion of the hot water that comes from eastern and deep parts. Thus, the hot water is directed to the west part of the field where almost no production or injection is performed and heats that region. Injected water also has effect on that region and cools the eastern part while hot water heats the western part.

That the injected water penetrates more to the western part is an expected result since most of the production is performed in that region and there is also flow of water to north in alluvium formation. The amount of water moving to one direction

may change depending on the location of the region from which hot water penetrates into the system. More data is needed to correctly determine the case.

At layers $z=0$ and $z=-15$, continuous decrease in temperature exists and the northern parts are hotter than the southern parts although reverse situation exists at initial condition. For the continuous decrease in temperature, there is effect of the injection through B-9 well in the early years of production, penetration of the surface water into the system and the injection through deep wells. Most of the production is done in wells B-5 and B-10 wells in shallow part. After produced from those wells, less cold water will flow to the northern part thus less cools that region compared to southern part. This may be the explanation of why northern parts are hotter in shallow zone.

Evaluating these information, it can be said that injection that will be performed in the region where BD-5 and ND-1 wells locate will prevent the hot water flowing to the western part and make it flow to production region.

In Scenario-2, areal temperature distributions at $z=0$, -15 , -85 , -350 , -550 and temperature distributions on cross-sections at $x=2500$, 2800 , 3000 , 3700 , 4400 were examined for years 2009, 2014, 2019 and 2024 (Figure 6.51 – 6.80). The following interpretations were made by analyzing the temperature distributions.

At layer $x=2500$, continuous increase in temperature with time can be observed from 2009 to 2029. Increase in temperature starts from deeper parts and finally reaches to shallow parts. At layer $x=2800$, decrease in temperature in the region where most of the production carried out can be seen. Decrease in temperature at that region can be more observable at layer $x=3000$ and $x=3700$. The shallow part of layer $x=3700$ has temperature of around 70 C.

At layers $z=0$ and $z=-15$, continuous decrease in temperature can be observed with time. The northern parts are hotter than the southern parts although reverse situation exists at initial condition. At layer $z=-15$, the region where B-10 well locates cools more than the region where B-5 well locates. This may be the result of cold water injection performed through well BD-10. (% 6.5 of total injection was performed through this well in year 2008). At layer $z=-85$, continuous decrease in temperature again can be seen. The hottest part takes place at the region where the wells B-5 and B-1 locate. Temperature decrease caused by injection of cold water can easily be observed at layers $z=-350$ and $z=-550$. Cold water that is mainly

injected through BD-8 penetrates more to the western part. Increase in temperature observed at layer $x=2500$ can also be seen at the west of these layers. As time passes, cold region extends to west and east part of the field but extends more to the west part where the most of the production is performed and as time passes the west part where ND-1 and BD-5 wells locate gets hotter.

The results obtained from Scenario-1 and Scenario-2 are similar. They have same kind of temperature distribution, increase and decrease in temperatures happen in the same manner. The difference is on the value of the temperatures. For example, at layer $x=2500$, the second model has higher temperatures than the first model. It can be observed that temperature decreases more sharply (especially in deeper parts) in the second model at layers $x=3000$ and $x=3700$. This is an expected result since more water is injected and produced. The second model has higher temperatures at layer $z=-15$ in years 2019 and 2024. That the cold water moves more to the deeper wells and so less to the shallow wells in the second model may be the explanation of this situation. Thus, compared to the first model, the deep wells cool more, shallow wells cool less but as less water flows to the shallow wells pressures around these wells decrease more in the second model. In both two models injection performed through deep wells blocks the hot water coming from deep eastern part and makes them move to the western part. This event is more clear in the second model as western deep parts are hotter and the region where most of the production is performed is cooler compared to the first model.

In these two models it is clear that some hot water flows through the west part of the field in which almost no production or injection is done and heats that region. A solution must be introduced to make this hot water to flow through the production region. Injection done through that region will prevent the hot water to gravitate to west part and thus it will flow through the production region but how much water will be injected through that region in that case is a point that must be considered. Another solution is to produce water from that region. In that case, cold water injected through deep wells will flow more through that region and cool it. How much injected water will flow and how much it cools that region is another point that must be considered.

In Scenario-3, areal temperature distributions at $z=0, -15, -85, -350, -550$ and temperature distributions on cross-sections at $x=2500, 2800, 3000, 3700, 4400$ were examined for years 2009, 2014 and 2019 (Figure 6.51 - 6.80). The following interpretations were made by analyzing the temperature distributions.

At layer $x=2500$, different from model 1 and 2, continuous decrease in temperature exists with time. At layer $x=3000$, continuous decrease in temperature can be observed for the deep part. This is related to cold water that is injected through that new well at the depth 1000 m. At layer $x=3700$, the region between the depths 800 m and 1000 is hotter than the same region of the second model. Continuous temperature decrease again can be seen in that part. At layer $z=-350$, cold water zone occupies less area compared to the second model. The region where most of the production wells crosses is hotter in the third model and hot zone extends more at east but the west part is colder as it can also be observed at layer $x=2500$. At layer $z=-550$, the same situation can also be observed. Hot zone that is represented with red color extends more at east in the third model but the west part is cooler. At layer $z=-15$, the regions where B-10 and B-5 wells occupies is a little bit hotter in the second model. It is important to notice that most of the production is done in wells B-10 and B-5 in shallow part.

In the first two models, water mainly injected through BD-8 and BD-3 wells blocks the hot water coming from deep parts and make it flow to western part as it flows to west it heats that region. However, in the third model, as the injection Scenario changes, some portion of the water is injected at the depth 1000 m through the new well taking place at the location of BT-1 well. This water cools the deep parts where it is injected and flowing to west cools the west part. Since it is directed to the west, the amount of cold water directed to east is reduced instead of that portion mainly hot water flows through that east part. This may be the explanation of why the east parts are hotter in the third model compared to the second model. Compared to the second model, less amount of water is injected through BD-8 so more hot water flows to the regions, especially to east portions, which are in the effect of cold water injected through BD-8 and BD-3 wells and heats that region more.

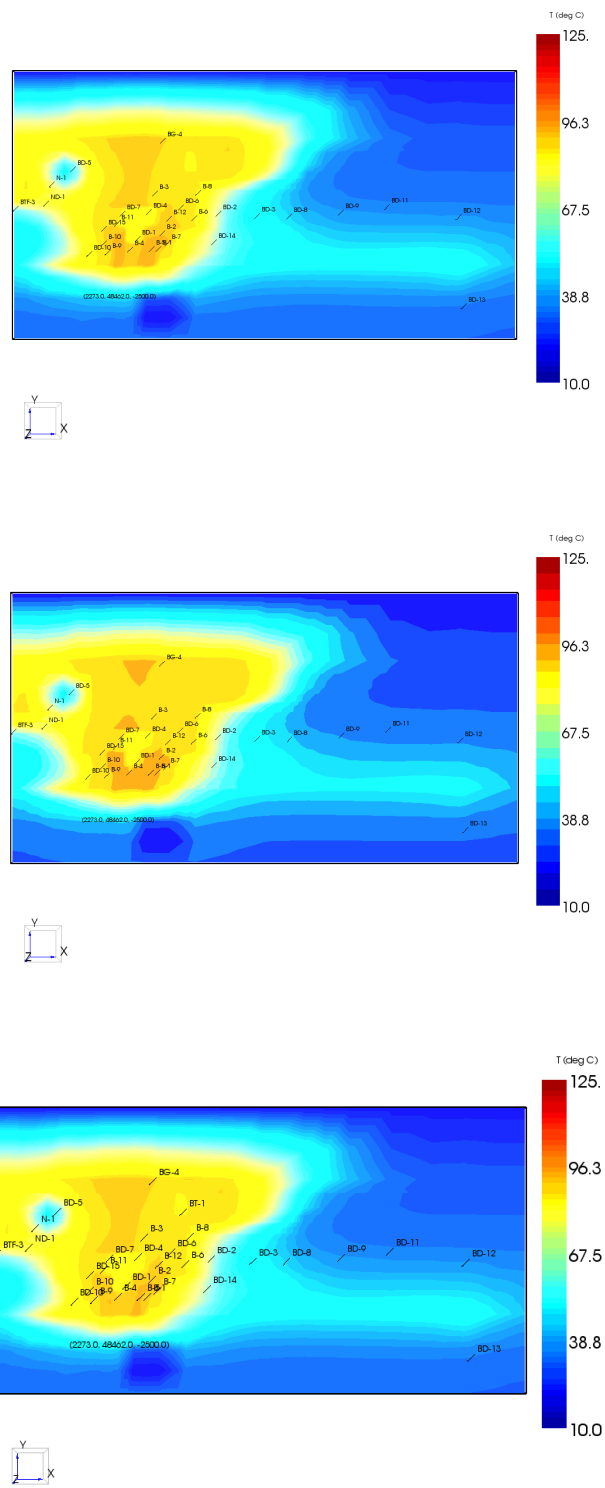


Figure 6.51- The areal temperature profile for cross-section Z=0 and year 2014 (Scenario 1, 2, 3).

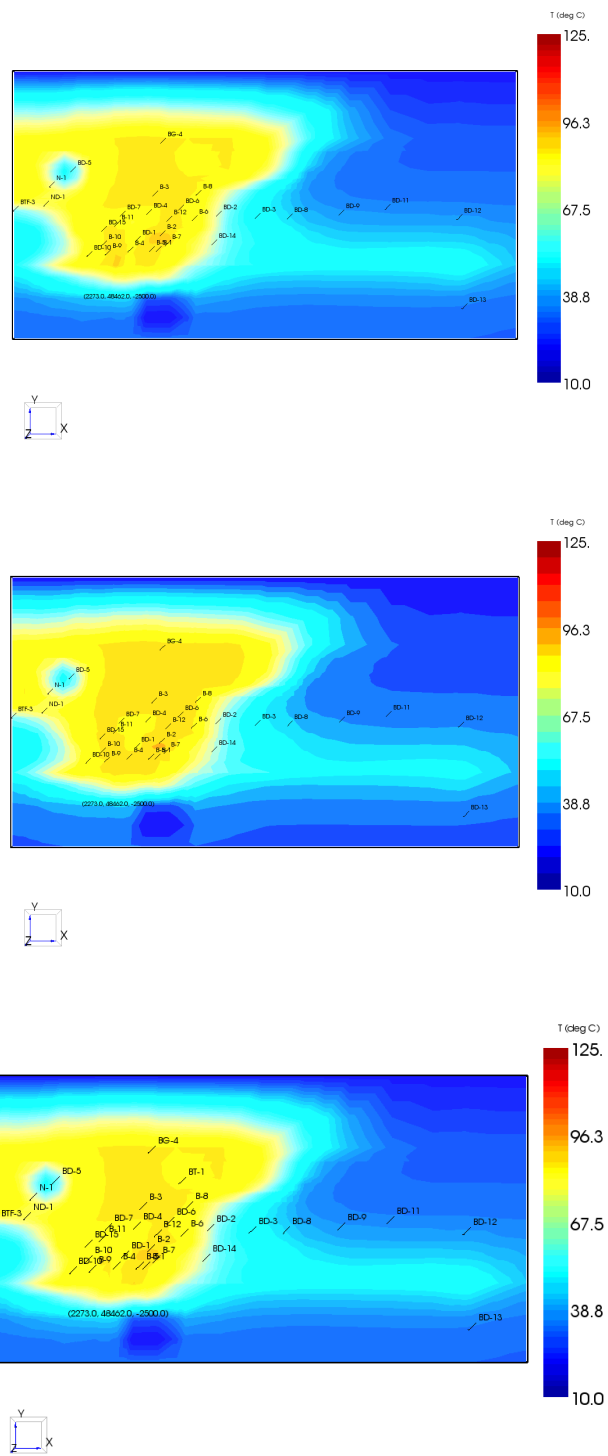


Figure 6.52- The areal temperature profile for cross-section Z=0 and year 2019 (Scenario 1, 2, 3).

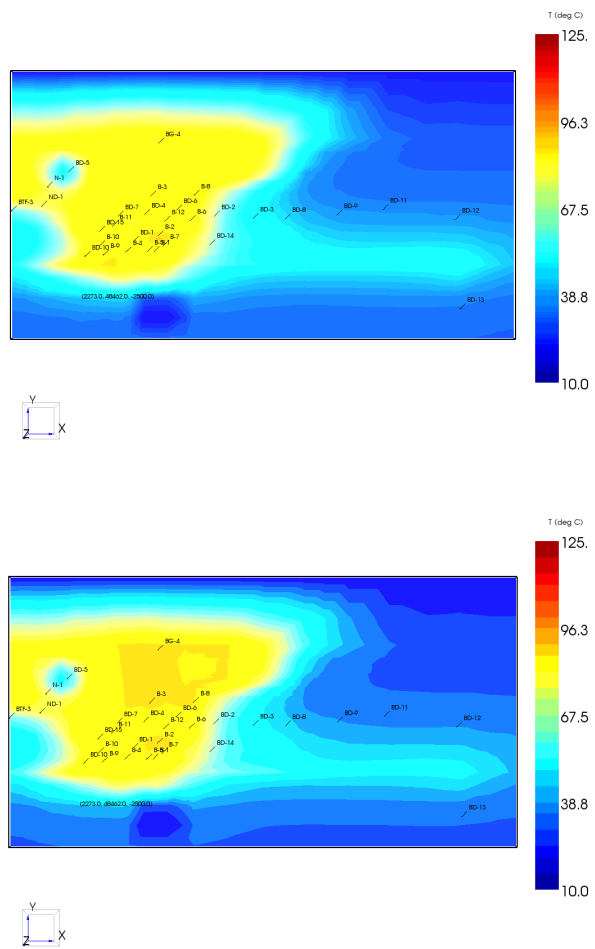


Figure 6.53- The areal temperature profile for cross-section Z=0 and year 2024 (Scenario 1, 2).

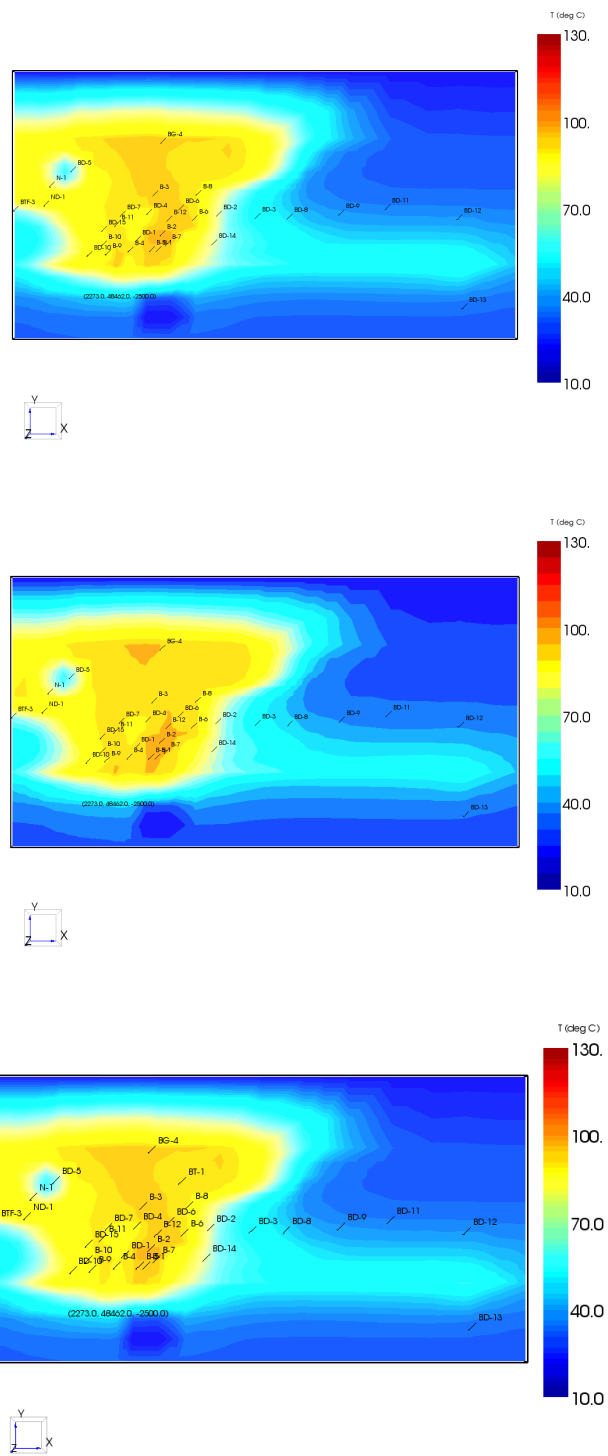


Figure 6.54- The areal temperature profile for cross-section Z=-15 and year 2014 (Scenario 1, 2, 3).

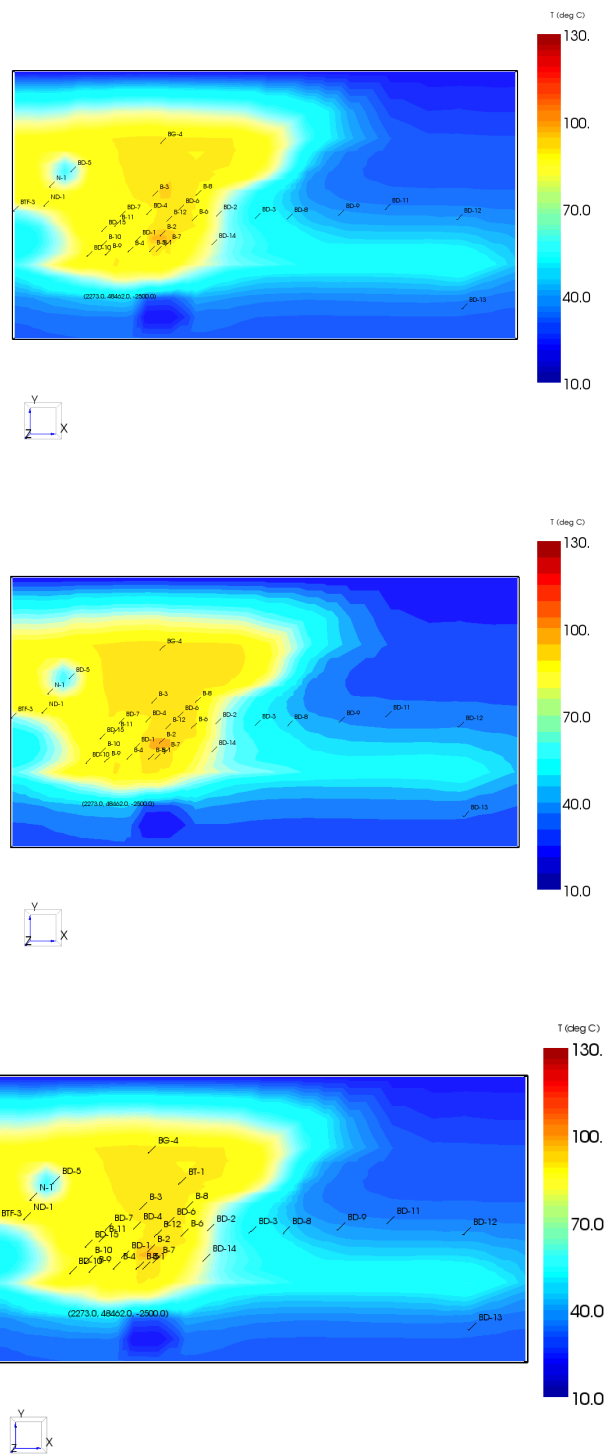


Figure 6.55- The areal temperature profile for cross-section Z=-15 and year 2019 (Scenario 1, 2, 3).

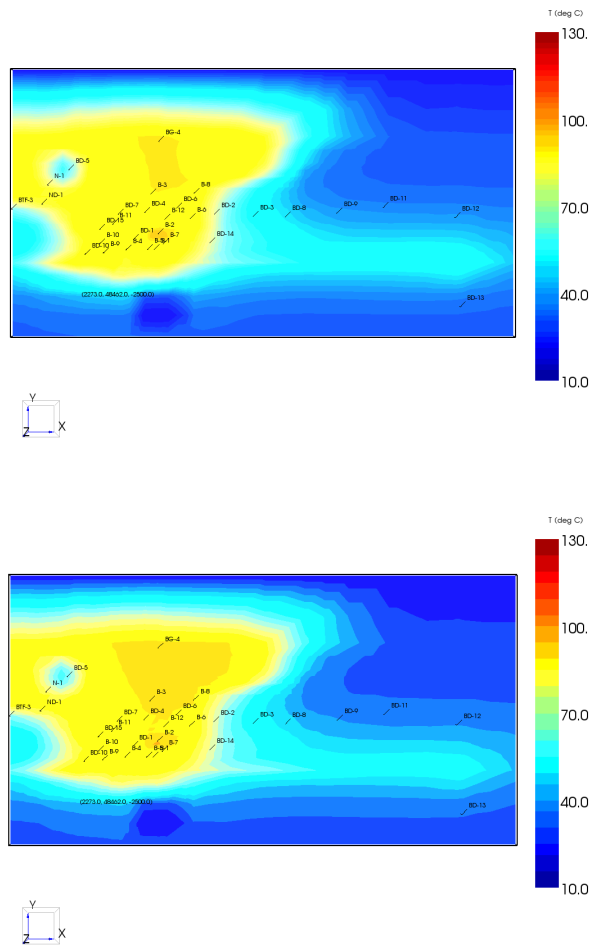


Figure 6.56- The areal temperature profile for cross-section Z=-15 and year 2024 (Scenario 1, 2).

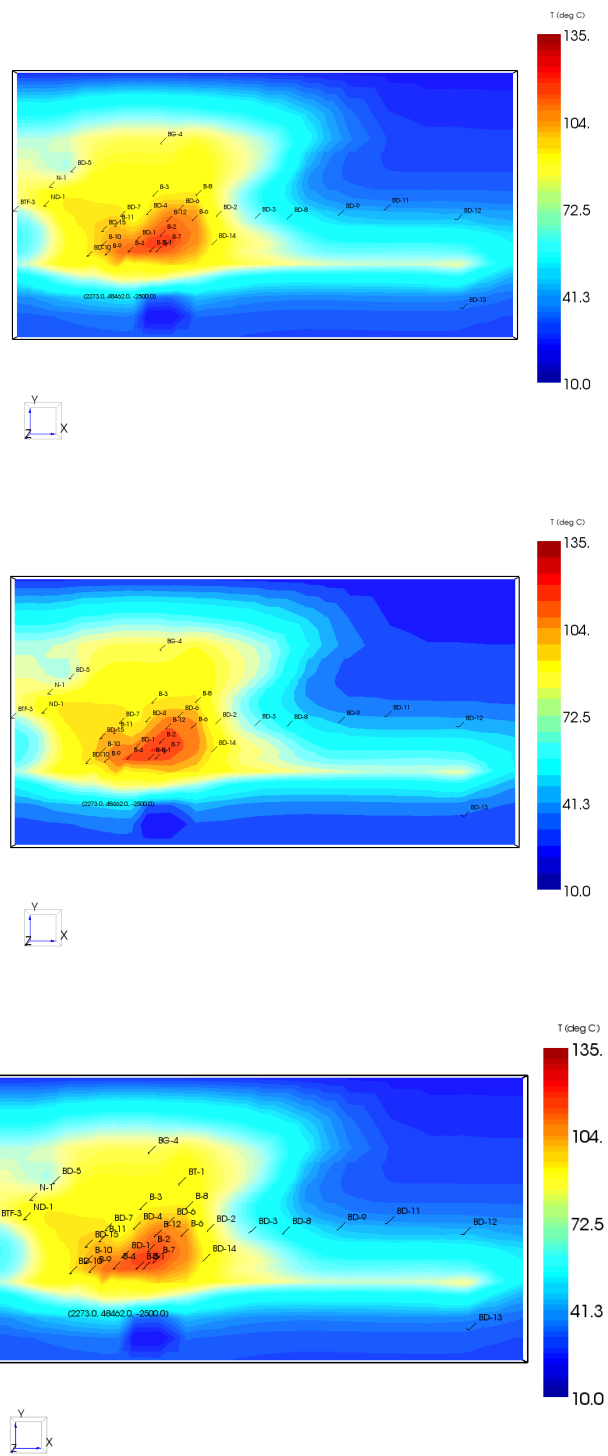


Figure 6.57- The areal temperature profile for cross-section Z=-85 and year 2014 (Scenario 1, 2, 3).

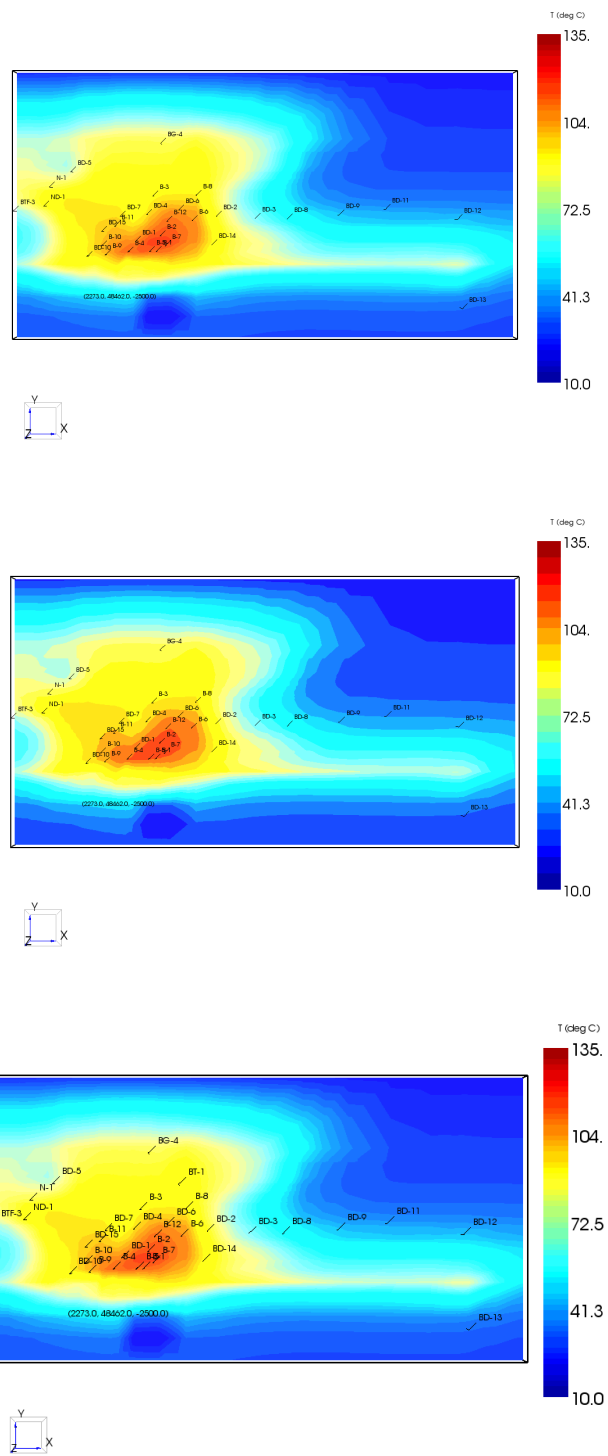


Figure 6.58- The areal temperature profile for cross-section Z=-85 and year 2019 (Scenario 1, 2, 3).

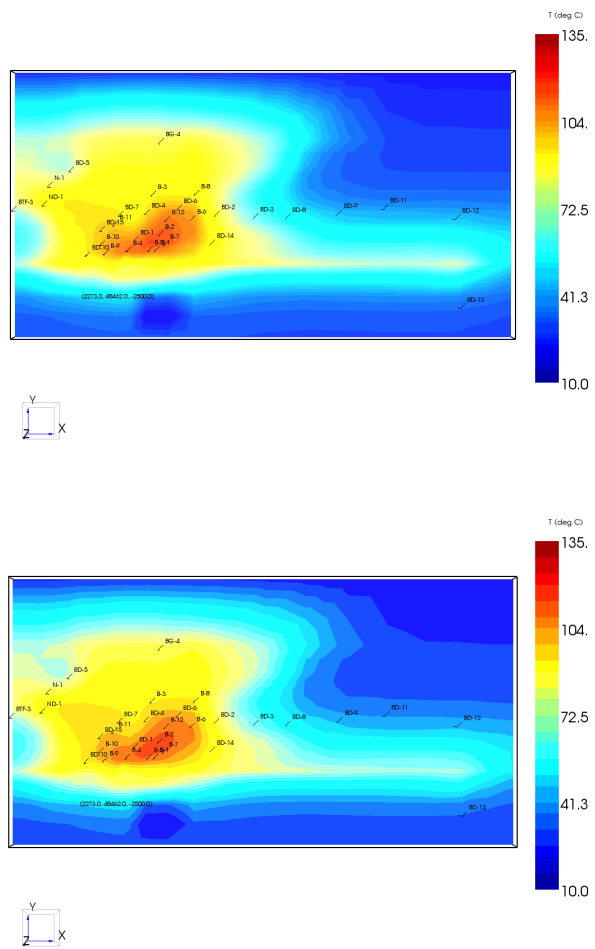


Figure 6.59- The areal temperature profile for cross-section Z=-85 and year 2024 (Scenario 1, 2).

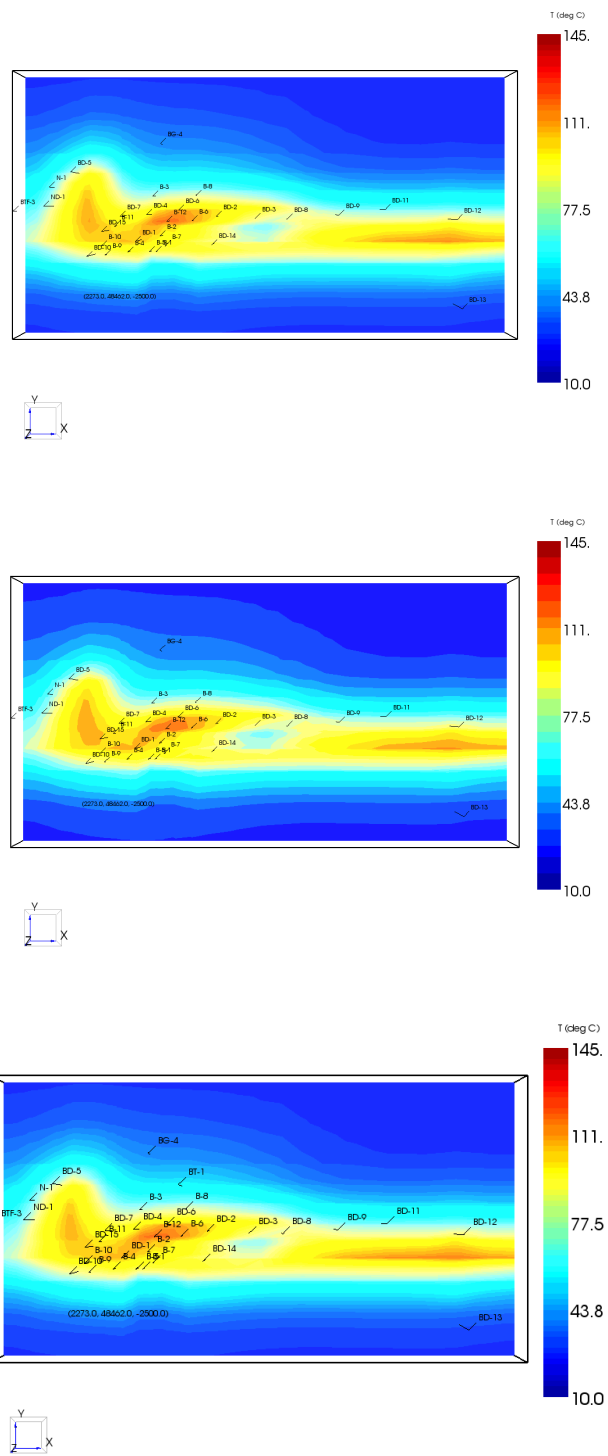


Figure 6.60- The areal temperature profile for cross-section Z=-350 and year 2014 (Scenario 1, 2, 3).

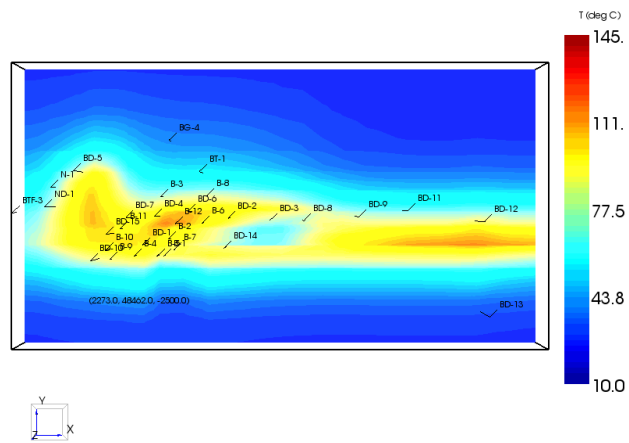
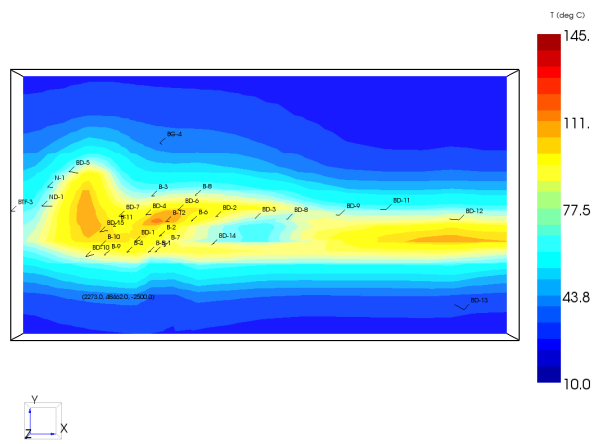
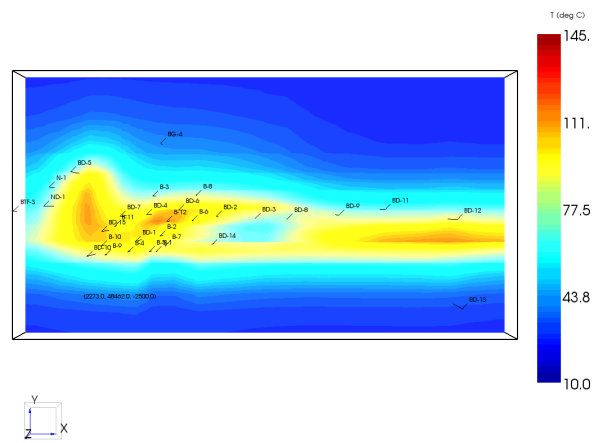


Figure 6.61- The areal temperature profile for cross-section Z=-350 and year 2019 (Scenario 1, 2, 3).

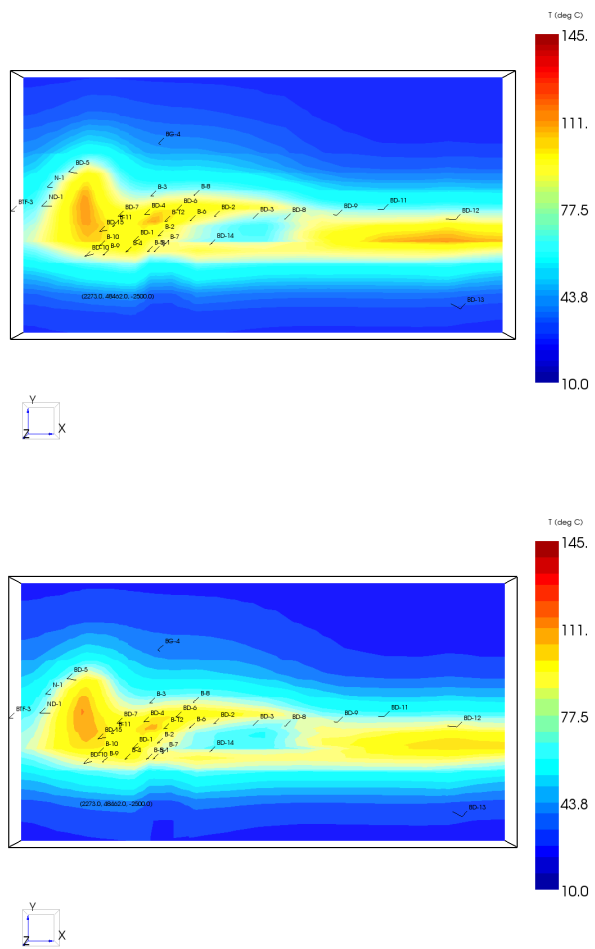


Figure 6.62- The areal temperature profile for cross-section Z=-350 and year 2024 (Scenario 1, 2).

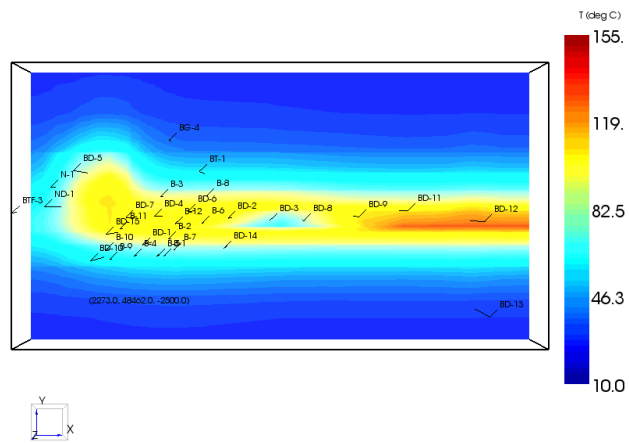
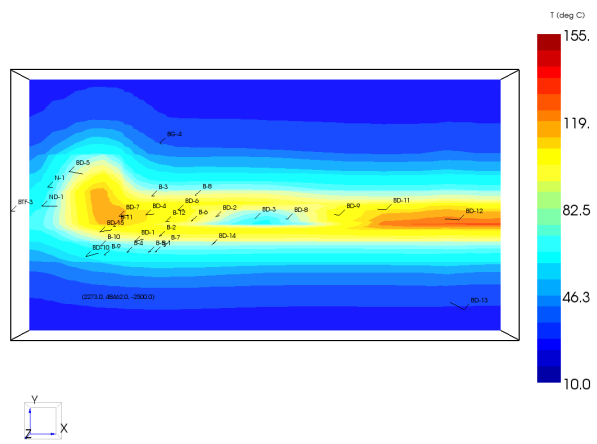
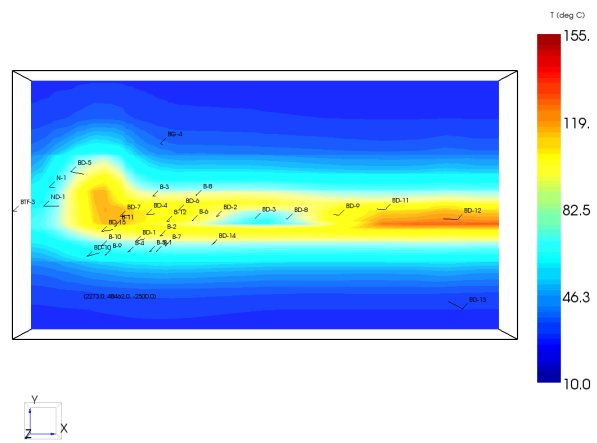


Figure 6.63- The areal temperature profile for cross-section Z=-550 and year 2014 (Scenario 1, 2, 3).

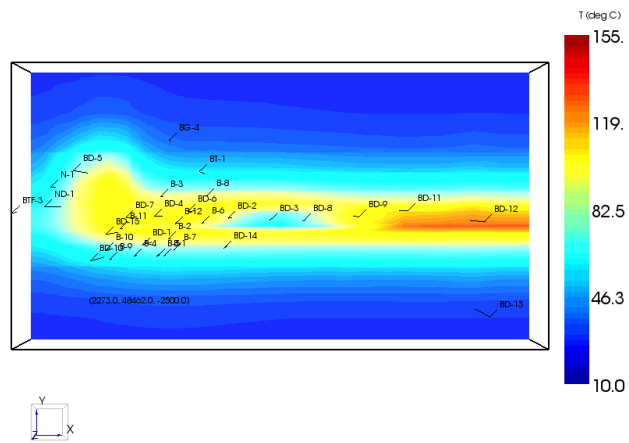
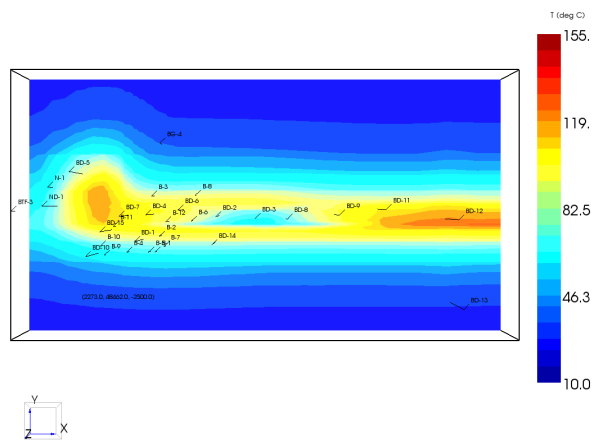
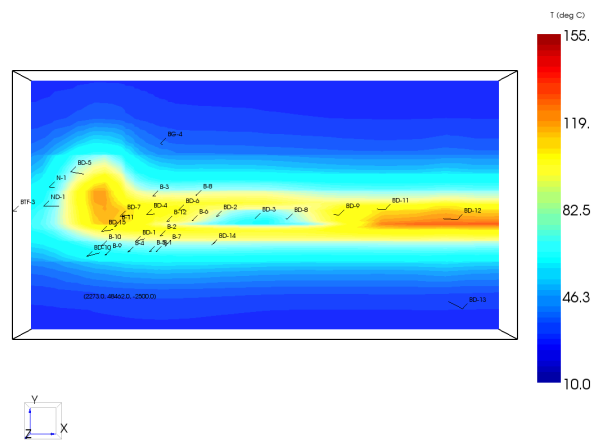


Figure 6.64- The areal temperature profile for cross-section Z=-550 and year 2019 (Scenario 1, 2, 3).

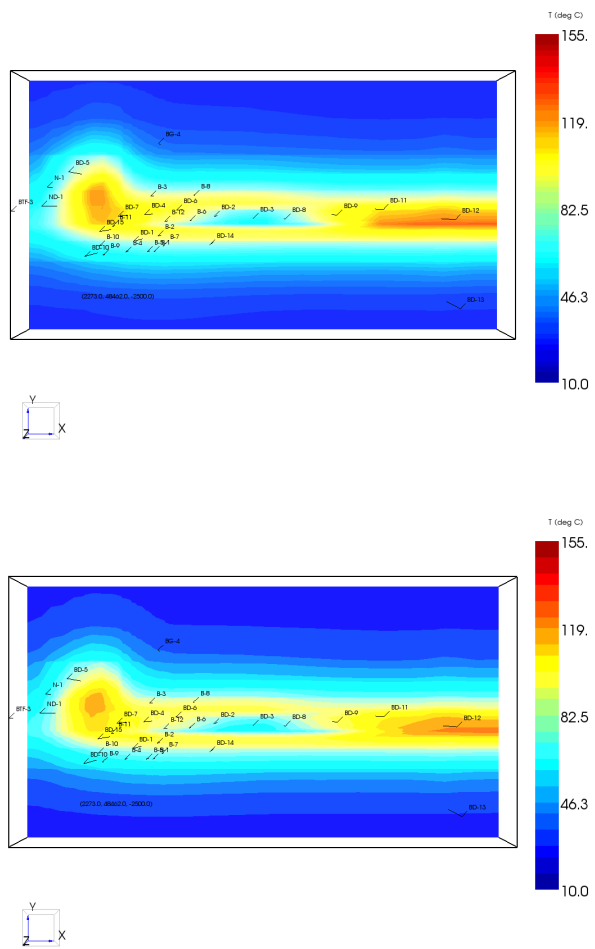


Figure 6.65- The areal temperature profile for cross-section Z=-550 and year 2024 (Scenario 1, 2).

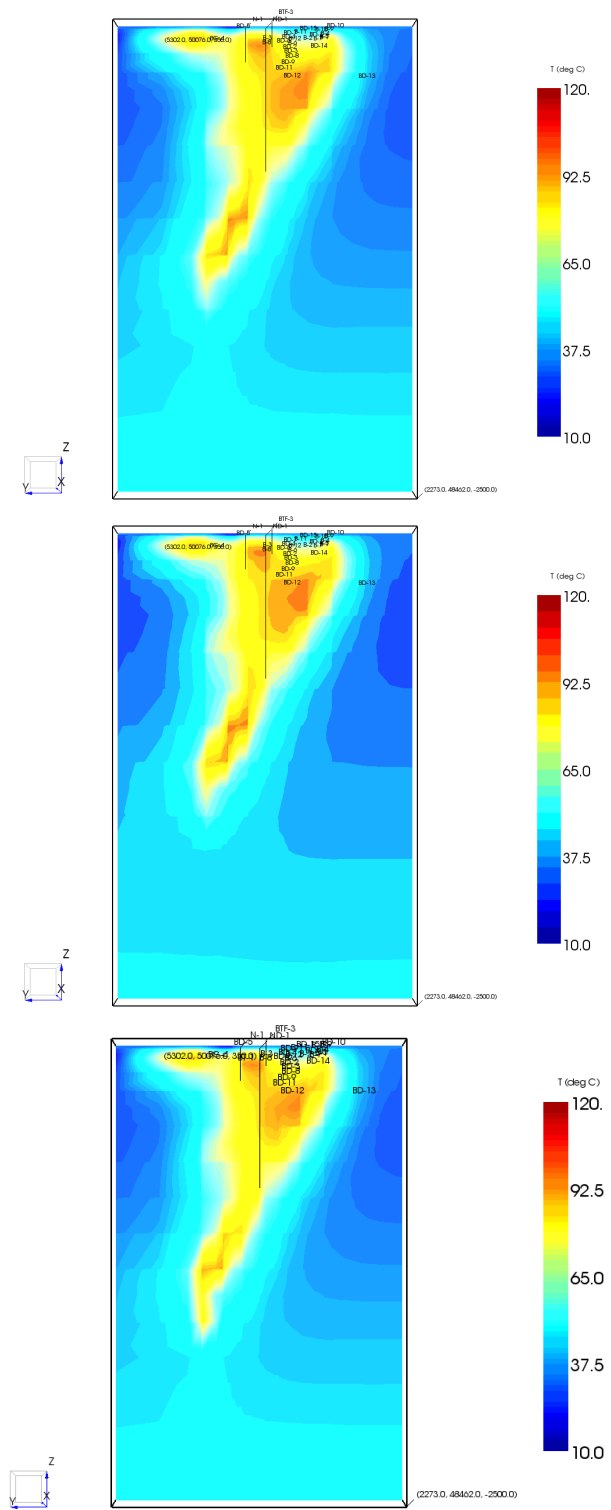


Figure 6.66- The areal temperature profile for cross-section X=2500 and year 2014 (Scenario 1, 2, 3).

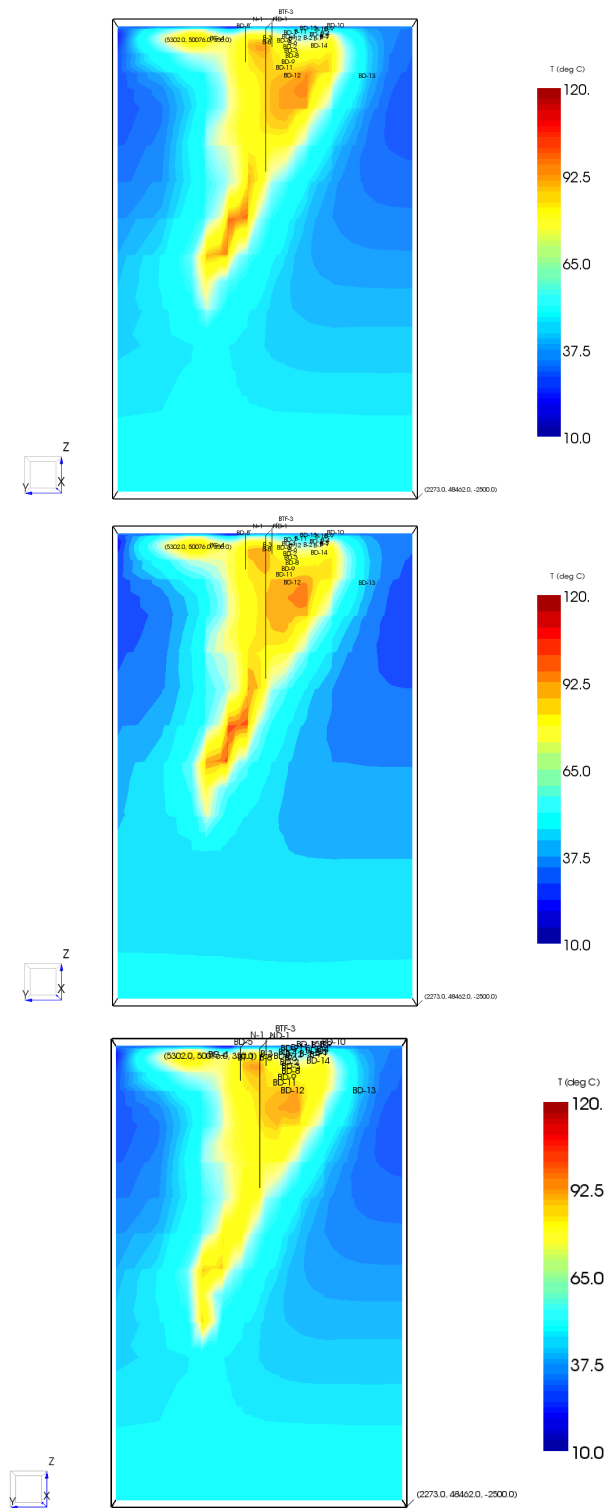


Figure 6.67- The areal temperature profile for cross-section X=2500 and year 2019 (Scenario 1, 2, 3).

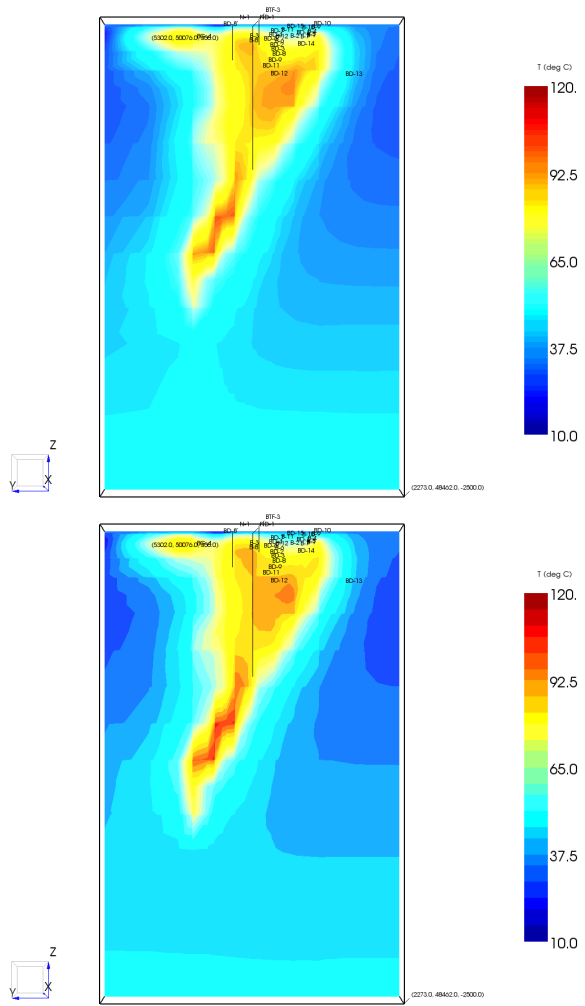


Figure 6.68- The areal temperature profile for cross-section X=2500 and year 2024 (Scenario 1, 2).

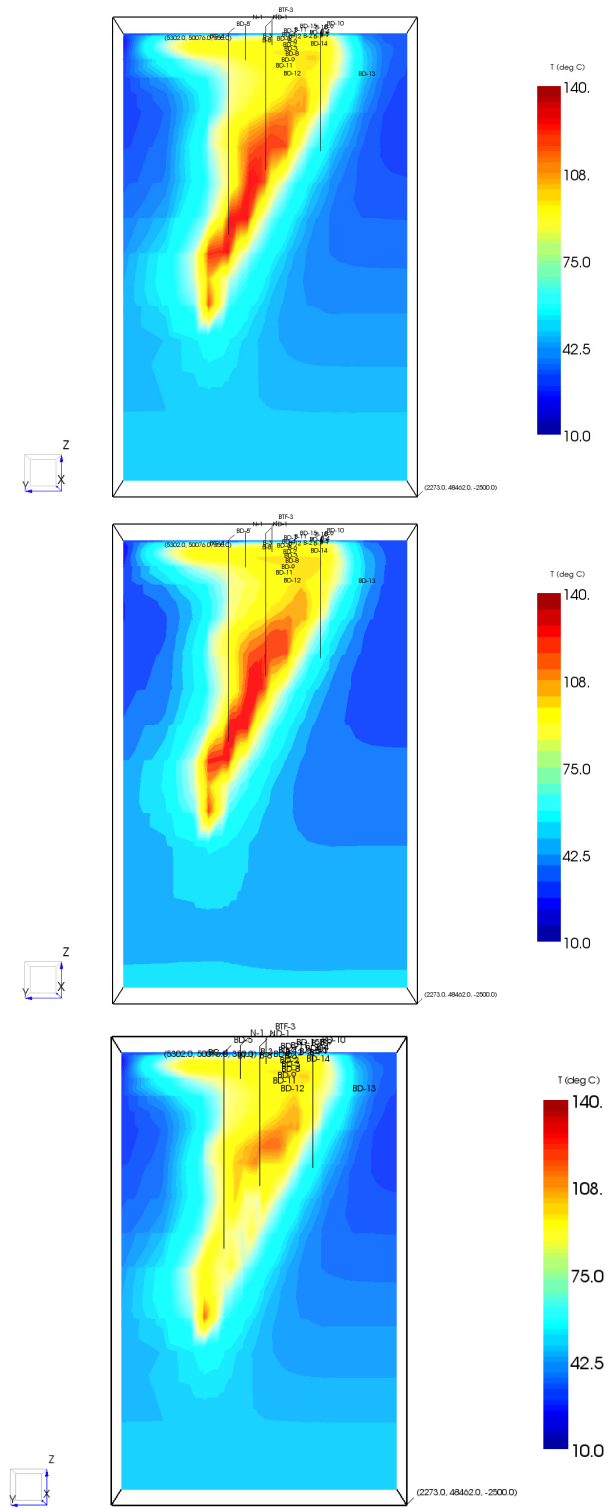


Figure 6.69- The areal temperature profile for cross-section X=2800 and year 2014 (Scenario 1, 2, 3).

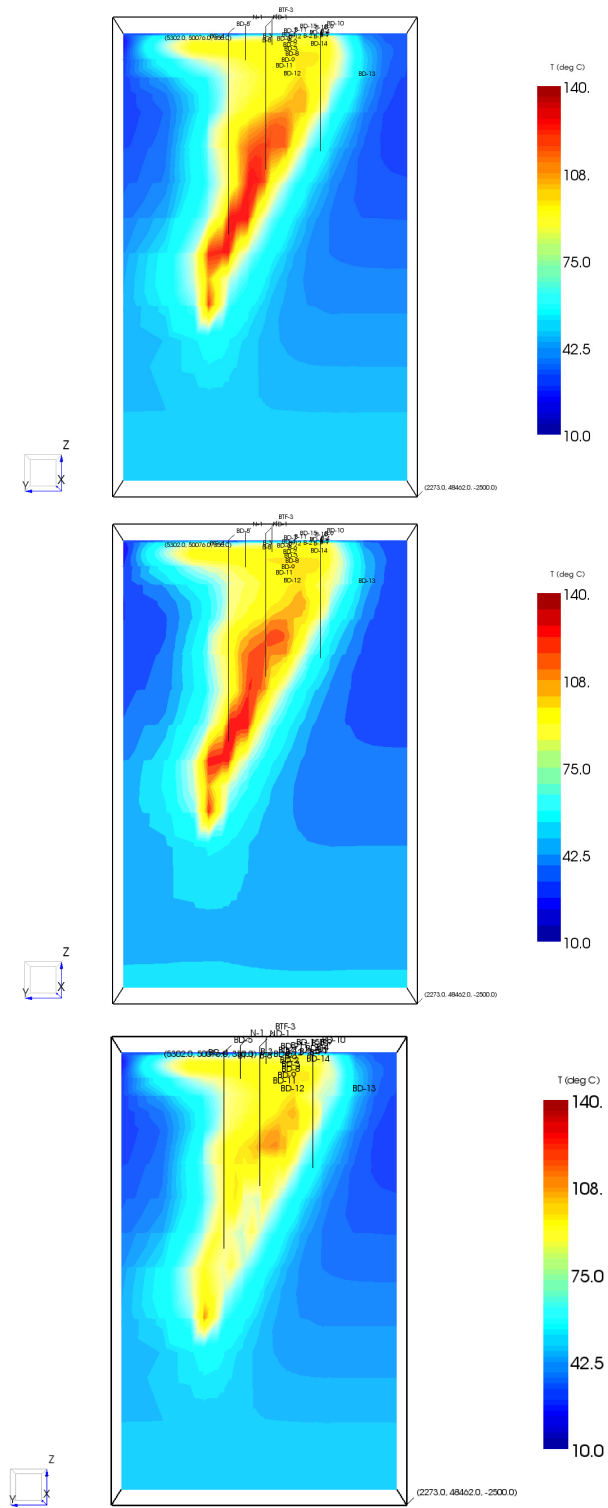


Figure 6.70- The areal temperature profile for cross-section X=2800 and year 2019 (Scenario 1, 2, 3).

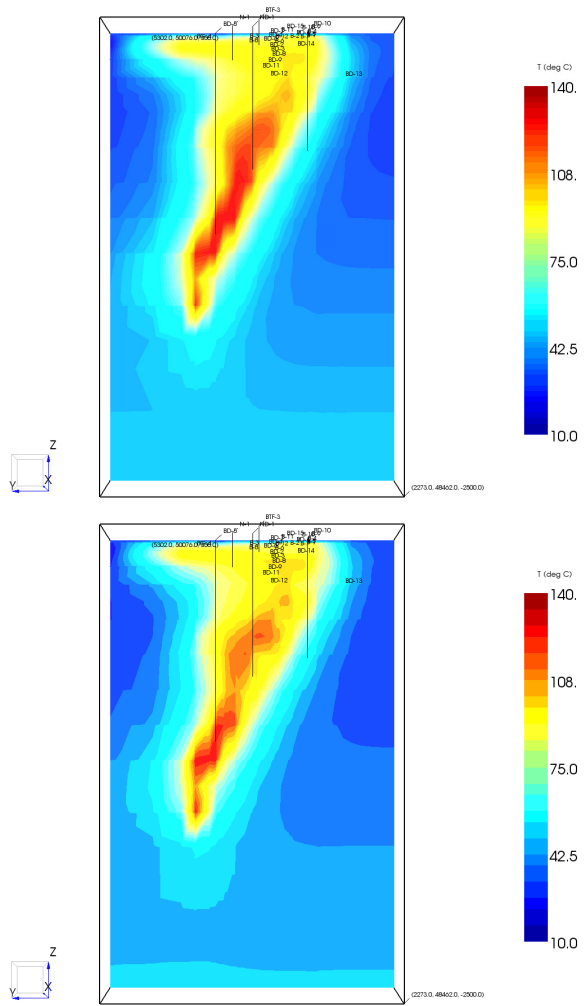


Figure 6.71- The areal temperature profile for cross-section X=2800 and year 2024 (Scenario 1, 2, 3).

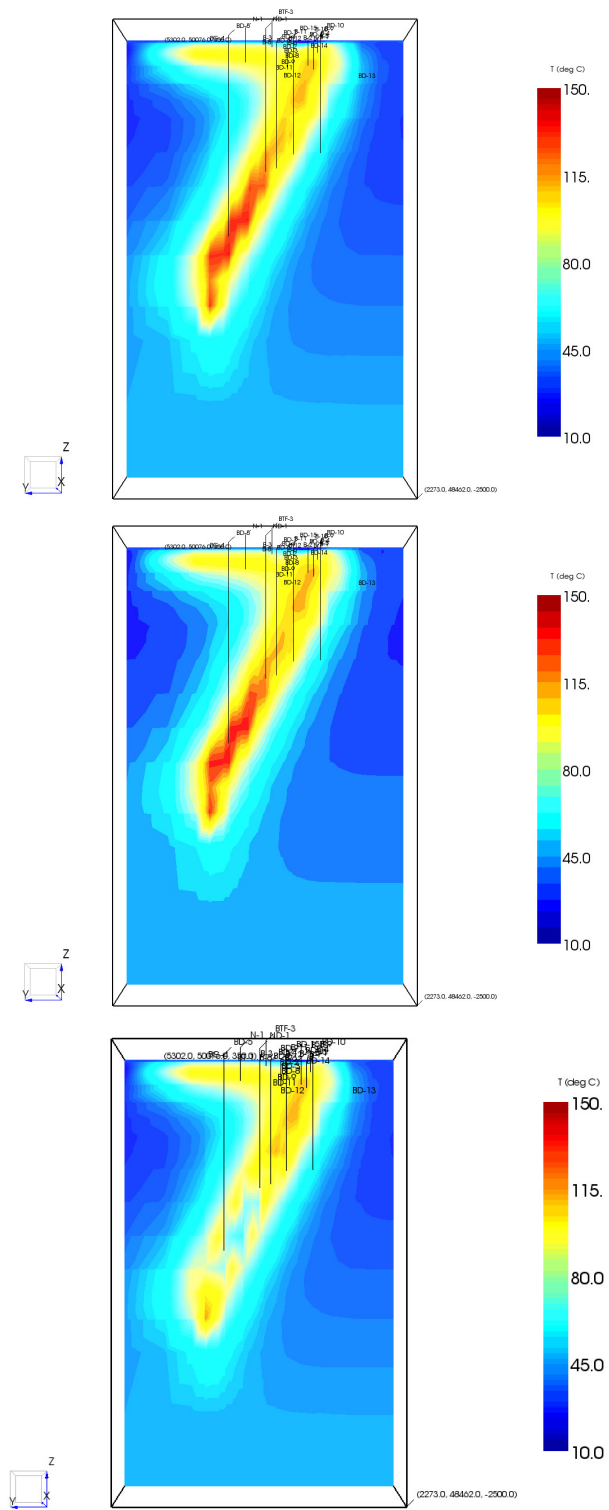


Figure 6.72- The areal temperature profile for cross-section X=3000 and year 2014 (Scenario 1, 2, 3).

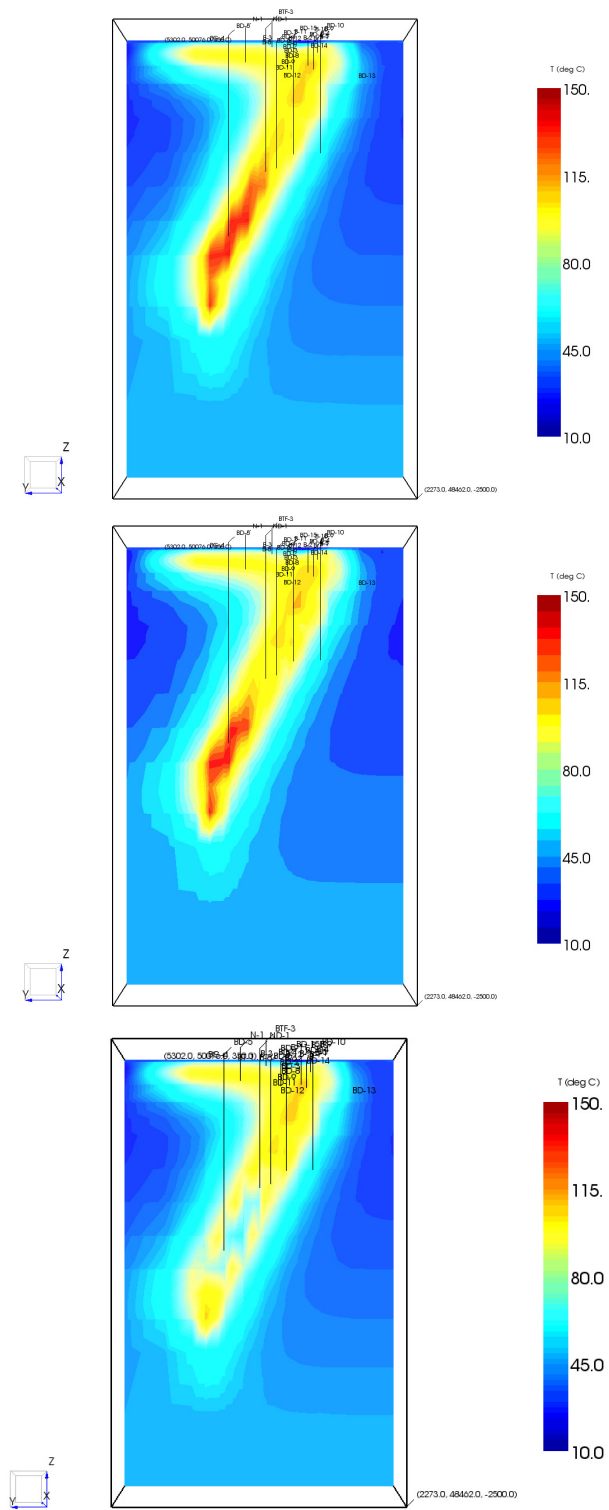


Figure 6.73- The areal temperature profile for cross-section X=3000 and year 2019 (Scenario 1, 2, 3).

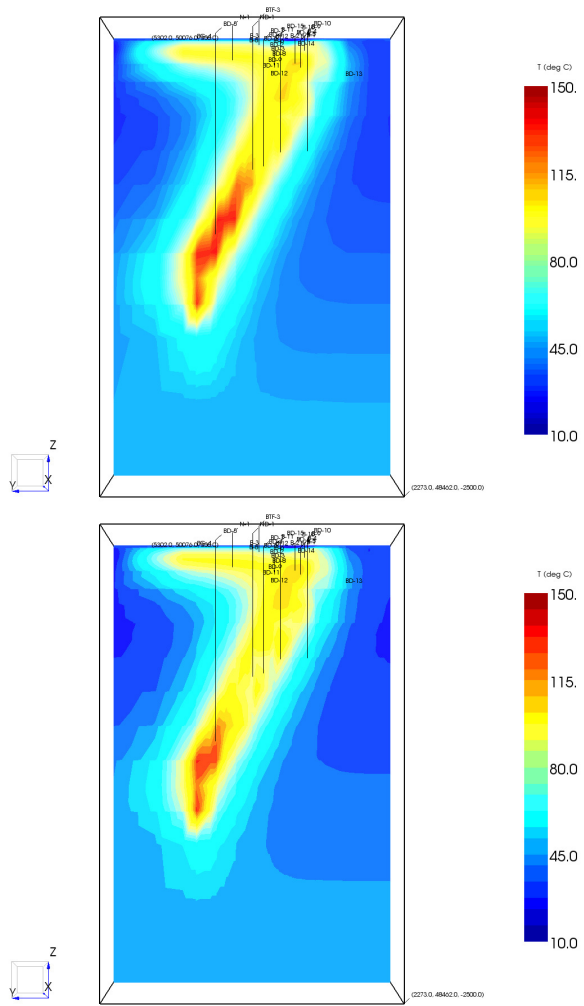


Figure 6.74- The areal temperature profile for cross-section X=3000 and year 2024 (Scenario 1, 2).

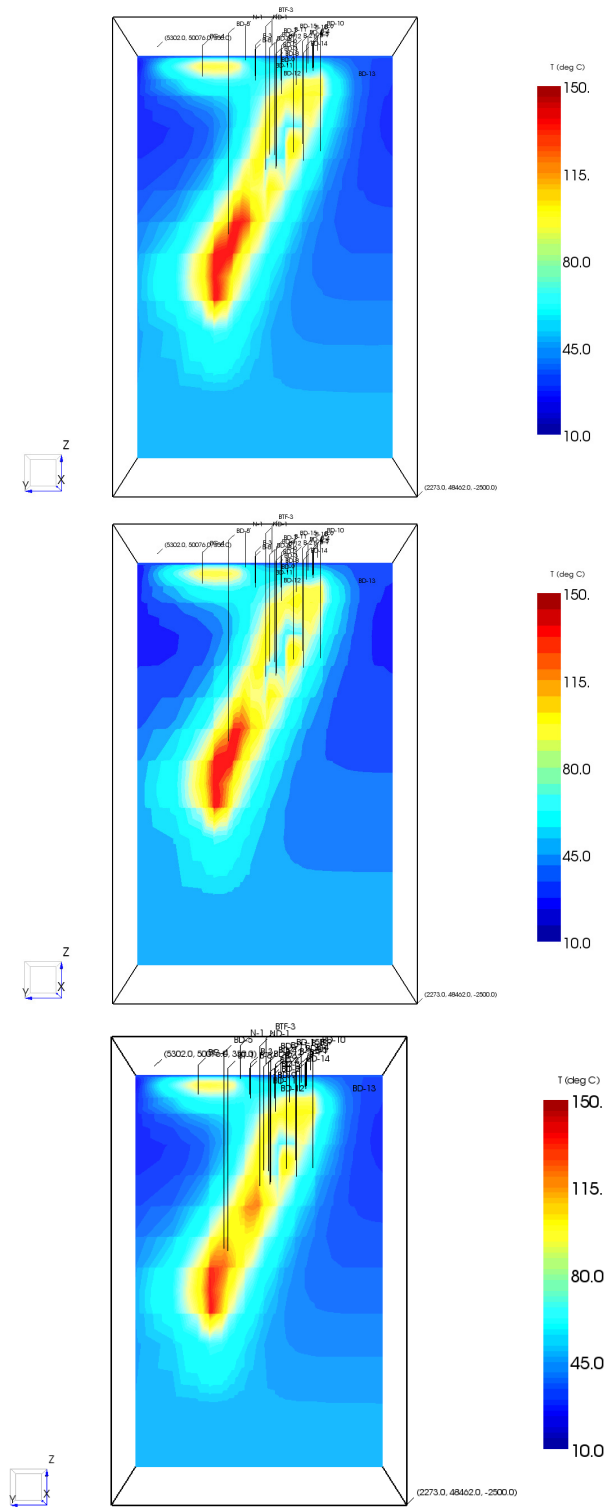


Figure 6.75- The areal temperature profile for cross-section X=3700 and year 2014 (Scenario 1, 2, 3).

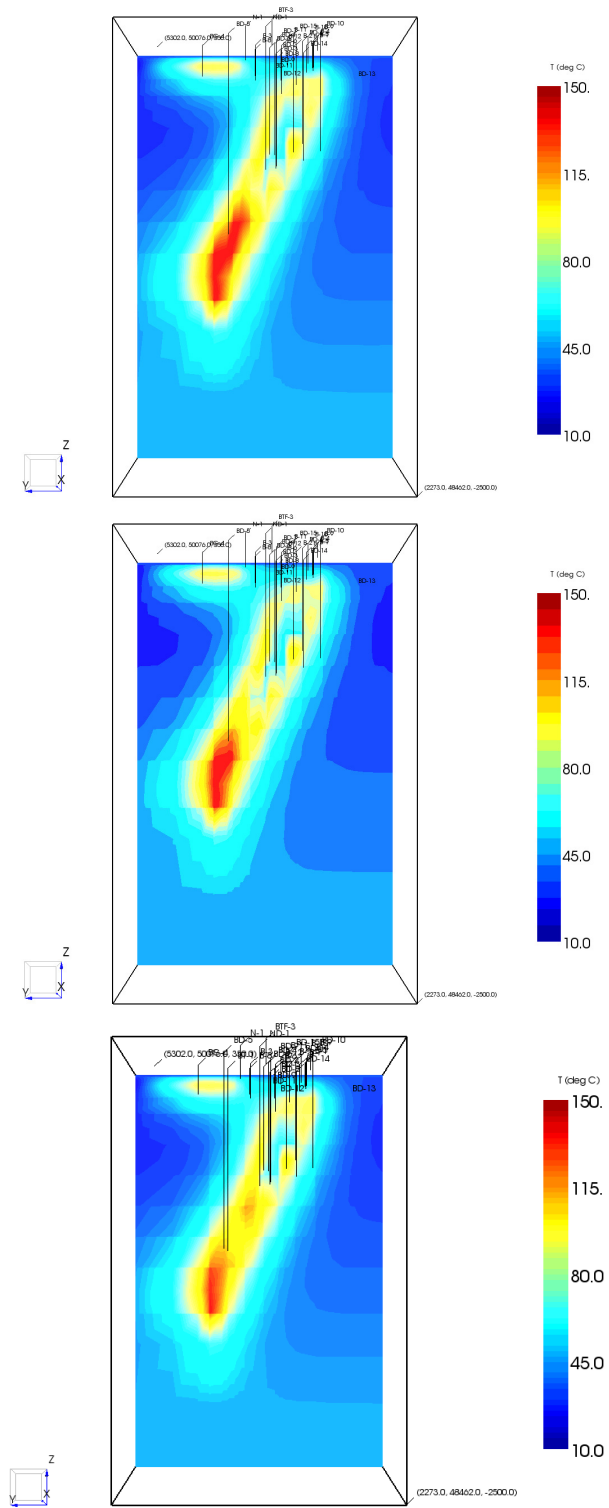


Figure 6.76- The areal temperature profile for cross-section X=3700 and year 2019 (Scenario 1, 2, 3).

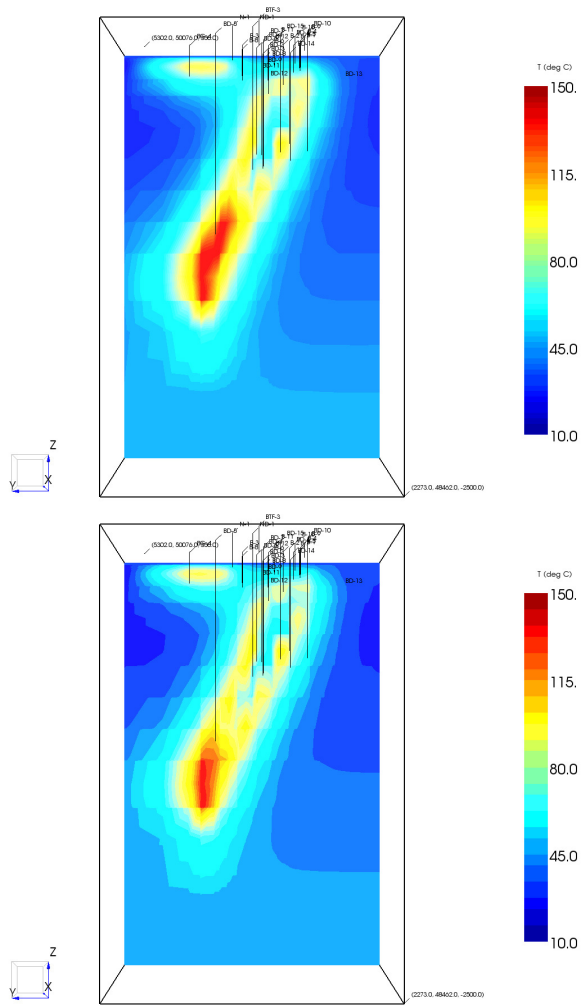


Figure 6.77- The areal temperature profile for cross-section X=3700 and year 2024 (Scenario 1, 2).

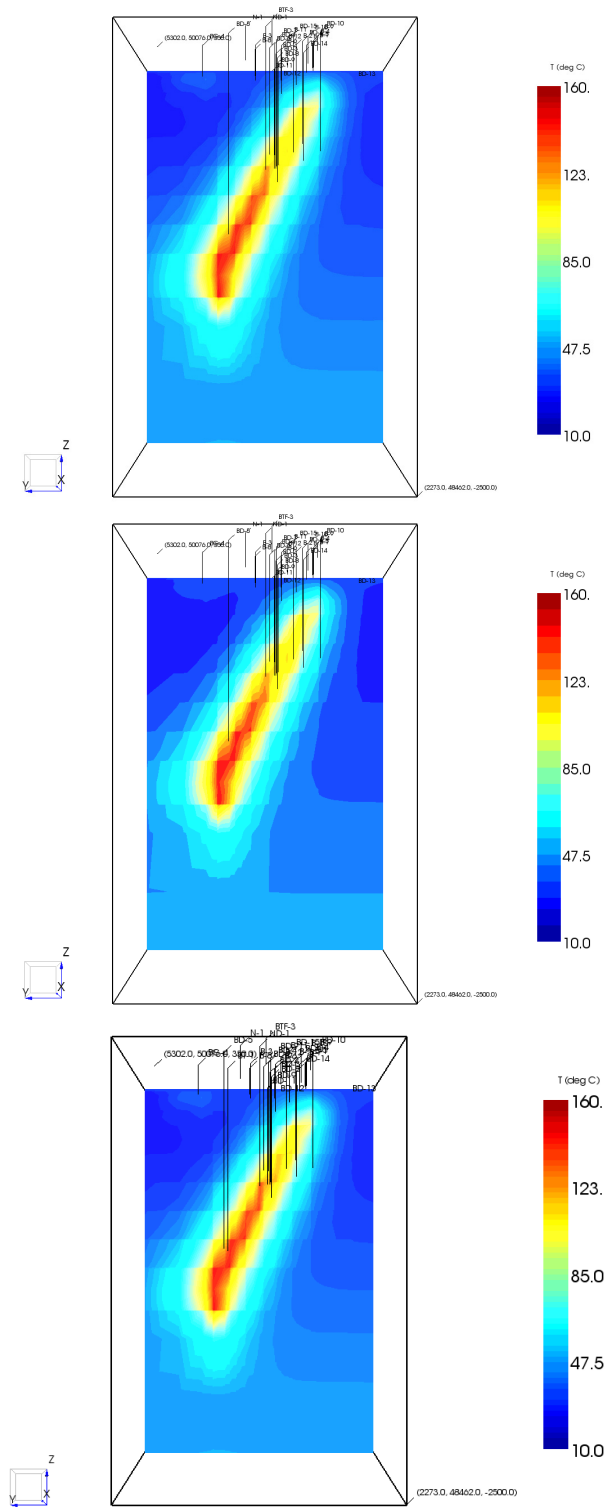


Figure 6.78- The areal temperature profile for cross-section X=4400 and year 2014 (Scenario 1, 2, 3).

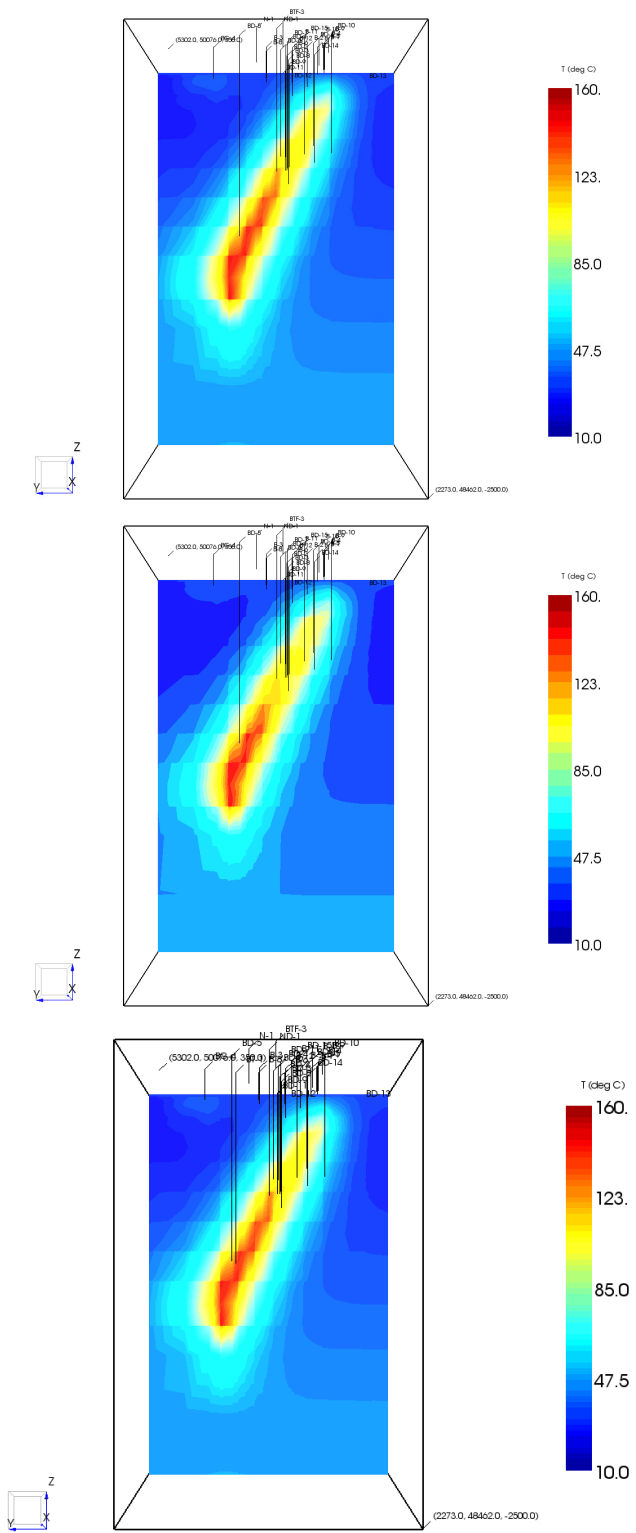


Figure 6.79- The areal temperature profile for cross-section X=4400 and year 2019 (Scenario 1, 2, 3).

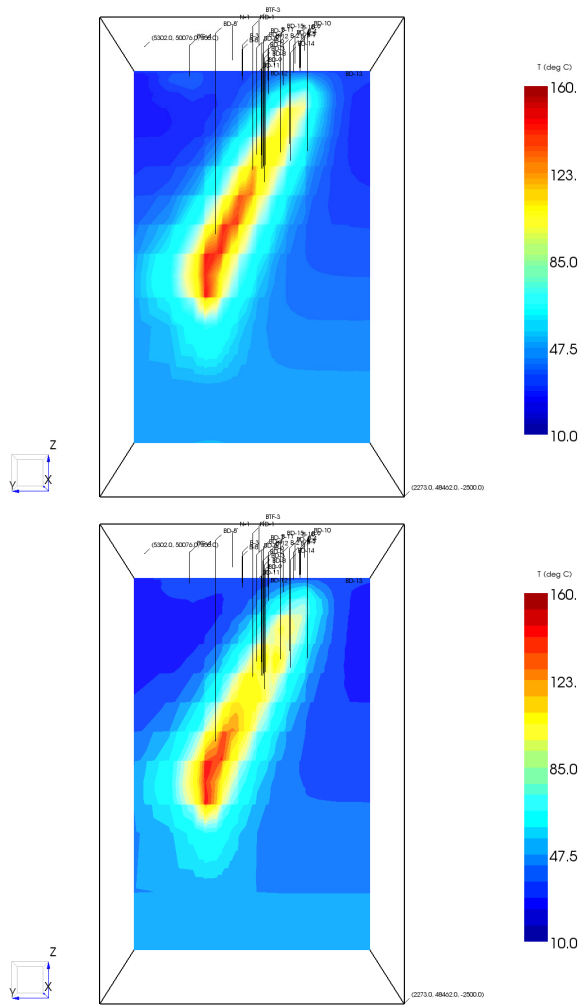


Figure 6.80- The areal temperature profile for cross-section X=4400 and year 2024 (Scenario 1, 2).

Evaluating the temperature profiles of the wells in Scenario 1, 2 and 3 (Figure 6.81 - 6.87) the following interpretations can be made.

- Temperature profiles of BD-1, B-1, B-4 and B-5 do not show significant differences in all Scenarios. Those wells are closely located to each other, having relatively long distances from the main injectors (BD-8 for Scenario 1 and 2 and BD-8 and BT-1 for Scenario-3).
- Having injection from BT-1 in Scenario-3 positively affected the temperature response of BD-2. Shifting some of the injected water from BD-8 to BT-1 resulted with higher temperatures of BD-2 throughout its production life. Since BD-8 and BD-2 are aligned on the same E-W line they must have affected by AG-I fault.
- The wells at the eastern part of the field (BD-9, BD-11 and BD-12) as well as BD-14 are heavily affected by the application of Scenario-2 in which the production as well as injection from BD-8 increased continuously. Their temperatures decreased continuously compared to results from Scenario-1 and 3.
- On the other hand, the wells that are affected by Scenario-3 are BD-7, BD-15 and B-10, which are located at the western side of the field. Shifting some of the injection from BD-8 to BT-1 resulted with this observation.
- The wells BD-4 and BD-6 were also affected by changing from Scenario-1 to Scenario-2. Increase in production and injection rates of the field caused these wells to cool down. On the other hand, Scenario-3 has opposite effects on the temperature profiles of these two wells. Shifting the injection partially from BD-8 to BT-1 did not cause a change in the temperature of BD-6 compared to the result of Scenario-1, but BD-4 experienced some small decrease in temperature.

Average block pressures obtained from all three Scenarios are presented in Figures 6.88 – 6.94. The followings are the observations by considering the average block pressures obtained from Scenario-1 as reference:

- Average block pressures of the wells ND-1, BD-4, BD-5, BD-7 and BD-15 are not affected by the increase in production and injection rates (Scenario-

2) or by shifting some of the injecting water from BD-8 to BT-1 (Scenario-3). This is attributed to the locations of those wells compared to main producers and injectors. They are relatively far from the wells where the main changes took place. At the same time the relatively small production from this section of the field is compensated by the water injection from the nearby well BD-10.

- On the other hand, there exists increase in the average block pressures of the following wells in Scenario-2: B-12, BD-1, BD-2, BD-6, BD-11, BD-12 and BD-14. As it was explained in the description of Scenario-2 that the increase in injected volume is always higher than the increase in production while keeping the locations of injection and production the same. As a result, more water injected by time resulted with an increase in pressure in the wells closer to injectors (BD-8 and BD-3).
- Three wells showed a decrease in pressure during the application of Scenario-2, namely, N-1, B-5 and B-10. B-5 and B-10 are among the main producers of the field producing from shallow depths. A longer production with increasing rates and carrying out the injection practices from deeper sections of the reservoir did not help to sustain the pressure level of these two wells. The decrease in shallow level pressures of the western part of the field is also felt by N-1, a shallow observation well as small decrease in pressure.

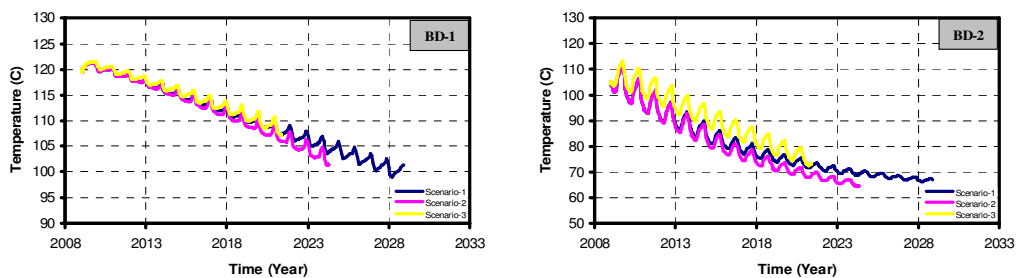


Figure 6.81– Simulated bottomhole temperature of BD-1 and BD-2 (Scenario 1, 2, 3).

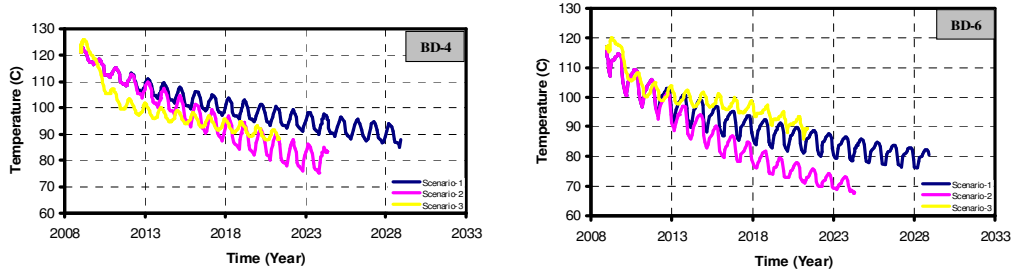


Figure 6.82- Simulated bottomhole temperature of BD-4 and BD-6 (Scenario 1, 2, 3).

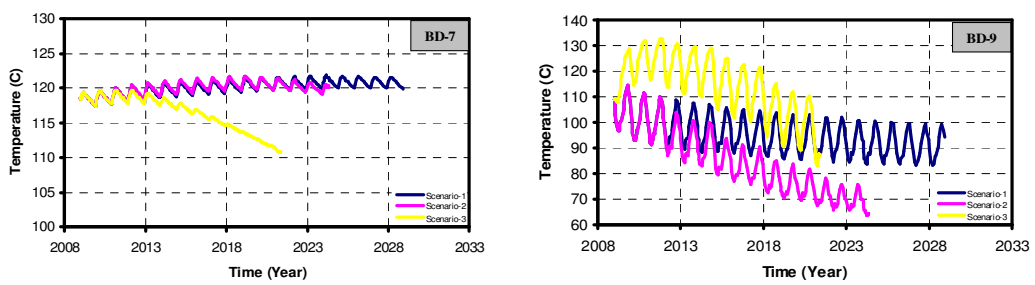


Figure 6.83- Simulated bottomhole temperature of BD-7 and BD-9 (Scenario 1, 2, 3).

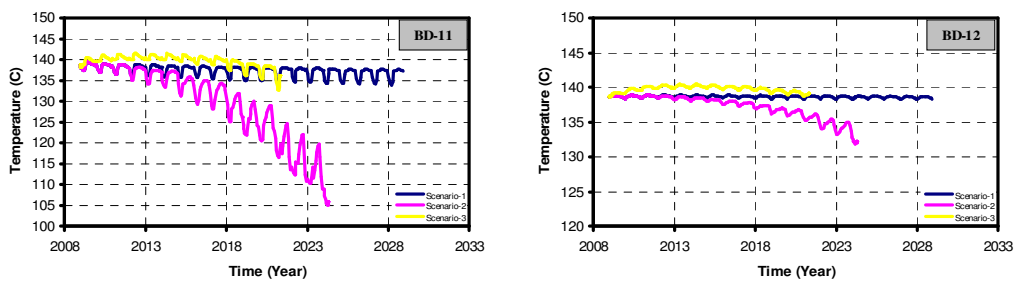


Figure 6.84- Simulated bottomhole temperature of BD-11 and BD-12 (Scenario 1, 2, 3).

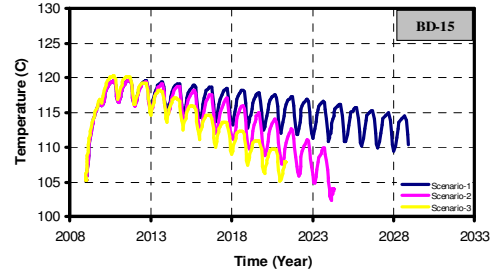
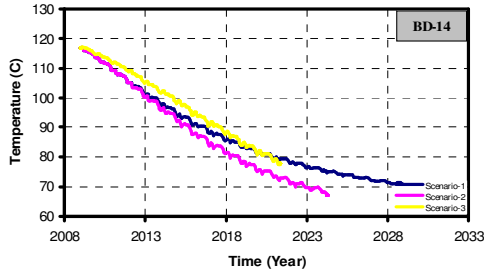


Figure 6.85- Simulated bottomhole temperature of BD-14 and BD-15 (Scenario 1, 2, 3).

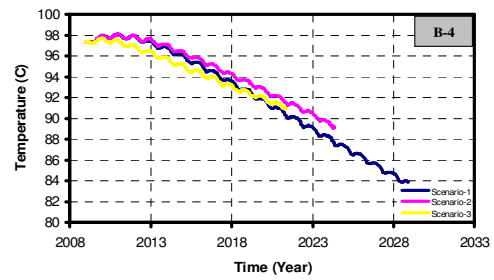
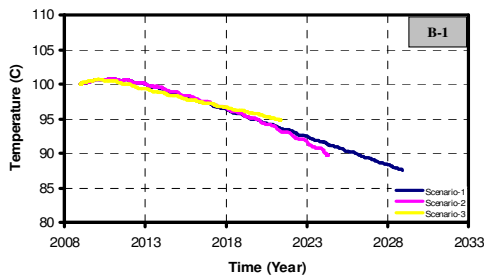


Figure 6.86- Simulated bottomhole temperature of B-1 and B-4 (Scenario 1, 2, 3).

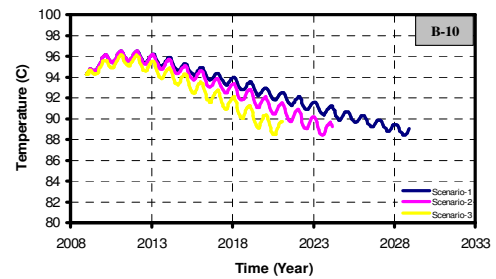
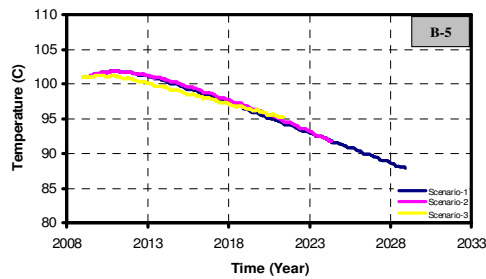


Figure 6.87- Simulated bottomhole temperature of B-5 and B-10 (Scenario 1, 2, 3).

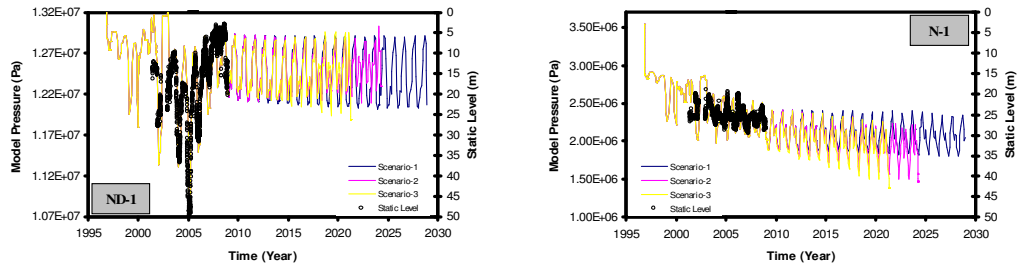


Figure 6.88- Simulated bottomhole pressure of ND-1 and N-1 (Scenario 1, 2, 3).

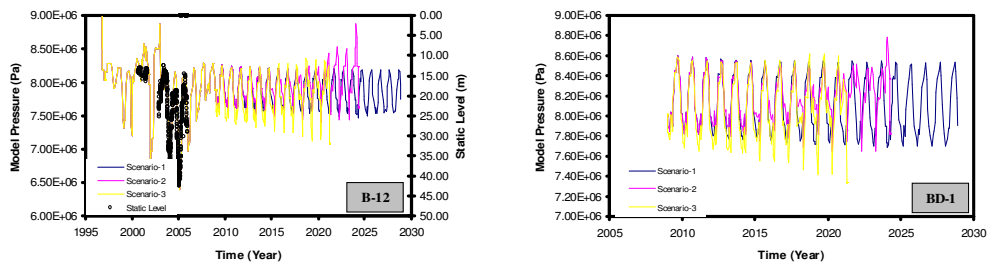


Figure 6.89- Simulated bottomhole pressure of B-12 and BD-1 (Scenario 1, 2, 3).

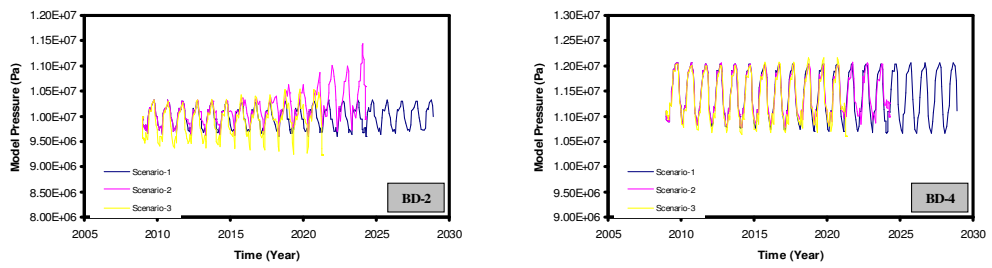


Figure 6.90- Simulated bottomhole pressure of BD-2 and BD-4 (Scenario 1, 2, 3).

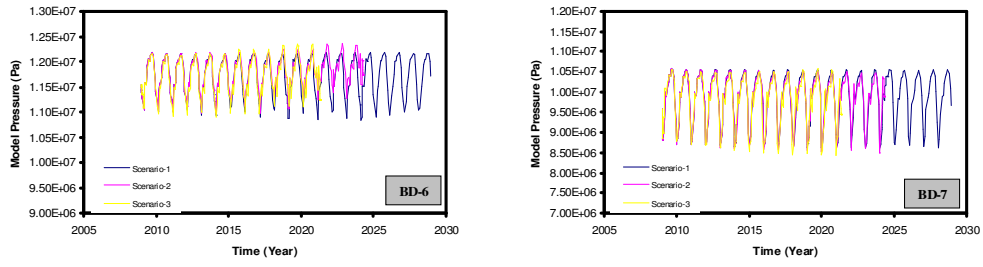


Figure 6.91- Simulated bottomhole pressure of BD-6 and BD-7 (Scenario 1, 2, 3).

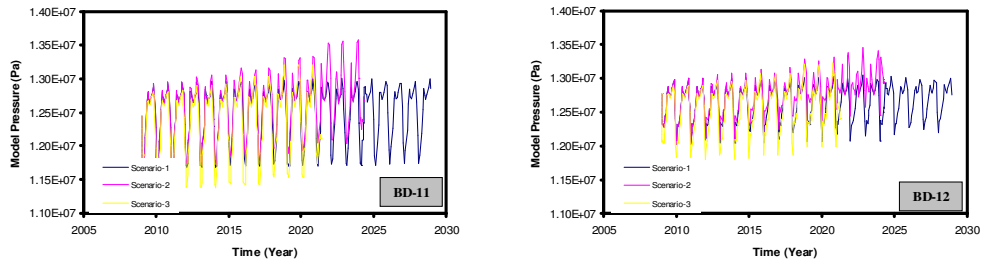


Figure 6.92- Simulated bottomhole pressure of BD-11 and BD-12 (Scenario 1, 2, 3).

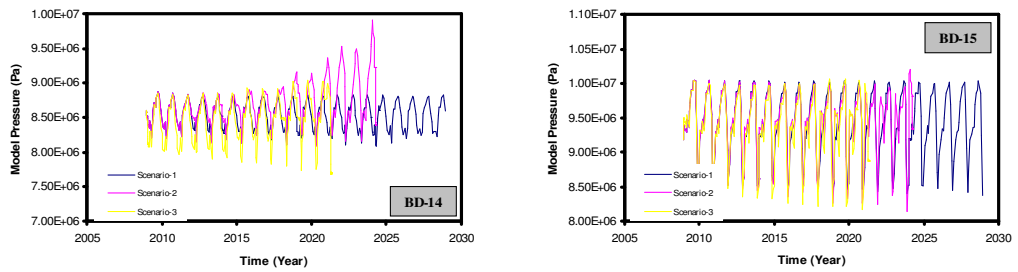


Figure 6.93- Simulated bottomhole pressure of BD-14 and BD-15 (Scenario 1, 2, 3).

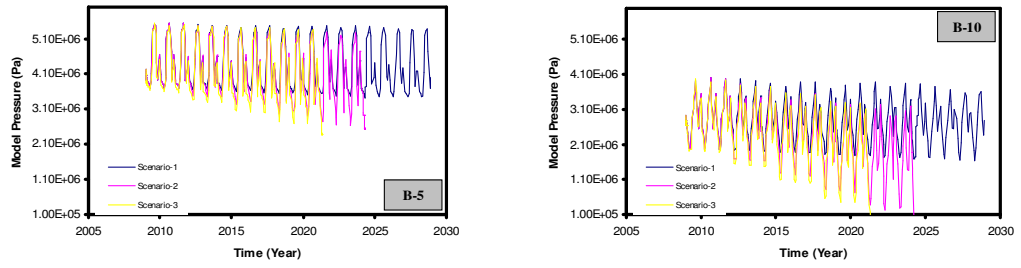


Figure 6.94- Simulated bottomhole pressure of B-5 and B-10 (Scenario 1, 2, 3).

CHAPTER 7

CONCLUSIONS AND RECOMMENDATION

The following conclusions are drawn from the modeling study of Balçova Geothermal Field:

1. Successful natural state modeling and production and injection history match of the period of 1996-2008 was achieved.
2. Under the light of performance prediction studies by applying three different scenarios (Table 7.1), the following conclusions are drawn.
 - a. In all three scenarios, temperature decreases observed for all production wells. In Scenario-2, compared to Scenario-1, both the temperatures of deep wells located at the eastern portion of the field (BD-6, BD-2, BD-14, BD-9, BD-11, BD-12) and the temperature of deep wells located at the western portion (BD-4, BD-15, BD-7, BD-5) decreased more.
 - b. In Scenario-3, compared to Scenario-1, the deep wells located at the eastern side experienced less temperature drops while the deep wells located at the western side experienced higher temperature drops.
 - c. In Scenario-3, compared to Scenario-2, the wells, BD-15 and BD-7, locating at the western side experienced higher temperature drops. These wells totally comprise small amount (10 %) of total production in year 2008.
 - d. It was observed that no significant temperature differences existed between the shallow wells of all three scenarios.
 - e. No significant changes in bottom hole pressures of deep wells occurred in both three Scenario. On the other hand, shallow wells, especially B-10 and B-5, responded to Scenario-2 and Scenario-3 as decrease in bottom hole

pressures because of the continuous increase in their flow rates but small contribution from the injection which is actually realized in deeper parts of the field. Such pressure drops in shallow wells did not occur in Scenario-1. Bottom hole pressures of B-10 and B-5 decreased more in Scenario-3 compared to Scenario-2.

- f. In Scenario 1 and 2, it was observed that water mainly injected through BD-8 and BD-3 wells blocked the hot water coming from deep parts and made it flow to western part and as it flowed to west it heated that region. However, in the third scenario, it was observed that discharge water used for injection through the new well taking place at the location of BT-1 well cooled the deep parts where it was injected and also cooled the west part. Since the portion of injected water directed to west increased and the amount of water directed to east was reduced then it became easier for hot water to flow through the east part.

Table 7.1- Explanation of Scenarios used in the future forecasting study.

Scenarios	Explanation
Scenario-1	Production and injection rates in year 2008 were repeated for 20 years.
Scenario-2	<ul style="list-style-type: none"> - Production and injection rates in year 2008 were repeated for the first three years. - After that, production rates were increased by 10 % and injection rates were increased by 17 % every 3 years.
Scenario-3	<ul style="list-style-type: none"> - A new well is added for injecting some portion of water that was injected through BD-8 well. - Production and injection rates in year 2008 were repeated for the first three years. - After that, production rates were increased by 10 % and injection rates (except the new well) were increased by 25 % every three years.

3. Evaluating both the temperature values of production wells and production amounts of those wells in both three scenarios, it can be said that reinjection procedure that includes the deep well that is planning to be drilled through BT-1 and to the depth 1000 m will probably result in less cooling in production zone if a similar production scenario to that was done in year 2008 is repeated. This means that more energy will be recovered from the field utilizing this new well for injection.

REFERENCES

- Aksoy, N., *Monitoring Balçova-Narlıdere Geothermal System With Tracers*, PhD Thesis, 9 Eylül University, Izmir, 2001.
- Aksoy, N., Filiz, S., *Investigation of Balçova-Narlıdere Geothermal Field by Isotopes*, Proceedings, 1st Environment and Geology Symposium (ÇEVJEO'2001), Izmir, 21-23 March, 2001.
- Aksoy, N., Serpen, U., *Reinjection Management in Balçova Geothermal Field*, In: Proceedings World Geothermal Congress, Antalya, Turkey, 2005.
- Aksoy, N., Serpen, U., Filiz, Ş., *Management of the Balçova–Narlıdere geothermal reservoir*, Geothermics, Turkey, 2007.
- Arkan, S., Parlaktuna, M., *Resource Assessment of Balçova Geothermal Field*, In: Proceedings World Geothermal Congress, Antalya, Turkey, 2005.
- Barenblatt, G. I., et al., *Basic concepts in the theory of seepage of homogeneous liquids in fissured rocks* (in Russian). Prikl. Mat. Mekh., 24 (5), 852-864, 1960.
- Corey, A., T., *The Interrelation Between Gas and Oil Relative Permeabilities*, Producers Monthly, 38-41, 1954.
- Çetiner, L., *İzmir Balçova Jeotermal Sahası BD-6 ve BD-7 Jeotermal Enerji Araştırma Sondaj Kuyuları Bitirme Raporu* (in Turkish), MTA, Ankara, 1999.
- Çetiner, L., *İzmir Balçova BD-8 Jeotermal Enerji Arama Sondaj Kuyusu Bitirme Raporu* (in Turkish), MTA, Ankara, 2004.
- Erinc, S., *Climatology and Methods*, Institute of Geography of Istanbul University, Yay, No. 35, Istanbul, 1969.
- Fatt, I. and W.A. Klikoff, *Effect of Fractional Wettability on Multiphase Flow Through Porous Media*, AIME Transactions, 216, 246, 1959.
- Genc, S.C., Altunkaynak, S., Karacik, Z., Yazman, M., Yilmaz, Y., *The Cubukludag Graben, South of Izmir: Its Tectonic Significance in the Neogenegeological Evaluation of Western Anatolia*, Geodina-Mica Acta, 14, 45–55, 2001.
- Grant, M., A., *Permeability Reduction Factors at Wairakei*, paper 77-HT-52, presented at AICHE-ASME Heat Transfer Conference, Salt Lake City, Utah, 1977.

Henry, B., C., *Modern Reservoir Engineering-A simulation Approach*, Prentice-Hall, Inc., New Jersey, 1977.

İZSU, *Alionbaşı Dam Planning Report*, General Directorate of İzmir Water and Canalisation Administration, 1997.

Leverett, M.C., *Capillary Behavior in Porous Solids*, Trans. Soc. Pet. Eng. AIME, 142, 152-169, 1941.

Mualem, Y., A., *New Model for Predicting the Hydraulic Conductivity of Unsaturated Porous Media*, Water Resour. Res., Vol. 12, No. 3, pp. 513 – 522, 1976.

Milly, P.C.D., *Moisture and Heat Transport in Hysteretic, Inhomogeneous Porous Media: A Matrix-Head Based Formulation and a Numerical Model*, Water Resour. Res., Vol. 18, No. 3, pp. 489 - 498, 1982.

Narasimhan, T.N., P.A. Witherspoon and A.L. Edwards. *Numerical Model for Saturated-Unsaturated Flow in Deformable Porous Media, Part 2: The Algorithm*, Water Resour. Res., 14 (2), 255-261, 1978.

Ongur, T., *Geological Report on İzmir-Urla Geothermal Exploration Area*, MTA report No. 4835, 1972.

Onur, M., Aksoy, N., Serpen, U., Satman, A., *Analysis of Pressure Transient Tests in Balcova-Narlıdere Geothermal field*, Turkish Journal of Oil and Gas, 8, 20–36, 2002.

Pickens, J.F., R.W. Gillham and D.R. Cameron, *Finite Element Analysis of the Transport of Water and Solutes in Tile-Drained Soils*, J. of Hydrology, 40, 243-264, 1979.

Pruess, K., Oldenburg, C., Moridis, G., *TOUGH2 User's Guide, Version 2.0*, Berkeley University Press, California, 1999.

Pruess, K., *Mathematical Modeling of Fluid Flow and Heat Transfer in Geothermal Systems – An Introduction in Five Lectures*, United Nations University Geothermal Training Programme Reykjavik, Iceland, 2002.

Satman, A., Serpen, U., Onur, M., *Reservoir and production performance of İzmir Balcova-Narlıdere geothermal field*, Report for İzmir City Council, Istanbul, 2001.

Serpen, U., Kayan, I., *Hydrologic balance of Balcova geothermal field*, Proceedings of 13th Inter-national Petroleum Congress and Exhibition of Turkey, Turkey, pp. 546–553, 2001.

Serpen, U., *Hydrogeological Investigations on Balcova Geothermal System in Turkey*, Geothermics 33, 2003.

Thunderhead Engineering, *Petrasim User Manual*, <http://www.thunderheadeng.com/petrasim/manual/html/index.html>, last visited on January 2010, 2009.

Toksoy, M., Aksoy, N., Serpen, U., *Proposal Report for the Izmir Energy Policy and Regional Geothermal Energy Plan*, Izmir Institute of Technology, Geothermal Energy Research and Application Centre, Report 2003/3, Izmir, Turkey , 14 pp, 2003 (in Turkish).

Tuncay, İ., *İzmir Balçova Sahası Jeotermal Enerji Aramaları, Jeofizik Kuyu Ölçüleri Etüdü*, MTA Report No. 8790, Ankara, 1989.

Udell, K.S. and J.S. Fitch., *Heat and Mass Transfer in Capillary Porous Media Considering Evaporation, Condensation, and Non-Condensable Gas Effects*, paper presented at 23rd ASME/AIChE National Heat Transfer Conference, Denver, CO, 1985.

Warren, J. E. & Root, P. J., *The behaviour of naturally fractured reservoirs*, Soc. Pet. Eng. J., 3, 245-255, 1963.

Van Genuchten, M., Th., *A Closed-Form Equation for Predicting the Hydraulic Conductivity of Unsaturated Soils*, Soil Sci. Soc. , Vol. 44, pp. 892 – 898, 1980.

Verma, A., K., K. Pruess, C.F. Tsang and P.A. Witherspoon, *A Study of Two-Phase Concurrent Flow of Steam and Water in an Unconsolidated Porous Medium*, Proc. 23rd National Heat Transfer Conference, Am. Society of Mechanical Engineers, Denver, CO, 135–143, 1985.

Yilmazer, S., *Geochemical Features of Balçova Hot Springs and Geothermal Energy Possibilities for the Area*, PhD Thesis, Akdeniz University, Isparta, Turkey, 1989.

Yilmazer, S., Karahan, Ç., İldem, F., Uygur, N., *Balçova BD-5 Sondajı Kuyu Bitirme Raporu* (in Turkish), MTA, 1999.

Yilmazer, S., Uygur, N., Yakabağ, A., Karahan, Ç., İldem, F., *Balçova BD-4 Kuyusunun Kuyu Bitirme Raporu* (in Turkish), MTA, 1998.

APPENDIX A

PERMEABILITY STRUCTURE

The pressure gradient of the field was calculated as 9.86 kPa/m with the help of the figure constructed using pressure and depth values (Figure A.1). The average temperature of the rising water was assumed to be 130 °C, 5m-wide permeable zone associated with AG-I fault, and the flowrate of the hot water flowing upwards was 50 k/s were assumed (Satman et al., 2001). Using these information, the vertical permeability of this 5-m wide zone was calculated as $2 \cdot 10^{-12} \text{ m}^2$ which is actually equal to 2000 md. Since used values seem to be reasonably acceptable, this permeability value was selected to be used in the modeling study. To match the initial temperatures of wells, the permeability of the west part of the AG-I fault was selected as two times of that permeability value.

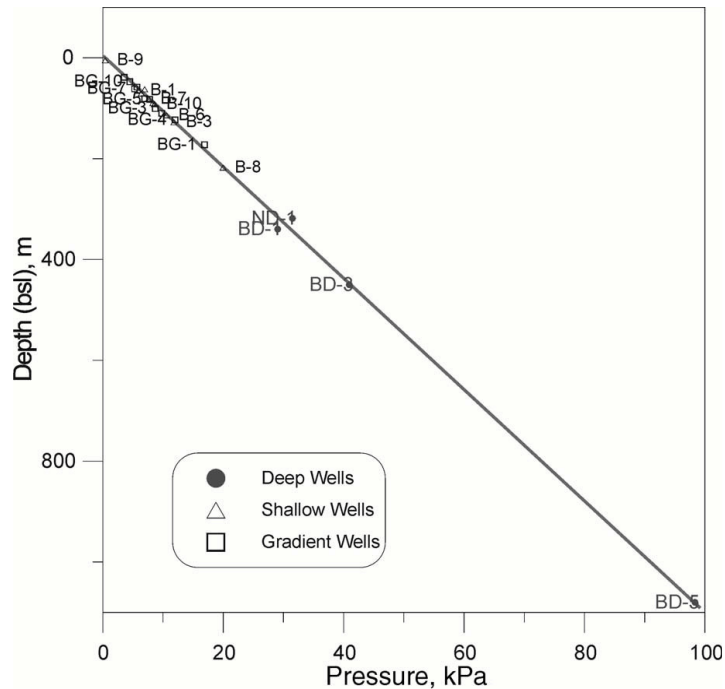


Figure A.1- Reservoir pressures of Balçova field with respect to depth (Serpen, 2003).

According to Darcy's law;

$$\frac{Q}{A} = \frac{k \Delta P}{\mu \Delta L} \quad (A.1)$$

Viscosity of water can be calculated using the formula

$$\mu_w = \exp(1.003 - 1.479 \times 10^{-2} T + 1.982 \times 10^{-5} T^2) \quad (A.2)$$

$$T = 130 \times 1.8 + 32 = 266 \text{ F}$$

$$\mu_w = \exp(1.003 - 1.479 \times 10^{-2} (266) + 1.982 \times 10^{-5} (266)^2)$$

$$\mu_w = 0.21680 \text{ cp} = 2.1680 \times 10^{-4} \text{ kg/m sec}$$

Adding the excess gradient the pressure gradient is assumed as 10000 Pa/m

The vertical flow is assumed to occur over the area that has 5 m wide and 100 m length, (the area is at the intersection of AG-I fault with alluvium), thus

$$A = 5 \times 100 = 500 \text{ m}^2$$

$$k = \frac{Q}{A} \mu \frac{\Delta P}{\Delta L} = \frac{0.05}{500} \times (2.1680 \times 10^{-4}) \times 10000$$

$$k = 2.168 \times 10^{-12} \text{ m}^2 = 2168 \text{ md}$$

Table A.1-Transmissivity values of İzmir flysh (Onur et al., 2002).

Wells	Inferred Faults	Transmissivity (m3)	Permeability (m2)	Inferred permeable zone thickness (m)
BD-2	CII	3E-11 - 6.1E-11	1.5E-13 - 3E-13	200
BD-5	DIV	2E-12 - 1.1E-11	1E-14 - 5.5E-14	200
BD-6	CII, DII	6E-11	3E-13	200
BD-7	DI	3.9E-11	3.9E-13	100

Table A.1 shows the results of tests conducted in several wells to estimate the transmissivity and permeability values in the related permeable zones. Injection and fall-off tests were performed in wells BD-2 and BD-5 and drawdown tests were performed in wells BD-6 and BD-7. The results indicate that the permeability of the 5-m wide zone associated with AG-I fault is at least one order of magnitude higher than the estimated permeabilities seen in Table A.1. Removing the effect of AG-I fault on the permeability values found with the help of tests conducted in wells, it can be stated that the permeability of the zone near the 5-m wide zone is lower than the permeability values found with the help of the tests conducted. 100 md may be selected as an average permeability value for the zone near that 5-m wide zone.

Collecting all these information and analyzing them, it can be stated that the main flow occurs in the AG-I fault as it has much more higher permeability compared to other zones.

The ascending water finally changes its direction to North and moves along the alluvium formation. Alluvium transport hot water, which was indicated by the boron contents of water from wells drilled in the northern plains (Yilmazer, 1989). From this situation the result that alluvium is a permeable zone can be obtained. However, the value of the permeability of alluvium is not known.

The talus formation existing in the southern part of the field serves as caprock, which was observed by analyzing the initial temperature distribution of wells drilled through that formation. This information shows that talus existing in the field does not transport water and so is impermeable.

The initial temperature distribution of wells indicates which zones are permeable and which zones are impermeable. The thickness of the permeable zone in the shallower part of the field is about 40 m in some region and can decrease to 0 m. Generally, this 40 m zone is more observable.

APPENDIX B

POROSITY DISTRIBUTION

In order to estimate the porosity of the formation from well logs, neutron porosity log and density porosity log data should be evaluated together. Moreover, values from density log maybe incorrect because of the measurement failures. Correction plot should be made to see whether the density log data of the depth considered is correct or not. Caliper log data is also needed to determine which parts of the wellbore has a higher diameter compared to other parts of the well. Enlargement exists in the wellbore may cause incorrect gamma ray and neutron porosity values.

Density log data only exists for some gradient wells and correction plot was not made so some parts of the data may need to be considered out of calculation. Caliper log data is missing so whether a correction for the neutron log data and gamma ray log data is needed can not be anticipated. General opinion about formation properties can be formed and average porosity values for some parts of the reservoir can be calculated using the given values consisting of neutron log, gamma ray log and density log data.

Three different parts, shallow, middle and deep, can be obtained by analyzing gamma ray and porosity logs which were conducted for gradient wells, shallow wells and deep wells. These parts can be more observable in the graphs prepared using data from wells BG-3, BG-4 and B-3. For the shallow part, a value close to 2.6 can be acquired from density log for BG-4. Besides, neutron log acquired from wells BG-3, BG-4 and B-3 gives a value around 25. By using these values and quick look up method, the porosity of the shallow part was estimated as 15 %. The middle part, on the other hand, has a lower neutron porosity value, which is about 10. The value of the density log in this part varies between 2.6 and 2.7. The quick look up method gives a value around 7 % for the porosity of the middle part. The deep part has density log value which changes between 2.7 and 2.8, while it has neutron log value close to 0. Combining these information, it can be said the porosity of the deep part is close to 0, maybe taken as 3 %. It is observable that the deep part is associated with flysch formation. That the middle part whose porosity

is estimated about 7 % is a permeable zone can be indicated from the temperature distribution of wells BG-4 and BG-1. The information that the shallow part serves as caprock may be seen as an outcome from the examination of the temperature distributions in gradient wells. In some part of the reservoir the effect of shallow part to the middle part is so much that it may increase overall porosity of the middle part. Keeping this information in mind, the average porosity of the permeable part can be taken as 10 %.

Values used in resource assessment of Balçova Geothermal field indicate that porosity of the flysch formation varies between 0.2 % and % 7 (Parlaktuna and Arkan, 2005). 7 % which was also found using log values may be interpreted to porosity value of the upper portions of the flysch formation. Porosity of flysch formation is estimated as 3 % with the help of log data. This value agrees well with the values used in resource assessment.

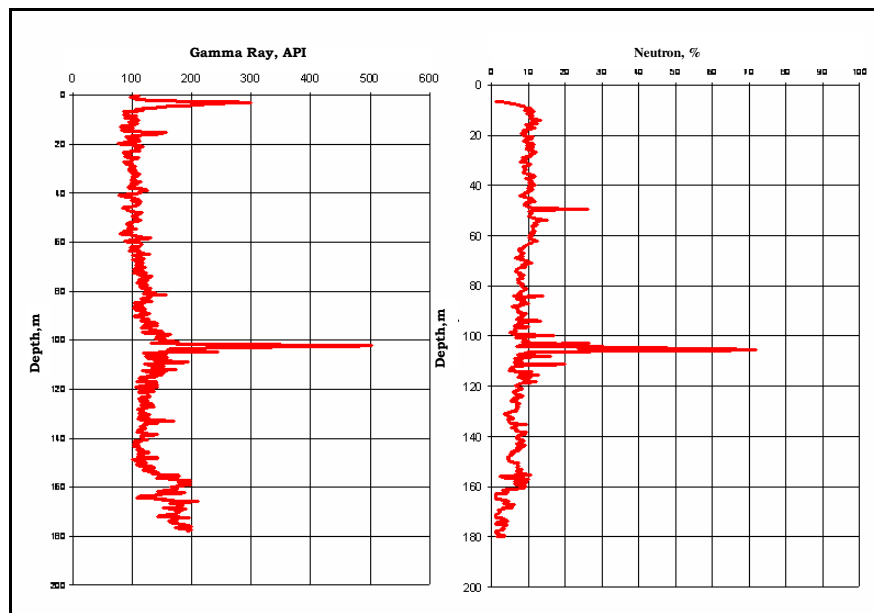


Figure B.1- Balçova BG-1 well gamma ray and neutron porosity logs (Tuncay, 1989).

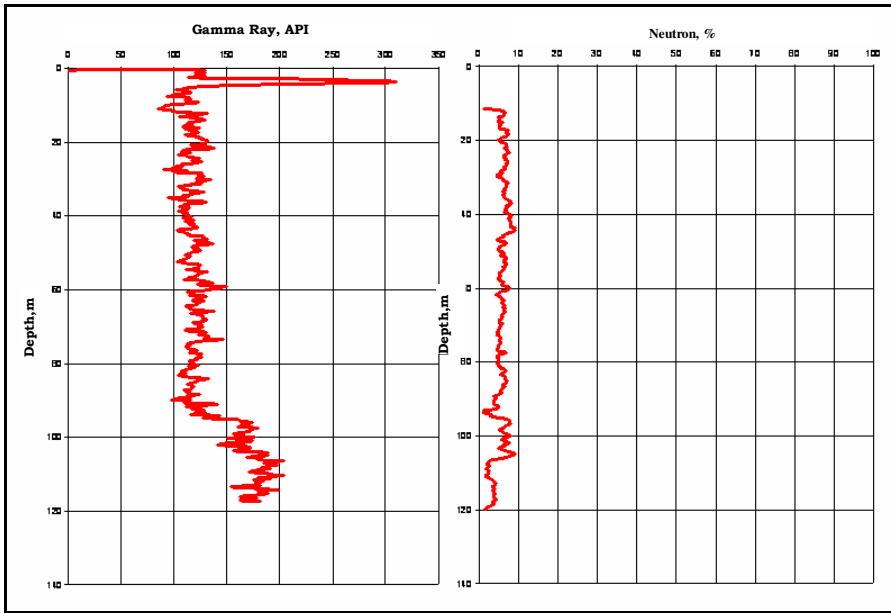


Figure B.2- Balçova BG-2 well gamma ray and neutron porosity logs (Tuncay, 1989).

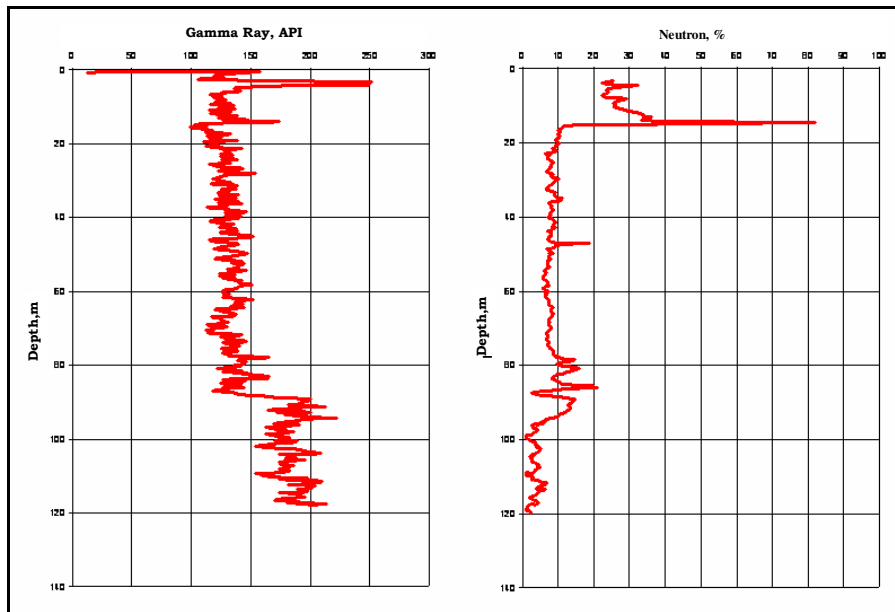


Figure B.3- Balçova BG-3 well gamma ray and neutron porosity logs (Tuncay, 1989).

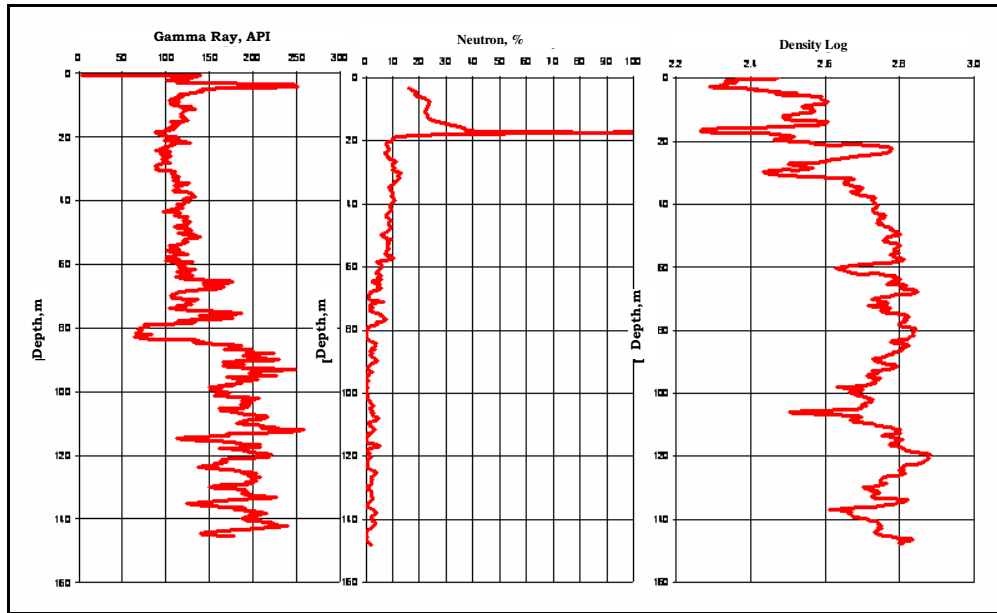


Figure B.4-Balçova BG-4 well gamma ray, neutron porosity logs and density logs (Tuncay, 1989).

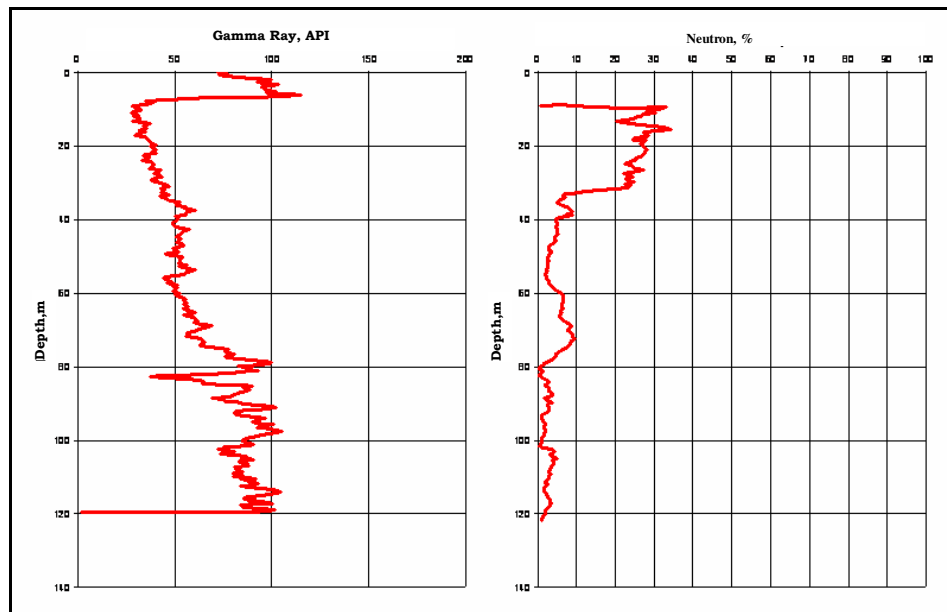


Figure B.5- Balçova B-3 well gamma ray and neutron porosity logs (Tuncay, 1989).

APPENDIX C

GENERAL EQUATIONS AND CALCULATION PROCEDURE IN TOUGH2

C.1. General Equations

The basic mass and energy balance equations solved by TOUGH2 can be written in the general form

$$\frac{d}{dt} \int_{V_n} M^{\kappa} dV_n = \int_{\Gamma_n} F^{\kappa} \cdot n d\Gamma_n + \int_{V_n} q^{\kappa} dV_n \quad (C.1)$$

The integration is over an arbitrary subdomain V_n of the flow system under study, which is bounded by the closed surface Γ_n . Here

M : Mass or energy per volume

κ : 1 ...NK, mass components

κ : NK+1, heat component

F : Mass or heat flux

q : sinks and sources

n : a normal vector on the surface element $d\Gamma_n$, pointing inward into V_n

The general form of the mass accumulation term is

$$M^{\kappa} = \Phi \sum_{\beta} S_{\beta} \rho_{\beta} X_{\beta}^{\kappa} \quad (C.2)$$

The total mass of component κ is obtained by summing over the fluid phases β (=liquid, gas, non-aqueous phase liquid). Here

Φ : Porosity

S_{β} : Saturation of phase β

ρ_{β} : Density of phase β

$X_{\beta\kappa}$: Mass fraction of component κ present in phase β

The heat accumulation term in a multiphase system is

$$M^{NK+1} = (1 - \phi)\rho_R C_R T + \phi \sum_{\beta} S_{\beta} \rho_{\beta} u_{\beta} \quad (C.3)$$

ρ_R : Grain density

C_R : Specific heat of the rock

T : Temperature

u_{β} : Specific internal energy in phase β

Mass flux is a sum over phases,

$$F^{\kappa} \Big|_{\text{adv}} = \sum_{\beta} X_{\beta}^{\kappa} F_{\beta} \quad (C.4)$$

Individual phase fluxes are given by a multiphase version of Darcy's law:

$$F_{\beta} = \rho_{\beta} u_{\beta} = -k \frac{k_{r\beta} \rho_{\beta}}{\mu_{\beta}} (\nabla P_{\beta} - \rho_{\beta} \mathbf{g}) \quad (C.5)$$

u_{β} : Darcy velocity in phase β

k : Absolute permeability

$k_{r\beta}$: Relative permeability to phase β

μ_{β} : Viscosity of phase β

\mathbf{g} : Vector of gravitational acceleration

$$P_{\beta} = P + P_{c\beta} \quad (C.6)$$

P_{β} : Fluid pressure in phase β

P : Reference pressure (usually gas pressure)

$P_{c\beta}$: Capillary pressure

Absolute permeability of the gas phase increases at low pressures according to the relation given by Klinkenberg

$$k = k_{\infty} \left(1 + \frac{b}{P} \right) \quad (C.7)$$

k_{∞} is the permeability at infinite pressure (true permeability)

b: Klinkenberg parameter which depends on the material to be used

Heat flux includes conductive and convective components

$$F^{NK+1} = -\lambda \nabla T + \sum_{\beta} h_{\beta} F_{\beta} \quad (C.8)$$

λ : Thermal conductivity

h_{β} : Specific enthalpy in phase β

Mass transport occurs by diffusion and hydrodynamic dispersion as follows

$$F^{\kappa} \Big|_{\text{dis}} = -\sum_{\beta} \rho_{\beta} \bar{D}_{\beta}^{\kappa} \nabla X_{\beta}^{\kappa} \quad (C.9)$$

The hydrodynamic dispersion is given by

$$\bar{D}_{\beta}^{\kappa} = D_{\beta,T}^{\kappa} \bar{I} + \frac{(D_{\beta,L}^{\kappa} - D_{\beta,T}^{\kappa})}{u_{\beta}^2} u_{\beta} u_{\beta} \quad (C.10)$$

Where

$$D_{\beta,L}^{\kappa} = \phi \tau_0 \tau_{\beta} d_{\beta}^{\kappa} + \alpha_{\beta,L} u_{\beta} \quad (C.11)$$

$$D_{\beta,T}^{\kappa} = \phi \tau_0 \tau_{\beta} d_{\beta}^{\kappa} + \alpha_{\beta,T} u_{\beta} \quad (C.12)$$

Neglecting the hydrodynamic dispersion

$$\bar{D}_{\beta}^{\kappa} = (\phi \tau_0 \tau_{\beta} d_{\beta}^{\kappa}) \bar{I} \quad (C.13)$$

α_L : Longitudinal dispersivity

α_T : Transverse dispersivity

τ_0 : Tortuosity coefficient for porous medium

τ_β : Tortuosity coefficient for phase saturation

$d_{\beta\kappa}$: Diffusion coefficient of component κ in bulk fluid phase β

$X_{\beta\kappa}$: Mass fraction of component κ in phase β

Diffusion coefficient for gases

$$d_{\beta\kappa}^k(P, T) = d_{\beta\kappa}^k(P_0, T_0) \frac{P_0}{P} \left[\frac{T + 273.15}{273.15} \right]^\theta \quad (\text{C.14})$$

At standard conditions, $P_0 = 1 \text{ atm} = 1.01325 \text{ bar}$, $T_0 = 0 \text{ C}$. Parameter θ for the temperature dependence is 1.80.

Diffusion coefficients of aqueous phases are taken as constants.

The following three formulations are used for tortuosity effects.

$$1- \tau_0 \tau_\beta(S_\beta) = \tau_0 k_{r\beta}(S_\beta) \quad (\text{C.15})$$

$$2- \tau_0 \tau_\beta = \phi^{1/3} S_\beta^{10/3} \quad (\text{C.16})$$

$$3- \tau_0 \tau_\beta = S_\beta \quad (\text{C.17})$$

In the first equation, tortuosity coefficient for porous medium is taken as constant while in the second equation it depends on porosity. Tortuosity coefficient for phase saturation depends on either phase saturation or relative permeability. Regarding the information that diffusive flux will vanish when the phase becomes discontinuous, relative permeability should be used for calculating the tortuosity coefficient. However, it should be kept in mind that relative permeability of one phase will be lower than 1, when the relative permeability of other phase is 0. Thus, it would predict weaker diffusion in that case.

C.2. Space and Time Discretization

The continuum equations are discretized in space using the integral finite difference method. Introducing appropriate volume averages,

$$\int_{V_n} M dV = V_n M_n \quad (C.18)$$

M_n : Average value of M over V_n

Surface integrals are approximated as a discrete sum of averages over surface segments A_{nm}

$$\int_{\Gamma_n} \mathbf{F}^\kappa \cdot \mathbf{n} d\Gamma = \sum_m A_{nm} F_{nm} \quad (C.19)$$

F_{nm} : Average value of the normal component of F over the surface segment A_{nm} between volume elements V_n and V_m

The discretized flux is expressed in terms of averages over parameters for elements V_n and V_m ,

$$F_{\beta,nm} = -k_{nm} \left[\frac{k_{i\beta} \rho_\beta}{\mu_\beta} \right]_{nm} \left[\frac{P_{\beta,n} - P_{\beta,m}}{D_{nm}} - \rho_{\beta,nm} g_{nm} \right] \quad (C.20)$$

Subscripts nm : Averaging at the interface (interpolation, harmonic weighting, upstream weighting) between the grid blocks n and m .

D_{nm} : Distance between the nodal points n and m

g_{nm} : Component of gravitational acceleration in the direction from m to n

Space discretization of diffusive flux

$$(f^\kappa)_{nm} = -(\Sigma_l^\kappa)_{nm} \frac{(X_l^\kappa)_m - (X_l^\kappa)_n}{D_{nm}} - (\Sigma_g^\kappa)_{nm} \frac{(X_g^\kappa)_m - (X_g^\kappa)_n}{D_{nm}} \quad (C.21)$$

Where

$$\Sigma_\beta^\kappa = \phi \tau_0 \tau_\beta \rho_\beta d_\beta^\kappa \quad (C.22)$$

Diffusive flux equation is re-written in terms of an effective multiphase diffusive strength coefficient and a single mass fraction gradient.

$$(f^k)_{nm} = - \left\{ \sum_l^k + \sum_g^k \frac{(X_g^k)_m - (X_g^k)_n}{(X_l^k)_m - (X_l^k)_n} \right\} \frac{(X_l^k)_m - (X_l^k)_n}{D_{nm}} \quad (C.23)$$

Harmonic weighting of diffusive strength coefficients are required for the conservation of diffusive flux across the boundary between two adjacent blocks.

Weighting of diffusive strength coefficients separately for liquid and gas phases is inadequate in some cases, for example, situations where phase partitioning effects occur. Thus, harmonic weighting is applied to the effective multiple diffusive strength coefficient which contains both liquid and gas diffusive strength coefficients.

C.3. Calculation Procedure

A set of first order ordinary differential equations in time

$$\frac{dM_n^k}{dt} = \frac{1}{V_n} \sum_m A_{nm} F_{nm}^k + q_n^k \quad (C.24)$$

The time discretization results in the following set of coupled non-linear, algebraic equations.

$$R_n^{k,k+1} = M_n^{k,k+1} - M_n^{k,k} - \frac{\Delta t}{V_n} \left\{ \sum_m A_{nm} F_{nm}^{k,k+1} + V_n q_n^{k,k+1} \right\} = 0 \quad (C.25)$$

Subscripts k+1 denotes the new time level, while subscript k denotes the previous time level. The treatment of the unknown terms is fully implicit and numerical stability can be obtained.

These equations are solved by Newton/Raphson iteration. Expanding the residuals in a Taylor series,

$$R_n^{k,k+1}(x_{i,p+1}) = R_n^{k,k+1}(x_{i,p}) + \sum_i \left. \frac{\delta R_n^{k,k+1}}{\delta x_i} \right|_p (x_{i,p+1} - x_{i,p}) + \dots = 0 \quad (C.26)$$

Subscript p+1 denotes the new iteration level, while subscript p denotes the previous iteration level.

x_i : Primary variables

Retaining only terms up to first order,

$$-\sum_i \left. \frac{\partial R_n^{k,k+1}}{\partial x_i} \right|_p (x_{i,p+1} - x_{i,p}) = R_n^{k,k+1}(x_{i,p}) \quad (C.27)$$

For each volume element (grid block) V_n , there are NEQ equations.

$$\text{NEQ} = \text{NK} + 1 \quad (C.28)$$

NK: The number of components

1 is added to include heat transfer.

Thus, for a flow system with NEL grid blocks, NEL*NEQ coupled non-linear equations exists.

There are NK1 primary variables for each volume element V_n (1 is added to include heat transfer), and totally NK1*NEL primary variables exists.

After determination of the primary variables, secondary parameters which consist of phase saturation, relative permeability, viscosity, density, specific enthalpy, capillary pressure, diffusion factor 1, diffusion factor 2 are calculated.

There are NB parameters needed for the accumulation and advective flow terms. NB = 8 if diffusion factors are considered, otherwise NB = 6. There are NK mass fractions of components in a phase. Thus in a phase, there are NBK = NB+NK secondary parameters. In a block, total number of phases is NPH, so that there are NSEC = NPH*NBK+2 secondary parameters. 2 is added to include temperature (miscellaneous). Due to the derivation of Residuals with respect to x_i is incremented, so, there are (NEQ+1)* NSEC secondary parameters for each grid block V_n . Totally, there are NEL*(NEQ+1)* NSEC secondary parameters.

Primary variables are taken from the previous run.

Secondary parameters are calculated after the determination of the primary variables.

Matrix structure is formed as follows

$$J.\Delta x = R \quad (C.29)$$

J represents $-dR_n^k/dx_i$ at iteration level p

Δx represents $x_{i,p+1}-x_{i,p}$

R represents R_n^k at iteration level p

Δx matrix is solved using one of the linear equation solvers: direct solver, bi-conjugate gradient solver, Lanczos-type bi-conjugate gradient solver, generalized minimum residual solver, stabilized bi-conjugate gradient solver.

Using new calculated primary variables continue the procedure mentioned above until the criteria

$$\left| \frac{R_{n,p+1}^{k,k+1}}{M_{n,p+1}^{k,k+1}} \right| \leq \varepsilon_1$$

(If accumulation terms are smaller than ε_2)

$$\left| R_n^{k,k+1} \right| \leq \varepsilon_1 \cdot \varepsilon_2$$

is satisfied. (Default value of ε_1 is equal to 10^{-5} and default value of ε_2 is equal to 1)

The calculated primary variables are for that new time. The new time is equal to previous time plus time step (Δt).

For other times the same procedure is followed.

Converge is usually reached in 3-4 iterations. If converge cannot be achieved within a certain number of iterations (default 8), the time step size is reduced and a new iteration process is started. If converge is achieved within a number iterations that is below the determined value (default 3), the time step size is increased. The aim is to use the highest time step size without exceeding certain number of iterations.

Phase saturation, viscosity, density, specific enthalpy can be calculated using steam tables or equations prepared for estimating these parameters.

Relative permeability and capillary pressure are functions of saturations.

C.4. Relative Permeability Functions

C.4.1. Linear Functions

k_{rl} increases linearly from 0 to 1 in the range

$$RP(1) \leq S_l \leq RP(3)$$

k_{rg} increases linearly from 0 to 1 in the range

$$RP(2) \leq S_g \leq RP(4)$$

Restrictions: $RP(3) > RP(1)$; $RP(4) > RP(2)$

C.4.2. Corey's Curves (1954)

$$k_{rl} = \hat{S}^4 \tag{C.30}$$

$$k_{rg} = (1 - \hat{S})^2 (1 - \hat{S}^2) \tag{C.31}$$

$$\hat{S} = (S_l - S_{lr}) / (1 - S_{lr} - S_{gr}) \tag{C.32}$$

Restrictions: $S_{lr} + S_{gr} < 1$

C.4.3. Grant's Curves (1977)

$$k_{rl} = \hat{S}^4$$

$$k_{rg} = 1 - k_{rl} \tag{C.33}$$

$$\text{Where } \hat{S} = (S_l - S_{lr}) / (1 - S_{lr} - S_{gr})$$

Restrictions: $S_{lr} + S_{gr} < 1$

C.4.4. All phases perfectly mobile

$k_{rg} = k_{rl} = 1$ for all saturations; no parameters

C.4.5. Functions of Fatt and Klikoff (1959)

$$k_{rl} = (S^*)^3 \quad (C.34)$$

$$k_{rg} = (1 - S^*)^3 \quad (C.35)$$

$$\text{Where } S^* = (S_1 - S_{lr}) / (1 - S_{lr}) \quad (C.36)$$

Restriction: $S_{lr} < 1$

C.4.6. Van Genuchten-Mualem Model (Mualem, 1976; van Genuchten, 1980)

$$k_{rl} = \begin{cases} \sqrt{S^*} \left\{ 1 - \left(1 - [S^*]^{1/\lambda} \right)^\lambda \right\}^2 & \text{if } S_1 < S_{ls} \\ 1 & \text{if } S_1 \geq S_{ls} \end{cases} \quad (C.37)$$

$$k_{rg} = \begin{cases} 1 - k_{rl} & \text{if } S_{gr} = 0 \\ (1 - \hat{S})^2 (1 - \hat{S}^2) & \text{if } S_{gr} > 0 \end{cases} \quad (C.38)$$

Restriction: $0 \leq k_{rl}, k_{rg} \leq 1$

$$\text{Here, } S^* = (S_1 - S_{lr}) / (S_{ls} - S_{lr}) \quad \hat{S} = (S_1 - S_{lr}) / (1 - S_{lr} - S_{gr})$$

C.4.7. Function of Verma et al. (1985)

$$k_{rl} = \hat{S}^3$$

$$k_{rg} = A + B\hat{S} + C\hat{S}^2 \quad (C.39)$$

$$\text{Where } \hat{S} = (S_1 - S_{lr}) / (S_{ls} - S_{lr}) \quad (C.40)$$

Parameters as measured by Verma et al. (1985) for steam-water flow in an unconsolidated sand:

$$\begin{aligned}
S_{lr} &= 0.2 \\
S_{ls} &= 0.895 \\
A &= 1.259 \\
B &= -1.7615 \\
C &= 0.5089
\end{aligned}$$

C.5. Capillary Pressure Functions

C.5.1. Linear Function

$$P_{cap} = \begin{cases} -CP(1) & \text{for } S_1 \leq CP(2) \\ 0 & \text{for } S_1 \leq CP(2) \\ -CP(1) \frac{CP(3) - S_1}{CP(3) - CP(2)} & \text{for } CP(2) < S_1 < CP(3) \end{cases} \quad (C.41)$$

Restriction: $CP(3) > CP(2)$

C.5.2. Function of Pickens et al. (1979)

$$P_{cap} = -P_0 \left\{ \ln \left[\frac{A}{B} \left(1 + \sqrt{1 - B^2/A^2} \right) \right] \right\}^{1/x} \quad (C.42)$$

$$A = (1 + S_1/S_{10})(S_{10} - S_{lr})/(S_{10} + S_{lr}) \quad (C.43)$$

$$B = 1 - S_1/S_{10} \quad (C.44)$$

Restrictions: $0 < S_{lr} < 1 \leq S_{10} \quad x \neq 0$

C.5.3. TRUST Capillary Pressure (Narasimhan et al., 1978)

$$P_{cap} = \begin{cases} -P_e - P_0 \left[\frac{1 - S_1}{S_1 - S_{lr}} \right]^{1/\eta} & \text{for } S_1 < 1 \\ 0 & \text{for } S_1 < 1 \end{cases} \quad (C.45)$$

Restrictions: $S_{lr} \geq 0 \quad \eta \neq 0$

C.5.4. Milly's Function (Milly, 1982)

$$P_{\text{cap}} = -97.783 \times 10^A \quad (\text{C.46})$$

$$A = 2.26 \left(\frac{0.371}{S_1 - S_{\text{lr}}} - 1 \right)^{1/4} \quad (\text{C.47})$$

Restriction: $S_{\text{lr}} \geq 0$

C.5.5. Leverett's Function (Leverett, 1941; Udell and Fitch, 1985)

$$P_{\text{cap}} = -P_0 \times \sigma(T) \times f(S_1) \quad (\text{C.48})$$

$$f(S_1) = 1.417(1 - S^*) - 2.120(1 - S^*)^2 + 1.263(1 - S^*)^3 \quad (\text{C.49})$$

$$S^* = (S_1 - S_{\text{lr}}) / (1 - S_{\text{lr}}) \quad (\text{C.50})$$

Restriction: $0 \leq S_{\text{lr}} < 1$

C.5.6. Van Genuchten Function (Van Genuchten, 1980)

$$P_{\text{cap}} = -P_0 \left(\left[S^* \right]^{-1/\lambda} - 1 \right)^{1-\lambda} \quad (\text{C.51})$$

Restriction: $-P_{\text{max}} \leq P_{\text{cap}} \leq 0$

$$S^* = (S_1 - S_{\text{lr}}) / (S_{\text{ls}} - S_{\text{lr}}) \quad (\text{C.52})$$

C.6. Deliverability Model

Wells may produce at constant flowing bottomhole pressure. With a given bottomhole pressure and productivity index, deliverability model can be applicable.

$$\hat{q}^k = \sum_{\beta} X_{\beta}^k q_{\beta} \quad (\text{C.53})$$

q^κ : Production rate for mass component κ

X_{β^κ} : Mass fraction of component κ in phase β

$$q_\beta = \frac{k_{r\beta}}{\mu_\beta} \rho_\beta \text{PI}(P_\beta - P_{wb}) \quad (\text{C.54})$$

$$(\text{PI})_1 = \frac{2\pi(k\Delta z_1)}{\ln(r_e/r_w) + s - 1/2} \quad (\text{C.55})$$

$$r_e = \sqrt{A/\pi} \quad (\text{C.56})$$

q_β : Mass production rate of phase β

$k_{r\beta}$: Relative Permeability

μ : Viscosity of phase β

ρ_β : Density of phase β

P_β : Phase pressure

P_{wb} : Flowing bottomhole pressure

$k\Delta z_1$: Permeability-thickness product in layer 1

s : Skin factor

A : Grid block area

$$P_{wb,1} = P_{wb,1+1} + \frac{g}{2} (\rho_1^f \Delta z_1 + \rho_{1+1}^f \Delta z_{1+1}) \quad (\text{C.57})$$

$$\rho_1^f = \frac{\sum_\beta \rho_{1,\beta} r_{1,\beta}^T}{\sum_\beta r_{1,\beta}^T} \quad (\text{C.58})$$

$$r_{1,\beta}^T = \sum_{m=1}^1 r_{m,\beta} \quad (\text{C.59})$$

$$r_{1,\beta} = \left(\frac{k_{r\beta}}{\mu_1} \right)_1 (\text{PI})_1 P_{1,\beta} \quad (\text{C.60})$$

g : Acceleration of gravity

ρ_1^f : Flowing density in the tubing opposite layer 1

$r_{1,\beta}$: Volumetric production rate of phase β from layer 1 (Wellbore pressure is assumed to be zero)

C.7. Heat Exchange with Confining Beds

For heat exchange with confining methods, the method of Vinsome and Westerveld (1980) which suggests that cap- and base-rock temperatures change smoothly in the case of strong and rapid temperature changes at the boundary of the conduction zone and that heat conduction perpendicular to the conductive boundary is more important than parallel to it is used in TOUGH2.

$$T(x, t) - T_i = (T_f - T_i + px + qx^2) \exp(-x/d) \quad (C.61)$$

$$d = \sqrt{\Theta t} / 2 \quad (C.62)$$

$$\Theta = \lambda / \rho C \quad (C.63)$$

x: Distance from the boundary

T_i: Initial temperature in cap or base rock

T_f: Time-varying temperature at the cap- or base-rock boundary

p,q: Time varying fit parameters

d: Penetration depth for heat conduction

Θ: Thermal diffusivity

λ: Thermal conductivity

ρ: Density of the medium

C: Specific heat

C.8. Coupled Wellbore Flow

At constant wellhead pressures, production from geothermal wells can be described by solving equations for flow in the reservoir and flow in the wellbore in a fully coupled manner or by generating a table of flowing bottomhole pressures for a range of flowrates and flowing enthalpies before the simulation starts.

$$P_{wb} = P_{wb}(q, h; P_{wh}, z, r_w) \quad (C.64)$$

q: Flowrate

h: Flowing enthalpy

P_{wh}: Wellhead pressure

z: Feed zone depth

r_w : Wellbore radius

P_{wb} : Flowing bottomhole pressure

Feed zone depth (z), wellhead pressure (P_{wh}), wellbore radius, (r_w) are constant values for a well. What change during the simulation are flowrate (q) and flowing enthalpy (h).

Using the Newton-Raphson iteration the unknown well flow rate and flowing bottomhole pressure can be calculated.

$$R(q) = q - \left(\sum \frac{k_{r\beta}}{\mu_\beta} \rho_\beta \right) PI(P - P_{wb}(q, h)) \quad (C.65)$$

APPENDIX D

PETRASIM

“Petrasim is a graphical interface for the TOUGH2 family of simulators that have been applied multi-phase, multi-component problems in one, two and three-dimensional porous and fractured media.

In the definition of model boundary, minimum and maximum values of X, Y, Z can be determined. In this part, there is an option to select the default material. If the model is to be an RZ axisymmetric model Y min is set to 0 and Y max is set to 1.

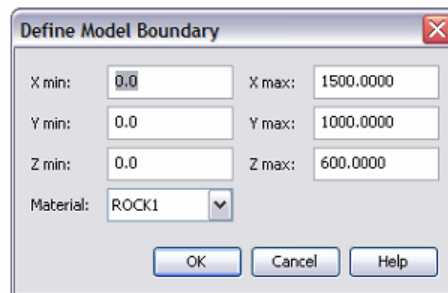


Figure D.1- Defining the boundary of the model

Internal boundaries, which are used to divide the model into regions, can be constructed using Strike+Dip option, 3 points on a plane option or Point+Normal option.

In Strike+Dip option, the coordinates of a point on the boundary plane, strike azimuth which is the degree from North in a clockwise direction, dip angle degree from horizontal of the plane are determined.

In 3 points on a plane option, the coordinates of three points on the boundary plane are written.

In Point+Normal option, the coordinates of a point on the boundary plane and the components of a vector normal to plane are determined.

Each region defined by internal boundaries can have specific material properties and initial condition.

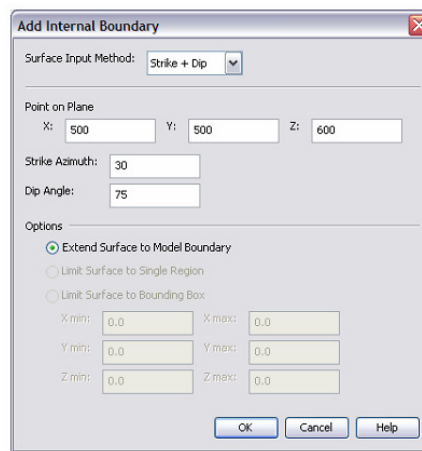


Figure D.2- Defining an internal boundary

Grids can be created with one of the division methods which are namely regular, meshmaker and meshmaker RZ. In regular method, grids are created by determining number of cells in X, Y and Z direction and factors used for each direction for increment. Grids can also be created by writing number of cells having same sizes in the specified direction and the magnitude of that size.

Material is created giving a name to it, specifying its properties such as density, porosity, permeability, wet heat conductivity, specific heat, relative permeability and capillary pressure functions related to this material. These materials and so their properties are assigned to individual cells or regions or to the entire model. Petrasim or TOUGH2 uses inheritance to determine any particular cell property: it

first looks in the cell, if the property is not found there, it looks in the region and finally to the default model.

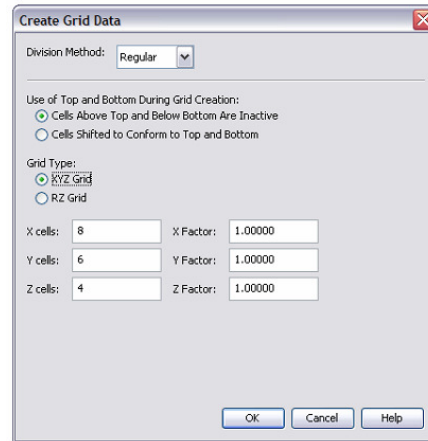


Figure D.3- Creating grid data

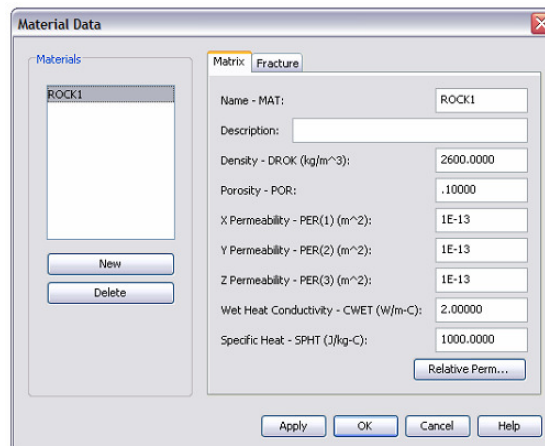


Figure D.4- Material Properties

Cell properties, permeability factor, volume factor, material type, its condition (whether it is enabled or fixed or disabled), production or injection values at that cell, initial conditions can be determined individually for each cell.

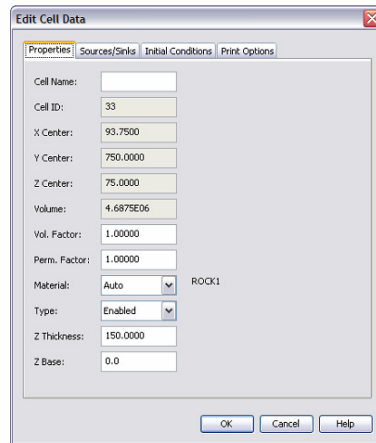


Figure D.5- Editing Cell Data

Fixed boundary conditions are set using fixed state option in Petrasim, creating inactive cells in TOUGH2. Another option to set fixed boundary conditions is to use large volumes. Thus, the change in variables can be made so small that it can be neglected. Changing permeability or conductivity, temperature and pressure effect can be adjusted. For time dependent boundary conditions, sinks and sources can be used. The option that includes heat exchange with confining beds can also be used.

How time step size changes during the calculation process can be watched on the running TOUGH2 dialog. Decrease in time step sizes indicates that number of iterations exceeds the value defined as max iterations per step or calculated parameters are out of range. As a rule of thumb, increase in time step size is a good sign of simulation progress.

The user can make 3D results using Petrasim. Isosurfaces and contours can be plotted for output parameters. Vectors can also be plotted so that direction and magnitude of different types of flows can be observed. 2D views and vectors on those planes can be constructed by selecting slice planes and selecting line plot option the user can observe how the output parameter changes between two points in the model.

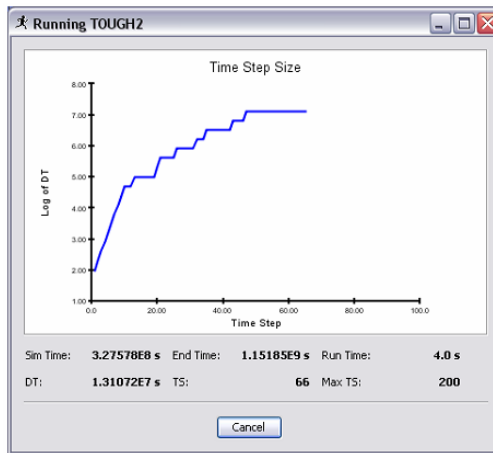


Figure D.6- Running TOUGH2

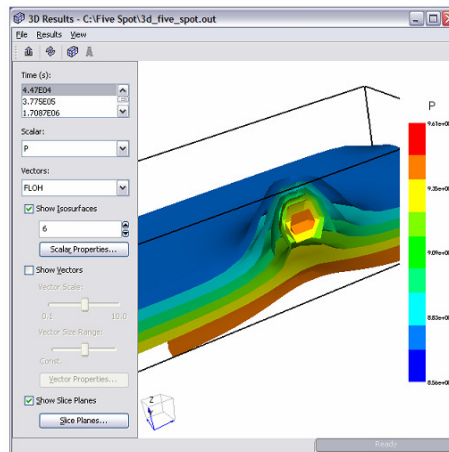


Figure D.7- The 3D results window

Selecting cell time history option, the user can observe how output parameters that are defined for the selected grid block changes with respect to time. Source, sink and connection plots can also be constructed.

It is possible to generate contour data consisting of the depth and a definition of contours at that depth to define 3D initial conditions or to define the topology of the top and bottom of the model.

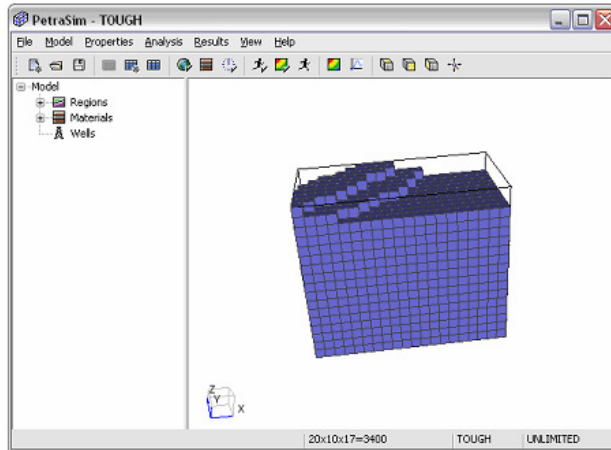


Figure D.8- 3D view of a model with top surface defined

Wells can be added as line objects in Petrasim. Production or injection occurs in matrix blocks which cross line that is drawn to represent a well and locate between the top completion depth and bottom completion depth. Production and injection can also be made by selecting a single cell or multiple cells and typing production or injection values to specified parts. The difference in using a well is that: Amount of production from a cell can be adjusted by defining permeability thickness product for that cell. Thus, cells having high permeability thickness product produces more compared to cells having low permeability thickness product.

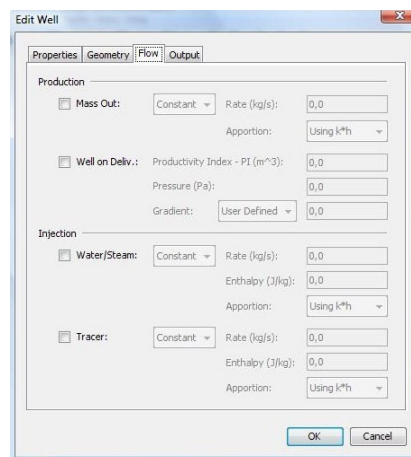


Figure D.9- Editing well data

Production can be made by three ways. The first way is a simple one: Typing production values with respect to time values. Specifying constant bottomhole flowing pressure for the upper most part and defining productivity index is the second way. For other parts pressure can be calculated with a gradient which can be calculated by the program or can be defined by the user. The method “coupled wellbore flow” in which the flow is described in both well and reservoir can be the third option.

In global properties option, the user can define the equation of state to be used, determine components to be used, type of water isothermal or non-isothermal, specify different gravity values, change the cosine of the gravity direction for X, Y and Z axes and determine if multiple interacting continua method is going to be used or not and specify flow option, fracture orientation, fracture spacing, number of interacting continua and volume fractions if multiple interacting continua method is going to be used.

Multiple interacting continua (MINC) method which is an extension of double-porosity concept and uses the assumption that fractures are well connected and have larger permeability and smaller porosity than they are in matrix (so flow happens mainly through the fracture) can be used to approximate modeling fluid and heat flow in fracture-porous media” (Thunderhead Engineering, 2009).

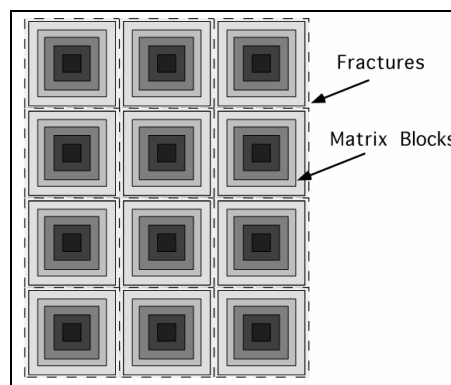


Figure D.10- Subgridding in the method of MINC.